ELECTRO-MICROFLUIDIC SENSOR FOR QUANTITATIVE DETECTION OF MICROPLASTICS IN SALINE FRESHWATER

Haider Warraich

A THESIS SUBMITTED TO THE FACULTY OF GRADUATE STUDIES IN PARTIAL FULFILLMENT OF THE REQUIREMENTS FOR THE DEGREE OF MASTER OF APPLIED SCIENCE

GRADUATE PROGRAM IN MECHANICAL ENGINEERING

YORK UNIVERSITY

TORONTO, ONTARIO

Abstract

This thesis investigates a DC microfluidic sensor incorporating a Wheatstone bridge and MXene-coated microwires to detect and quantify microplastics in freshwater with varied salinity. The study addresses the limitations of traditional detection methods, particularly in higher freshwater salinity where microplastics exhibit reduced electrophoretic mobility. The sensor's performance was evaluated across a range of microplastic concentrations (1–25 ppm) suspended in saline solution with varying NaCl concentrations (0–1000 ppm) to assess sensitivity and detection limits. Results demonstrated a significant reduction in electrical resistance as microplastics accumulated at the anode, indicating successful detection at lower salinities. However, at higher salt concentrations, microplastic accumulation and sensor sensitivity declined. Modifications, including constant current application and MXene functionalization, enhanced accumulation rates, and detection performance. Future research is required to investigate diverse microplastic types, shapes, and biological interferences to improve real-world applicability. This work provides a foundation for low-cost, sensitive microplastic detection in aquatic environments.

Dedication

To my mother, whose resilience through countless challenges instilled in me a passion for learning and engineering. Her sacrifices and unwavering support have been the foundation of this journey. And to my sister, for her constant encouragement.

Acknowledgements

I would like to extend my heartfelt gratitude to my M.Sc. supervisors, Dr. Pouya Rezai and Dr. Shoka Karimpour, for their exceptional guidance, encouragement, and support throughout my research journey. Their mentorship has been invaluable, and I am grateful for the opportunity to learn from their expertise, which has helped me grow both professionally and personally.

I am also deeply appreciative of my defense committee members, Dr. Razieh (Neda) Salahandish and Dr. Gerd Grau, for their time, insightful feedback, and critical review of my thesis. Their constructive input has been instrumental in refining my work.

A special acknowledgment goes to Dr. Alireza Zabihihesari, whose mentorship during my initial days in the program provided me with essential skills and knowledge, setting a strong foundation for my research.

I would also like to thank all the talented and dedicated members of the Advanced Center for Microfluidics Technology and Engineering (ACμTE) lab. Their camaraderie, support, and insightful discussions have greatly enriched my experience.

Finally, I would like to express my deepest gratitude to my mother and sister. Their unwavering love, encouragement, and support have been a constant source of strength throughout my academic journey, and I am forever grateful to have them by my side.

Table of contents

List of Figures

List of Tables

Chapter 1: Introduction

1.1 Introduction and Research Motivation

The continuous increase in synthetic plastic production and poor waste management have resulted in the disposal of plastic waste into aquatic ecosystems, leading to the creation and distribution of microplastics in water bodies [1]. Microplastics, defined as plastic particles less than 5 millimeters in diameter, have become a significant environmental concern due to their widespread presence and potential harmful effects on ecosystems and human health. These tiny plastic fragments originate from various sources, including the breakdown of larger plastic debris, microbeads in personal care products, and synthetic fibers from textiles [2]. Once introduced into the environment, microplastics can persist for extended periods due to their resistance to degradation.

The introduction of microplastics into aquatic environments occurs through multiple pathways. Urban runoff, wastewater effluents, and atmospheric deposition are significant contributors [1,2]. For instance, microbeads from exfoliating products and fibers from washing synthetic clothes often escape wastewater treatment processes and enter freshwater systems [3,4]. Additionally, larger plastic debris, such as bottles and packaging materials, degrade into microplastics over time through photodegradation and mechanical abrasion [4]. Microplastics have been detected in various environments, from the surface waters of oceans to the sediments of freshwater bodies. Their small size enables them to be easily transported by wind and water currents, leading to widespread distribution [5]. The varying salinity levels in these environments, from the high salinity of ocean water to the lower salinity of freshwater bodies, can significantly influence the physical and

chemical properties of microplastics, such as their buoyancy, aggregation behavior, and interaction with other pollutants [6]. In marine environments, microplastics have been found from coastal areas to the deep sea, highlighting their persistent nature and the challenges associated with their removal [4].

The pervasive presence of microplastics poses significant threats to aquatic ecosystems. Marine and freshwater organisms, ranging from plankton to larger fish and mammals, can ingest microplastics, mistaking them for food [7–9]. This ingestion can lead to physical harm, such as internal injuries and blockages, and chemical harm due to the leaching of toxic additives present in plastics [9]. Furthermore, microplastics can act as vectors for other pollutants, such as heavy metals and persistent organic pollutants, which can absorb onto their surfaces and be transported across different environmental compartments [10,11]. Microplastics have also been found in various food products, including seafood, honey, and drinking water, raising concerns about human exposure [12]. The ingestion of microplastics by humans can potentially lead to health issues, although the full extent of these effects is still under investigation. Potential risks include physical damage to the gastrointestinal tract, exposure to harmful chemicals, and the transfer of pollutants that microplastics can carry [13]. Understanding and mitigating these risks is essential for public health.

The presence of microplastics in the environment also has economic implications [14,15]. The contamination of seafood can affect fisheries and aquaculture industries, leading to economic losses [15]. Additionally, the cost of cleaning up plastic pollution and addressing its impacts on tourism and recreation can be substantial.

Developing effective detection and mitigation strategies for microplastics is thus crucial for protecting the environment, human health, and the economy. Regular monitoring must be fast, reliable, affordable, and capable of performing *in-situ* analysis. Additionally, these methods must be quantitative and sensitive to the size, type, and shape of microplastics to accurately assess their presence and impact.

Various detection methods have been developed to identify and quantify microplastics in water, and the most important ones will be reviewed in the next chapter. Traditional techniques, such as visual inspection [16], Fourier-transform infrared (FTIR) [17,18], and Raman spectroscopy [18,19], are commonly used but come with notable limitations. These methods often require labor-intensive sample preparation, lengthy analysis times, and may struggle to accurately detect smaller microplastic particles, especially in complex environmental matrices like saline freshwater. Moreover, these conventional techniques require the expertise of trained professionals, making them costly and time-inefficient for rapid and widespread monitoring [18].

Varying salt concentrations in different water bodies introduces different ions into the sample which can interfere with many detection methods, particularly those based on optical or electronic properties. To overcome these challenges, there is a pressing need for innovative detection technologies that combine sensitivity, speed, and the ability to handle detection of microplastics in saline freshwater.

The use of microfluidic sensors has been able to address these needs by leveraging their precision and sensitivity of detection [20]. These sensors offer high sensitivity, allowing for the detection of

low concentrations of microplastics and the differentiation of particles by size [21]. This enhances the accuracy of environmental assessments. Additionally, microfluidic sensors enable rapid, real-time analysis, significantly reducing the time required compared to traditional methods. Their versatile design allows for application in diverse settings, including laboratories, field stations, and on-site monitoring platforms. This adaptability, combined with cost-effectiveness, simplifies the detection process by minimizing extensive sample preparation and lowering overall analysis costs. As a result, microfluidic sensors provide a reliable and accessible solution for the widespread and urgent task of detecting and monitoring microplastics, which is essential given their pervasive presence and potential risks to ecosystems and human health

1.2 Research Opportunity and Thesis Objective

The research opportunity arises from research gaps found in literature which underscore the critical need for point-of-need (PoN) detection of microplastics in saline waters. Previous studies have relied heavily on detection of microplastics in DI water [16,22]. The novel aspect of our study lies in the detection of microplastics in salty water, a challenging environment for traditional detection methods especially if sensing is based on electrical measurement of fluid properties. As discussed further in Chapter 2, earlier works have demonstrated the detection of microplastics in KCl-diluted water using a resistive pulse sensor (RPS) [20]. One of the studies focused on particles ranging in size from 2 to 30 μm and explored salt concentrations from 2.5×10^{-4} to 0.1 M KCl (18.64 to 7455 ppm) [20]. The study revealed an inverted sensor response at lower ionic strength compared to the

results obtained at higher KCL concentrations [20]. Yet, the study did not extend to elaborate on detecting microplastics in lower (freshwater) conductivity ranges, focusing instead on higher salt concentrations, in the spectrum of seawater conductivity (3727.5 ppm KCL), and exceeding seawater's conductivity (7455 ppm KCl), further elaborated on in chapter 2. In another work, Pollard et al. [23] created an innovative multi-RPS sensor capable of detecting particles from 0.1 to 30 micrometers, still calibrated for seawater conductivity. This sensor covered a wide range of microplastic sizes, but its sensitivity to varying particle concentrations remained unexplored, discussed in depth in chapter 2. Prior study utilizing a microfluidic sensor coupled with electrophoretic force, has shown promise in the separation [24], extraction [22,25], and detection of microplastics in deionized water [22]. Nonetheless, the role of the conductivity of the aqueous medium hosting the microplastics remains an underexplored area particularly in the PoN sensors domain, suggesting a gap in our comprehensive understanding of these interactions. These gaps and opportunities for improvement are further detailed for each detection method in Table 1-1, which presents various detection methods, discussing their capabilities in measuring the smallest particle sizes, as well as their limit of detection (LOD), limit of quantification (LOQ), specificity, and sensitivity. The table also briefly addresses the gaps associated with each detection method.

Table 1-1: Comparative analysis of microplastic detection methods in water: highlighting detection capabilities and identifying critical gaps for future innovation.

		Detection Method	Smallest measured Size	Limit of Detection (LOD)	Limit of Quantification (LOQ)	Specificity	Sensitivity	Gaps/Room for Improvement
Conventional Detection Methods		**Visual Inspection of Microplastics** [16,26]	~50 µm	~50 µm	NA	Low (prone to human error)	Low (observer-dependent)	Prone to human error, not suitable for detecting small microplastics. Can't differentiate between synthetic and natural particles.
		Spectroscopy [18,27]	~20 µm (ATR-FTIR)	~25 µg/mL	~60 µg/mL	High (Capable of identifying specific polymer types/size/shape)	Medium (high signal-to-noise ratio)	Samples must be IR active; smaller particles (<20 µm) may not produce clear spectra; expensive equipment; interference from biofilms
Advanced Detection Methods		**Flow Cytometry** [28,29]	-0.2 µm	~1 µg/mL	~10 µg/mL	Medium (particle size/material, fluorescence-based differentiation)	High (low concentration detection)	Expensive, requires specialized equipment. Limited by detection of smaller particles and inability to distinguish between similar-sized biological particles.
	Microfluidic Based Detection	**Microfluidic Sensors with Optical Spectroscopy** [30]	~1 µm	~0.016 µg/mL	~0.2 µg/mL	High (design-dependent)	High (Can detect much smaller concentration and particle size)	Integration with optical techniques can be complex. Improvement needed in simplifying the design for practical use.
		Nile Red Staining with Microfluidics [31,32]	~5 µm	~5 µm	NA	Medium (staining can target microplastics, but also stains natural particles)	High (sensitive to small particles, influenced by flow rate and temperature)	Cannot distinguish between microplastics and organic matter. Improvement needed in reducing false positives

		Microfluidic-based Electrical Sensor (Resistive Pulse Sensor) [23,33,34]	~ 60 nm (57 particles per mL)	0.031 µg/mL	1.04 µg/mL (1.89×10^3 particles per mL)	Medium (depends on particle size/material)	High (sensitive to changes in electrical properties)	Limited by the electrical properties of the medium. Improvement needed in broadening the range of detectable materials.
		Electrophoretic-based Electrical Microfluidic Sensor [35]	~1 µm	5 µg/mL (5 ppm)	5 µg/mL (5 ppm)	Medium (correlation with microplastic concentration)	High (dependent on flow rate and microplastic size)	Dependent on particle size and concentration, need for optimization in real-world conditions with varying conductivity

There have been significant advancements in the development of various sensing devices, but many of these technologies remain expensive, involving complex fabrication processes. There is a clear need for a low-cost sensor that can be easily tailored to detect microplastics within freshwater. In this context, "low-cost" refers to the materials and fabrication processes of the sensor, excluding the costs associated with operation and mass production, which should be considered in future work.

This thesis focuses on the development of a direct current (DC) electro-microfluidics sensor designed to detect and quantify microplastics in saline freshwater environments. The proposed sensor aims to provide a reliable, cost-effective solution for detection and monitoring of microplastics, addressing the shortcomings of existing methods. To achieve this goal, the research in this thesis involves optimizing a microfluidic sensor for detecting polystyrene microplastics (1µm, 5µm, 10µm) of varying concentration (1 ppm, 5 ppm, 25 ppm) in saline freshwater range (300 - 1000 ppm). The initial sensor configuration was adopted from an existing microfluidic sensor that was used to detect microplastics in DI water [22]. This sensor was effective in previous

application, but its sensitivity and ability to detect microplastics in saline fresh water were unknow. To address this gap, we evaluated the sensors characteristics in saline water. The goal was to improve the sensor for reliable detection of microplastics in such an environment. Our sensor represents a proof of concept for a broader application in environmental monitoring. While the current focus is on microplastics, the platform has the potential to be adapted for detecting other types of contaminants in the future. The specific objectives of this thesis are:

1. **Characterize sensor parameters to detect microplastics in saline water:** This objective involves detailed analysis of the sensor's sensitivity, specificity, and detection limits under different saline (300, 650, and 1000 ppm) and microplastic (1, 5, and 25 ppm) concentrations.
2. **Improve the sensor's electrical response and optical performance for effective detection of microplastics across the complete range of freshwater salinity:** This entails refining the sensor to improve its electrical sensitivity and optical accuracy, ensuring it can accurately identify the presence and measure the concentration of microplastics (1, 5, and 25 ppm) in freshwater salinity ranging from 300 to 1000 ppm. Additionally, a numerical study will be conducted to understand the accumulation phenomenon, which will aid in optimizing the sensor's design and performance.
3. **Evaluate the sensor's capability to detect microplastics of varying sizes (1, 5, and 10 µm) in saline freshwater:** This involves testing and validating the optimized sensor's performance in detecting and differentiating between microplastic particles of different sizes, ensuring comprehensive monitoring capabilities.

Through experimental investigations, partly supported by computational frameworks, this research aims to develop a microfluidic sensor that meets the critical need for effective, low-cost detection of microplastics. The outcomes of this work will contribute to enhanced environmental monitoring and ultimately supporting efforts to mitigate the adverse impacts of microplastic pollution on ecosystems and human health.

1.3 Thesis Organization

The first chapter introduces the research background, motivation, existing gaps, and the objectives that this research aims to achieve. It sets the stage for the necessity of developing a low-cost, sensitive, and effective microfluidic sensor for detecting microplastics in saline freshwater environments.

The second chapter presents a detailed literature review of conventional and advanced environmental monitoring techniques. It begins with an overview of traditional methods for microplastic detection and their limitations, followed by a discussion of advanced techniques that include nanomaterial functionalization and microfluidic detection platforms. This chapter also identifies research gaps and key challenges that current methods face, particularly in detecting microplastics in saline freshwater environments.

The third chapter details the theory behind the developed microfluidic sensor, including the principles of electrophoresis and the impact of saline environments on microplastic detection. It also covers the design, fabrication, and experimental setup of the sensor, along with the

methodologies used for data acquisition and analysis. This chapter provides a comprehensive explanation of the sensor's working mechanism and the rationale behind the experimental procedures.

The fourth chapter presents the preliminary results and discusses the sensor's performance in detecting microplastics under varying conditions. It explores the effects of salt concentration and microplastic concentration on the sensor's detection capabilities, providing insights into the challenges and effectiveness of the sensor in saline freshwater environments. The chapter also compares the sensor's performance with existing detection methods, highlighting its potential advantages and limitations.

The fifth chapter focuses on the simplification and improvement of the sensor design. It discusses the implementation of a constant current operation, the integration of a Wheatstone bridge for enhanced measurement accuracy, and the functionalization of microwires with MXene to improve microplastic accumulation. This chapter also includes a numerical analysis that validates the experimental findings and provides a deeper understanding of the sensor's performance.

The sixth and final chapter summarizes the key findings of the research, discusses the limitations of the current work, and offers suggestions and recommendations for future research. It reflects on the implications of the study for environmental monitoring and proposes pathways for further development and optimization of the sensor for broader applications.

Chapter 2: Literature Review and Research Gaps

2.1 Conventional Microplastic Detection Methods

Conventional methods for detecting microplastics such as visual inspection, microscopy, and vibration spectroscopy have been leading environmental monitoring research for many years. Although effective, these methods are labour-intensive and require effort to accurately identify and quantify microplastics. This section will discuss some of these conventional methods used to detect microplastics.

2.1.1 Visual Inspection and Microscopy

Visual inspection is one of the initial methods used for detecting microplastics in environmental samples. It heavily relies on the manual counting and sorting of particles using the naked eye or optical microscopes. This method is often considered labor-intensive, yet it remains widely used due to its simplicity and minimum equipment requirements. According to Hidalgo-Ruz et al. [36], visual inspection usually involves collecting samples from various environments, then followed by density separation techniques to isolate microplastics from sediments. After that, samples are examined under a microscope, where particles are identified and characterized based on size, shape, and color.

Microscopy techniques which include optical microscopy, scanning electron microscopy (SEM), and transmission electron microscopy (TEM), have been widely used for identification and characterization of microplastics in the environment. These techniques provide high-resolution

imaging capabilities, allowing for detailed analysis of the morphology, size, and surface characteristics of microplastic particles. Studies by Wang et al. [37] and Rocha-Santos et al. [38] have demonstrated the effectiveness of SEM in identifying microplastics in marine and freshwater sediments, highlighting its ability to reveal intricate surface features and degradation patterns that are not visible with optical microscopy. SEM can also be coupled with energy-dispersive X-ray spectroscopy (EDS) to provide elemental analysis, enabling researchers to determine the chemical composition of microplastic particles [38,39], as shown in Fig. 2-1.

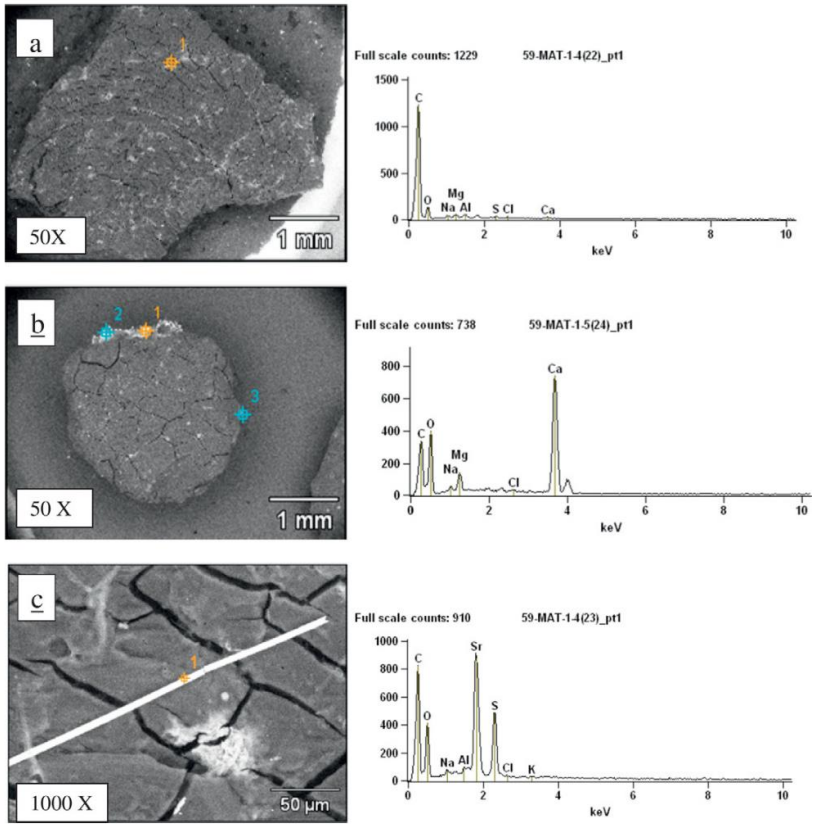

Fig. 2-1: SEM images and EDS of Pacific Ocean trawl microplastic particles showing characteristic environmental exposure surface cracks and adhered surface species: Ca or Mg-Ca crusts and radiolarians[37]. Figure reprinted with permission from Elsevier

TEM offers even higher resolution imaging than SEM, making it possible to visualize the internal structure of microplastics at the nanometer scale. This technique has been employed to investigate the fine structural details of microplastics, including the presence of additives and the effects of environmental weathering [40]. TEM's ability to provide detailed internal images is essential for understanding the interactions between microplastics and other environmental contaminants. However, both SEM and TEM require extensive sample preparation, including drying and coating for SEM or ultra-thin sectioning for TEM, which can be time-consuming and may alter the samples.

In addition to SEM and TEM, fluorescence microscopy using Nile Red staining has emerged as a valuable technique for detecting and quantifying microplastics. Nile Red is a lipophilic dye that binds to hydrophobic plastic polymers, making microplastics fluoresce under specific wavelengths of light. This method, as shown in studies by Fernandez-Fonzalez et al. [40] and Shruti et al. [41], is particularly effective for identifying small microplastics (down to 1 μm) in complex environmental matrices. The fluorescence microscopy approach allows for rapid screening and quantification of microplastics with minimal sample preparation, and it can be combined with image analysis software to enhance detection accuracy and efficiency [42]. However, the technique may face challenges in distinguishing between microplastics and other hydrophobic materials, and the fluorescence intensity can vary depending on the polymer type and degree of weathering. Various studies have highlighted the effectiveness and also the limitations of this method. For example, a study on microplastics [43] utilized visual inspection to identify and quantify microplastics in marine sediments. Their study emphasized the method's ability to detect a wide range of plastic types, although it required significant manual effort. Similarly, Ng and Obbard [44] applied visual

inspection to beach sand samples, demonstrating its utility in identifying microplastics in coastal environments. However, they also stated that recognizing microplastics from other similarly sized particles, such as natural fibers and organic debris, posed a great challenge.

The potential of human error in visual inspection were further underscored by Imhof et al. [36] who called for standardized protocols to improve reliability and reproducibility. They suggested that variability in operator skill and experience could lead to inconsistencies in data collection and interpretation. In another study [44], the need for complementary analytical techniques, such as FTIR spectroscopy, to confirm the polymer composition of visually identified particles, thus reducing the likelihood of misidentification was emphasized. Improvements in visual inspection methods have been proposed to enhance accuracy and efficiency. Coppock et al. [45] introduced a semi-automated system that combines visual inspection with image analysis software to reduce the workload and increase the consistency of particle identification.

Despite these advancements, visual and microscopy inspections remain a time-consuming process, especially when dealing with large sample sizes or environments with high microplastic contamination levels. The method's reliance on human observers also limits its scalability and throughput. The need for extensive training to ensure accurate identification further adds to the challenges associated with this technique. Furthermore, the effectiveness of visual inspection can be compromised by environmental factors. For instance, microplastics that are heavily weathered can be difficult to distinguish from natural particles. A study by Eriksen et al. [46] highlighted that weathering processes can alter the appearance of microplastics, making them less recognizable under a microscope.

2.1.2 Spectroscopy

Vibrational spectroscopy techniques, such as FTIR and Raman micro-spectroscopy, are currently considered among the most reliable and effective methods for identifying synthetic polymeric hydrocarbons. These methods employ a size-specific approach to qualify microplastics by analyzing the interaction between infrared (IR) and laser sources with the physical characteristics of particles. This enables the identification of both natural and synthetic polymers by analyzing their vibrational spectra [17].

Raman and FTIR micro-spectroscopy are typically coupled with microscopes, providing spectral and spatial information for small particles, less than 100 μm, while attenuated total reflection (ATR)-FTIR is used for larger microplastics usually greater than 300 μm [47,48]. Depending on the analyzed sample size, a few dozen to several million spectra may be produced similar to the ones illustrated in Fig. 2-2, requiring sophisticated interpretation. Imaging techniques produce large data cubes with numerous variables corresponding to recorded wavenumbers, not all of which are needed for accurate interpretation. Consequently, the large amount of data acquired necessitates intensive data analysis to identify and interpret the molecular information of the sample [16,17].

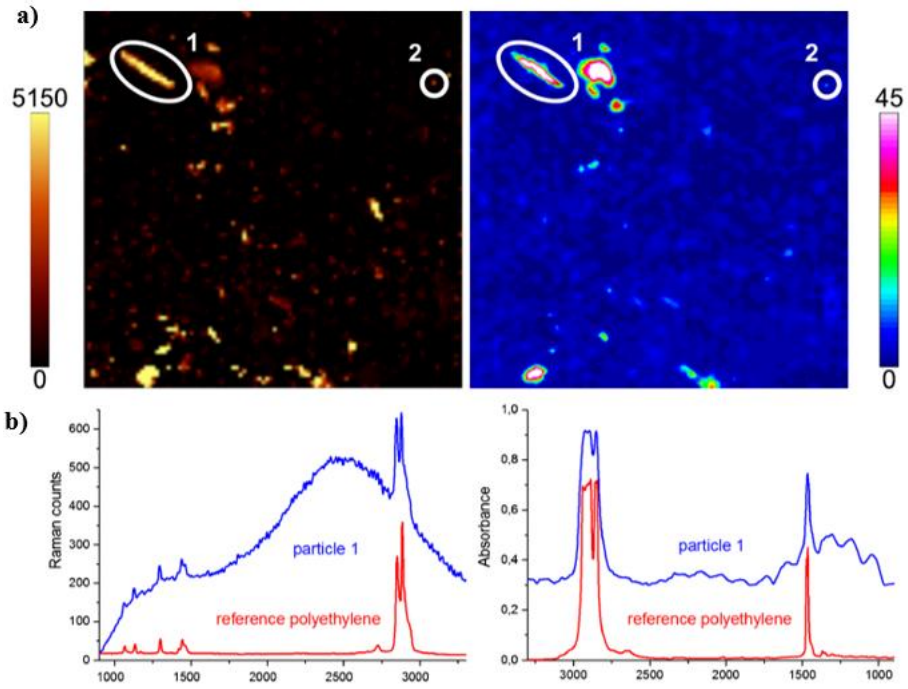

Fig. 2-2: a) Raman image (left) and FTIR image (right) of PE particles within a selected sample area by choosing a spectral range of 2780–2980 cm^{-1} . The colour scale bar represents the intensity of the integrated spectral band (arbitrary units). **b)** Complete Raman spectra (left) and FTIR transmission spectra (right) of PE particle [17]. Figure reprinted with permission from Springer Nature.

The appropriate data analysis routine depends on the instrumental workflow. Analyzing and assigning the spectra to a substance is challenging due to diverse microplastic and matrix types, large data sets, and complex microplastic spectra. The quality of microplastic spectra can be compromised by factors such as weathering, noise, baseline distortion, and other distortions, thereby adding complexity to the analysis process [27]. Pre-processing techniques, such as baseline correction or smoothing, can facilitate the data analysis procedure. These techniques can speed up substance identification, but any manipulation via pre-processing must preserve the vibrational band signals and shapes of the spectra [49].

FTIR and Raman spectroscopy are widely regarded as dependable methods for detecting microplastics, but they come with some limitations. Both methods require specialized equipment, intensive data analysis, and technical expertise, which can be expensive and time-consuming. Detecting particles smaller than 10 µm can be particularly challenging for both techniques [27,45]. Moreover, the data analysis for FTIR and Raman can be complex, requiring specialized software and interpretation skills to accurately identify and characterize microplastics [17].

2.2 Advanced Detection Technologies

2.2.1 Flow Cytometry

Flow cytometry has proven to be a powerful analytical technique traditionally used in cell biology and immunology to analyze the physical and chemical characteristics of particles in a fluid as they pass through a laser beam [29]. Recently, its application has been extended to environmental science, particularly for the detection and characterization of microplastics [50,51]. This technique allows for high-throughput analysis and can provide detailed information about the size, granularity, and fluorescence properties of microplastic particles. Flow cytometry works by suspending microplastic particles in a fluid stream, which is then passed through a focused laser beam. As the particles pass through the beam, they scatter light and emit fluorescence, which are detected by various sensors as observed in Fig. 2-3. The light scattering provides information on the size and internal complexity of the particles, while the fluorescence signals can be used to identify different types of plastics based on their intrinsic or dye-induced fluorescence properties [52].

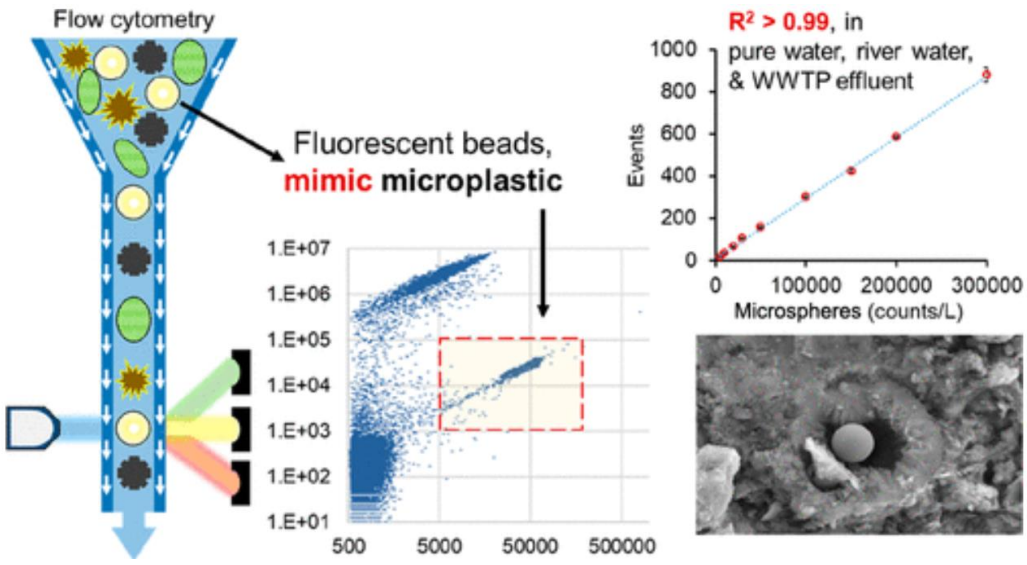

Fig. 2-3: Flow cytometry analysis of fluorescent microplastics: A flow cytometer is used to analyze fluorescent beads that simulate microplastics. The scatter plot shows the distribution of events, highlighting a strong correlation between microsphere counts and events in different water types (pure water, river water, and wastewater treatment plant effluent) [52]. Figure reprinted with permission from American Chemical Society

One of the earliest studies demonstrating the potential of flow cytometry for microplastic detection was conducted by Angelica et al.[53]. They developed a method of detecting polyethylene microplastic particles within the range of 0.6 - 15µm by combining flow cytometry with Nile Red staining. This approach enabled rapid and accurate quantification of microplastics in Milli-Q quality water. This approach demonstrated 90s sample analysis time, which is significantly faster than the hours typically required for micro-Raman and other spectroscopic techniques [53]. Further advancements in flow cytometry for microplastic analysis were reported by Chaoran et al.[54]. In this study they integrated automated sample analysis and high sample throughput with flow cytometry analysis to streamline the detection process. Their system encompasses the analysis of

microplastics in various water types, including ultrapure water, tap water, and surface water. It examines microplastics of different compositions, densities, and sizes (10, 50, and 100 μm) [54]. This automated approach significantly reduced the time and labor required for sample processing, making it a viable option for routine monitoring of microplastic pollution. Flow cytometry also offers the advantage of being able to analyze a wide range of particle sizes, from nanometers to micrometers. Yuet-Tang et al.[51] demonstrated the technique's sensitivity in detecting smaller microplastics (down to 1 μm) in sea water samples. By using a combination of forward and side scatter measurements, they were able to accurately size and quantify microplastic particles, which is critical for assessing the full extent of microplastic pollution.

Despite its advantages, the application of flow cytometry in microplastic research faces several challenges. Firstly, there is a high cost of purchasing and maintaining flow cytometers which can be prohibitive for many laboratories, limiting their accessibility [51]. Another primary limitation is the need for pre-treatment steps to remove organic matter and other debris that can interfere with the analysis. Interference from organic and inorganic particles in the samples can lead to false positives and inaccurate results, further complicating the analysis [54]. Staining of microplastics which is necessary for detection with flow cytometry, can be impractical for environmental monitoring due to the difficulty in uniformly staining diverse microplastic types in natural water samples. Additionally, this requirement complicates on-site detection efforts, making it hard to implement flow cytometry methods effectively in field conditions.

2.2.2 Microfluidic Sensors

Microfluidic technology is gaining popularity in recent times as it has revolutionized many fields. This technology allows for manipulating and analyzing fluids at a small scale, furthermore, requiring small sample sizes. Microfluidic technology has emerged as a promising method for the detection of microplastics in water. Several microfluidic methods have been developed for the detection and analysis of microplastics. These methods include optical spectroscopy [55], staining dyes [32], and various electrical based methods [20,22], as seen in Fig.2-4.

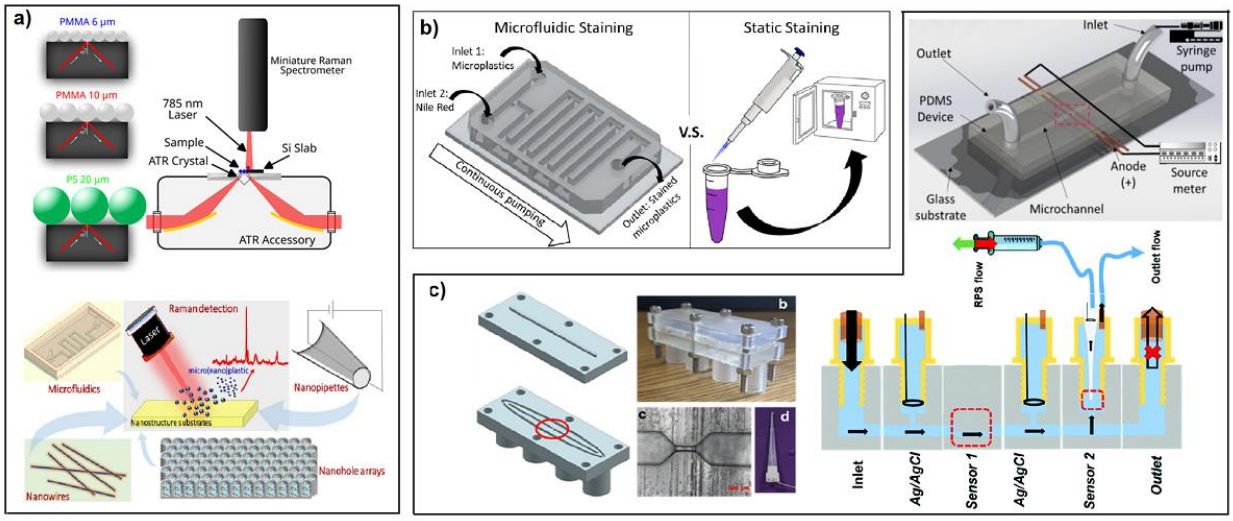

Fig. 2-4: Various microfluidics methods used to detect microplastics in water. **a)** optical spectroscopy [55], **b)** Nile red staining of microplastics particles [32], and **c)** various electrical sensors all integrated with the microfluidic technology[20,22]. Figures reprinted with permissions from Springer Nature, MDPI journals, Royal Society of Chemistry, and New journal of chemistry.

2. 2. 2. 1 Optical Spectroscopy with microfluidics

Microfluidic optical spectroscopy is an emerging technique that combines microfluidics and optical spectroscopy for the analysis and detection of microplastics in water. This technique allows for the precise analysis of the chemical composition of microplastic particles captured within a microchip. Once the microplastics are entrapped, they are aligned with the laser for detailed examination [30,56]. Both Raman and FTIR spectroscopy are commonly used in conjunction with a microfluidic chip, as illustrated in the experimental setup shown in Fig. 2-4a.

Raman spectroscopy with the use of microfluidic chips enables a swift and precise analysis of microplastics. To implement this approach, a sample containing microplastics is injected into a microfluidic channel or chamber, where a laser is used to stimulate the sample [55]. The scattered light is then gathered and examined by a Raman spectrometer, which provides information on the microplastics' chemical composition [17,18,55]. FTIR spectroscopy approach has the same working principle as the Raman spectroscopy method. The microplastics introduced into a microfluidic channel are exposed to infrared light. The interaction between the sample and the infrared light results in characteristic absorption spectra, which can be analyzed by a FTIR spectrometer to provide information on the chemical composition of the microplastics [19]. Both these methods of using optical spectroscopy have many advantages over traditional bulk spectroscopy. Firstly, the use of small sample volumes in microfluidic chips can reduce analysis time and increase detection sensitivity [30]. Secondly, microfluidic chips can assist in capturing and isolating microplastics, resulting in more targeted analysis [30]. Furthermore, the miniaturization of the system can lead to the development of more portable and cost-effective instruments.

However, there are also some limitations to this approach. One of the major limitations of using microfluidic chips with Raman or FTIR spectroscopy for microplastic detection is the small sample volumes and channels, which limits the sample throughput and can result in longer analysis times [16]. This can be a disadvantage for real-time monitoring applications that require quick analysis. Additionally, the initial setup costs can be high due to the complex and costly design and fabrication of microfluidic chips containing nanoporous, which may limit the accessibility of this approach for some researchers. Another limitation is the potential for clogging [55], particularly when dealing with microplastic-containing samples, which can compromise the accuracy and reliability of the results and necessitate additional measures to unclog the microfluidic channels. Moreover, microfluidic chips can pose difficulties for collecting smaller microplastics that may not fit within the microchannels, resulting in incomplete or biased analysis. Researchers should, therefore, carefully consider the choice of sample preparation methods to optimize microplastic collection. Finally, the sample matrix or background, such as water or sediment, can interfere with the signal obtained from Raman or FTIR spectroscopy [44,53], lowering the detection accuracy.

2. 2. 2. 2 Nile Red Staining with microfluidics

Recently, fluorescent dyes have been increasingly exploited for the detection of microplastics in water due to their high sensitivity and selectivity. Nile red, a lipophilic fluorescent dye, meaning it can stain lipids in their natural environment (Fig. 2-4b). This dye has been widely employed to measure the lipid content in various organisms, including mammalian cells, bacteria, yeasts, and microalgae [57–59]. Due to its promising results, it has gained popularity as a staining agent for the detection of microplastics.

In order to identify microplastics in environmental samples, the samples are treated with Nile Red dissolved in an organic solvent following the microplastic extraction and sample preparation procedures. The sample preparation procedure involves a series of steps, including filtration of the water sample to eliminate larger particles and debris, as well as acid digestion to eliminate organic substances and enhance measurement accuracy [59]. In most studies the microplastics are filters using a plankton net consisting of a mesh size of about 0.33 m [57,59]. In order to decrease the likelihood of false positives and to eliminate the presence of natural particles, chemical breakdown of natural organic matter is utilized. Hydrogen peroxide (H_2O_2) or potassium hydroxide (KOH) solutions are the most widely used reagents [42,60]. Alternatively, specific enzymes such as cellulase, protease, and chitinase may be utilized as less harsh alternatives. It is imperative to utilize a technique that does not harm the microplastic particles during this procedure. Once the sample preparation is complete, Nile red can be applied to the microplastics and observed under a florescent microscope as seen in Fig. 2-5.

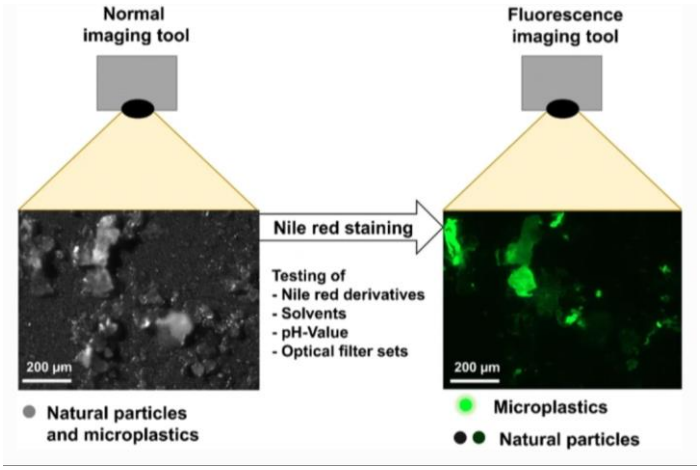

Fig. 2-5: The Nile red stained microplastic particles can be observed under the florescent microscope, although some fluorescent illumination could be false positives. [61]. Figure reprinted with permissions from Springer Nature

Despite the extensive preparation, it may not be possible to completely separate all natural organic particles from the microplastic, leading to false positives. Nile red can bind to materials besides microplastics resulting in an overestimation of microplastic contamination in a given sample [61].

Staining techniques like Nile Red have been effectively used for identifying small (50-500 µm) and very small (0.1-50 µm) microplastics, either by staining the biological content associated with the particles or directly staining the polymers [60,61]. While Nile Red is a readily available dye, detecting the fluorescence signal from the stained microplastics require specialized equipment such as a fluorescence microscope or a flow cytometer [61]. Advancements in this field are necessary to make this method viable for in-field testing. Moreover, expertise in handling and interpreting fluorescence data is necessary for precise analysis.

2. 2. 2. 3 Microfluidic-based electrical sensors

Microfluidic electrical sensor technology holds the potential to provide point-of-need detection of microplastics (Fig.2-4c), due to their simple working mechanism and design. There are several electrical-based methods used for detecting microplastics in water. The most commonly used approaches to excel towards point-of-need detection include resistive pulse sensors and sensors that utilize electrophoretic force to enhance microplastic accumulation for subsequent detection, as discussed below.

2. 2. 2. 3. 1 Resistive pulse sensor

Resistive Pulse Sensing (RPS) is an advanced analytical technique that has gained traction in the detection and characterization of microplastics due to its high sensitivity and capability to analyze particles in various environmental matrices, including saline waters. RPS sensors have diverse applications in environmental monitoring, such as detecting algae, bacteria, heavy metals, and recently, microplastics [20,21,23,62]. These sensors operate by measuring changes in impedance resulting from the movement of small particles through a sensing nano- or micro-scale gate, allowing for particle counting, shape and volume estimates [63], as seen through Fig. 2-6.

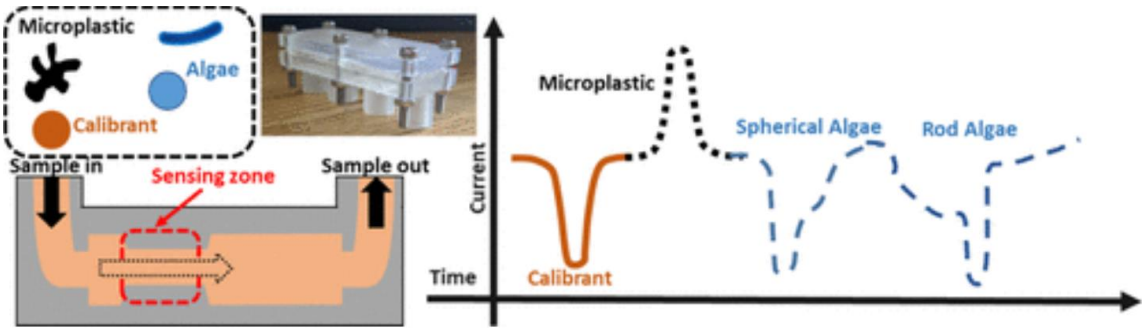

Fig. 2-6: A resistive pulse senor and its working mechanism is illustrated. As the sample passes the sensing zone of the microfluidic sensor a change in the current determines the particle characteristics [63]. Figure reprinted with permissions from American Chemical Society.

One of the pioneering studies employing RPS for microplastic detection was conducted by Ran-Peng et al. [64], where they utilized a microfluidic device with a nanopore to detect polystyrene beads. The study demonstrated the technique's ability to differentiate particles based on size, successfully detecting particles as small as 60 nm when diluted in pure water [64]. This early work highlighted RPS's potential for detecting even the smallest microplastic particles, a significant advantage over many conventional methods. In another significant study, Pollard et al.[34] developed a multi-nanopore RPS system to improve the throughput and sensitivity of microplastic detection. They successfully detected polystyrene (PS) particles ranging from 2 to 30 µm in saline solutions with salt concentration of approximately 18.64 ppm (2.5×10^{-4} KCl) [34]. The device was capable of detecting particles as small as 2 µm in diameter, marking a tenfold increase in sensitivity compared to its previous version, showcasing its capability to detect microplastics in low concentration saline environments. The study also noted that the presence of salt slightly increased the noise level but did not significantly impact the detection accuracy.

Kim et al.[65] addressed the limitations of traditional RPS techniques, such as noise during detection and low throughput due to single sensing apertures. Their microfluidic chip employs multiple detection gates in the main channel, utilizing a hydrodynamic particle focusing method. The channel structure is modulated to ensure uniform particle positioning and minimize noise. A reference gate is included to improve detection accuracy. The working principle is based on Coulter's principle, where the presence of particles alters the resistance in the electrolyte solution (KCl) [65]. The device demonstrates sensitivity in detecting and analyzing 200 nm polystyrene particles. Han et al. [66] enhanced the application of RPS by incorporating a reference electrode to reduce noise. The device features a bridging nanochannel as the sensing gate, with sensing and excitation electrodes placed symmetrically upstream and downstream [66]. The addition of the reference electrode beside the excitation electrode significantly reduces noise, improving the overall accuracy and reliability of the RPS device.

A recent study by Ruiting et al. [67] further optimised the RPS to achieve high-throughput analysis of microparticles. The device incorporates a unique multiplexing strategy where the central electrode is exposed at different locations inside parallel sensing channels. This setup allows for signal multiplexing, enabling the simultaneous processing of signals from multiple channels [67]. The central electrode generates bipolar template waveforms with varying pulse widths which are then decoded using machine learning algorithm. The multiplexing approach demonstrated to increase the throughput significantly making the device suitable for rapid applications. Further, this approach demonstrated high accuracy in particle counting and sizing, with errors of 2.6% and 6.1%, respectively [67]. This advancement addresses the limitations of traditional RPS systems, which often suffer from low throughput and high noise levels.

Despite its advantages, RPS faces several challenges that hinder its reliability in detecting microparticles. These sensors rely on small channels to detect and characterize particles with high sensitivity [23]. The small channels create a narrow sensing zone, enhancing the detection of changes in electrical resistance as particles pass through. The necessity for small channels brings the challenge of channel clogging. As particles move through these narrow apertures, there is a higher likelihood of blockages, particularly in heterogeneous samples with particles of varying sizes [66]. Clogging can interrupt measurements, reduce accuracy, and necessitate frequent maintenance or cleaning of the device. Furthermore, sensitivity to ionic strength variations in the sample causes inconsistent signal responses, requiring careful calibration and electrolyte control [34]. Noise and signal interference from electrical, temperature, and mechanical sources demand advanced and costly signal processing techniques [66]. Also, traditional RPS sensors suffer from low throughput due to single sensing apertures, though recent advancements in multi-nanopore systems aim to improve this by increasing parallel sensing channels [67].

2. 2. 2. 3. 2 Electrophoresis based sensor

Electrophoresis manipulates microplastics based on their surface charge as they come in contact with an induced electric field. The microplastics can be attracted or repelled by the electric field and moved towards or away from electrodes depending on the strength of the electric field. This method can be used to separate microplastics from other particles in the water sample [68]. This approach has been recently used for the extraction of microplastics in DI water sample followed by their detection [22].

A straight microchannel with two microwires fixated perpendicular to it are used to detect microplastic in water using DC current. As a current is applied to the microwires, an electric field is formed. As the electric field comes in contact with the charged particles, electrophoretic force is applied to the particles [22]. This sensor utilises electrophoresis force to accumulate microplastics near the anode, due to the negative charge associated with them, as seen in Fig. 2-7. Microplastics consistently accumulated at the anode, regardless of the direction of the hydrodynamic drag force, although the force direction influenced the concentration of accumulation (Fig. 2-7 b-c). The accumulation of the microplastics resulted in the drop of the normalised resistance being measured between the two microwires, as seen in Fig. 2-7d.

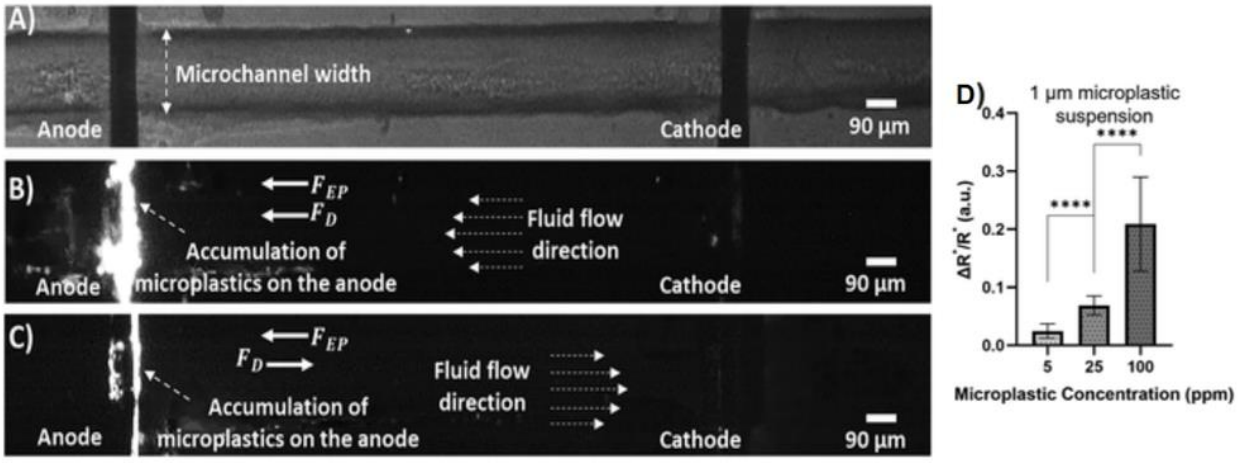

Fig. 2-7: Visualization of microplastic accumulation in the sensor's detection zone; **a)** no microplastics present in the solution; **b)** microplastics accumulation at the anode when the drag force (F_D) and electrophoretic force (F_{EF}) are aligned in the same direction; **c)** microplastics accumulation at the anode with drag force and electrophoretic force in the opposite direction; **d)** the corresponding normalized decrease in resistance as microplastic accumulation increases at the anode [22]. Figure reprinted with permission from new journal of chemistry.

Transforming the DC-based detection method into a portable sensor for on-site microplastic identification offers several key advantages over traditional methods. Its simplicity, low power requirements, and potential for real-time analysis make it particularly well-suited for field applications. Unlike other approaches, this method can be adapted for direct detection in varying environmental conditions. However, to fully realize its potential as a portable sensor, several challenges must be addressed, including the need to assess and improve its detectability across different salt concentrations in conductive water. Additionally, further research is required to optimize the sensor's sensitivity to microplastics. One promising approach to enhance this sensitivity is through nanomaterial (e.g., MXene) functionalization of electrodes as pursued in this thesis, which can potentially improve the sensor's ability to capture microplastics at lower concentrations and in challenging environmental conditions.

2.3 MXene-based Microplastic Capturing

MXene with its unique 2D design has shown remarkable characteristics when it comes to water purification. These materials are derived from MAX phases, characterized by a layered structure consisting of alternating layers of transition metals (M), aluminum or silicon (A), and carbon or nitrogen (X). MXenes have shown an excellent efficiency in eliminating various contaminants for aquatic environments such as metals, per- and poly-fluoroalkyl substances (PFAS), and microplastics [69,70]. Their high conductivity and multifunctional properties result in an increased surface area, and further facilitating strong physical and electrostatic interactions that improve microplastic adsorption [69]. Additionally, the adaptable nature of MXenes in various water treatment applications underscores their potential in enhancing purification techniques.

Recently, MXene has gained attention as an effective material for microplastic removal from water, owing to its outstanding structural and chemical properties. For example, a recent study by Urso et al. [70] used MXene-based oxide microrobots to demonstrate high efficiency in microplastic removal due to their extensive surface area and active sites, facilitating both adsorption and nano plastic detection [70]. This highlights the crucial role of nanomaterials like MXenes and their nano-scale interactions in capturing microplastics. Additionally, MXenes show promise as membranes for treating microplastic-contaminated water [71]. Ti3C2Tx (MXene) membranes can effectively remove and separate microplastics from water as observed in Fig. 2-8. Moreover, Ti3C2Tx composite electrode membranes have been explored for their potential to reduce microplastic fouling [72]. The metallic conductivity of MXenes is primarily due to the presence of transition metal layers, which facilitate efficient electron transport. For instance, Ti3C2Tx, one of the most extensively studied MXenes, exhibits metallic behavior attributed to its conductive titanium layers, which also enhances its performance in environmental remediation processes, including visible light-driven hydrogen evolution and microplastic degradation [72,73].

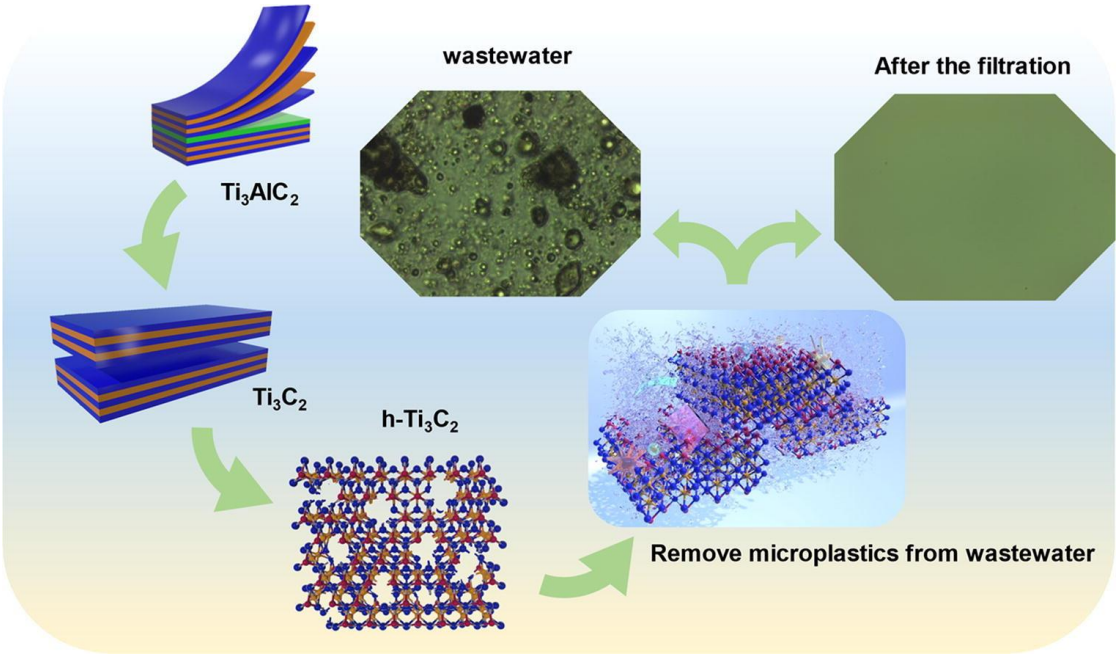

Fig. 2-8: The process of microplastic removal from wastewater using Ti_3C_2 (MXene) materials [74]. Figure reprinted with permission from Elsevier.

Despite their promising properties, MXenes face challenges such as stability in oxidative environments. Enhancing their durability without compromising conductivity remains a focus of ongoing research [69]. Additionally, developing scalable and cost-effective synthesis methods is crucial for their widespread application, and exploring new functionalization strategies to tailor MXenes' properties for specific uses is an area of active investigation [69]. In this thesis, MXene has been utilized to coat the anode of microwires within a microfluidic sensor, leveraging its strong affinity for microplastics to explore enhancing their accumulation and, consequently, improving the sensor's electrical resistance signal.

Chapter 3: Materials and Methods

In this chapter, we will discuss the experimental and numerical methodologies used in the development and optimization of the DC electro microfluidics sensor. This includes detailing the procedures involved in the sensor's development and the principles underlying its operation for the detection of microplastics in saline freshwater.

3.1 Microfluidic Sensor Overview: Theory and Initial Fabrication

This section will elaborate on the fabrication process of the microfluidic sensor. Additionally, the underlying theory and equivalent circuit of the sensor will be discussed.

3.1.1 Sensor's Woking Principle

Research has established that microplastics in marine environments typically possess a surface charge. The specific charge of microplastics, positive or negative, depends on factors like the type of plastic and its exposure to environmental conditions, e.g., the pH level, ionic strength of the fluidic matrix, exposure to sunlight, and weathering processes. Additionally, biofouling and the absorption of environmental pollutants profoundly alter microplastics' surface chemistry. These elements collectively dictate microplastics' electrical charge, consequently affecting their movement and interactions within marine ecosystems. Utilizing electrophoretic force, which is contingent upon the surface charge, has shown promise in the separation, extraction, and detection of microplastics in deionized water [35,75]. Nonetheless, the role of the conductivity of the aqueous

medium hosting the microplastics remains an underexplored area particularly in the PoN sensors domain, suggesting a gap in our comprehensive understanding of these interactions.

The process of electrophoretic accumulation is governed by the movement of charged microplastics towards oppositely charged electrodes, driven by an applied electric field. The efficiency of this technique for microplastic detection in environments with high electrolyte conductivity, such as saline water, remains a subject of investigation [76]. Our study aims to examine the influence of increased electrolyte conductivity on the strength of the electrophoretic force applied to microplastics and to investigate how this variable influences the electrophoretic accumulation and detection of microplastics in microfluidic devices.

According to Ohm's law (eq. 3-1), an increase in the conductivity of the carrier solution reduces the electrical resistance (R) between two electrodes, resulting in a decrease in voltage (V) for a constant current (I).

$$V = I \times R \tag{3-1}$$

The change in the voltage directly influences the strength of the resulting electric field, as described by the electric field-potential relationship:

$$E = -\frac{dV}{dx} \tag{3-2}$$

where, E represents the electric field strength, and dV/dx denotes the voltage gradient in the x direction, which refers to the linear distance between the two points of measurement along a single axis. Assuming the distance between two parallel electrodes in a channel (e.g., two inserted microwires in a microchannel as shown in Fig. 2-7) remains constant, electric field strength (E) decreases as V decreases due to the increased conductivity of the solution when the current between electrodes is kept constant. This reduction in E causes a decrease in the electrophoretic force (F_{EP}) exerted on the microplastics as described by eq. 3-3.

$$F_{EP} = 6\pi\epsilon\delta aE \tag{3-3}$$

In equation 3-3 particle's radius is a, dielectric constant of the medium is ϵ, and zeta potential of the particle is δ. The dielectric constant of DI water is approximately 78.5 at room temperature (25°C). As salt is dissolved in water, increasing its salinity, ϵ decreases to as low as 20, depending on the specific salt concentration present in the solution. Furthermore, previous studies have shown that as the concentration of salt in a solution increases, there is a corresponding decrease in the zeta potential of microplastics (δ). This reduction is attributed to the compressed electric double layer (EDL) around the particles. Therefore, while the particle properties such as radius (a) in eq. 3-3 remain constant, ϵ, δ and E all decrease due to the higher conductivity associated with saline water. This reduction diminishes the magnitude of the electrophoretic force (F_{EP}) applied on microplastics.

We can further explore the impact of salt concentration on the electrophoretic accumulation of microplastics by examining the interactions between ions and particles, ions and electrodes, and

the formation of the EDL around the charged microplastics and electrodes. The dissociation of NaCl in water into sodium (Na^+) and chloride (Cl^-) ions increases the solution's ionic strength and leads to the formation of an EDL around the electrodes and the charged microplastics (Fig. 3-1a). The EDL consists of the Stern layer, where ions are tightly adsorbed directly onto the charged surface, forming a dense layer, and the diffusion layer, where ions are more loosely arranged and decrease in concentration with distance from the surface (Fig. 3-1(b-c)). The thickness of the diffusion layer, known as Debye length, signifies the range within which the electric potential away from the surface of a charged particle diminishes to an insignificant level. As a result, a longer Debye length is linked to a solution with lower salinity, as illustrated in Fig. 3-1b. Consequently, a shorter Debye length correlates with densely clustered ions in the Stern layer and a shorter diffusive layer (Fig. 3-1c).

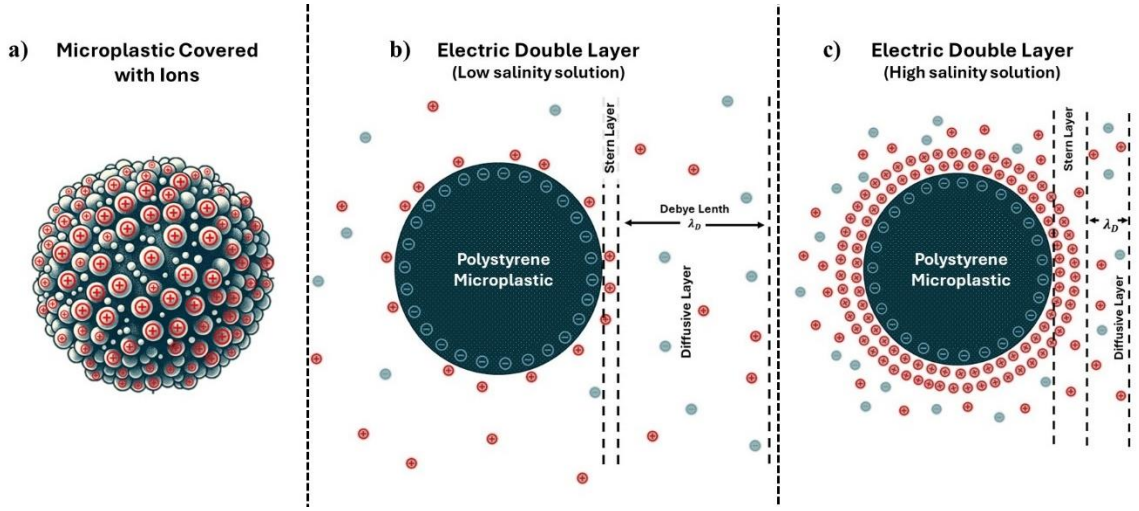

Fig. 3-1: a) The Electric Double Layer (EDL) around charged microplastics in **b)** low and **c)** high salinity waters.

The thickness of the diffusion layer can be modeled by the Debye length equation:

$$\lambda_D = \sqrt{\frac{\epsilon\epsilon_0 kT}{2N_A e^2 J}} \tag{3-4}$$

where, ϵ *is* the dielectric constant of the medium, ϵ_0 is the vacuum permittivity, k is the Boltzmann constant, T is the temperature in Kelvin, N_A is Avogadro's number, e is the elementary charge, and J is the ionic strength of the solution which can be calculated as:

$$J = \frac{1}{2}\sum_{i=1}^{n} c_i z_i^2 \tag{3-5}$$

where, c_i represents the molar concentration of the ions, z_i is the charge number for the ions and n is the number of different ions. According to eq. 3-5, higher conductivity implies higher c_i (concentration of ions) which in turn suggests a higher ionic strength J.

In salty water, the combination of higher ionic strength (J) and a lower dielectric constant (ϵ) result in a shorter Debye length (eq. 3-4). This implies that the electric potential associated with the charged particles diminishes over a shorter distance compared to DI water.

The high concentration of ions in the solution also leads to a screening effect[77,78]. As the concentration of ions increases, there are more ions in the vicinity of the charged particle, and they can partially screen the charge on the particle, reducing the effective zeta potential (Fig. 3-1c).

3.1.2 Experimental Setup

The experimental setup, depicted in Fig. 3-2, comprised the following components: a microfluidic sensor, a Keithley Instruments Model 2410 DC source-meter, a Legato 110 syringe pump from KD Scientific, a Leica DMIL LED inverted fluorescence microscope, and a computer equipped with KickStart software for controlling the source-meter and recording its electrical signals.

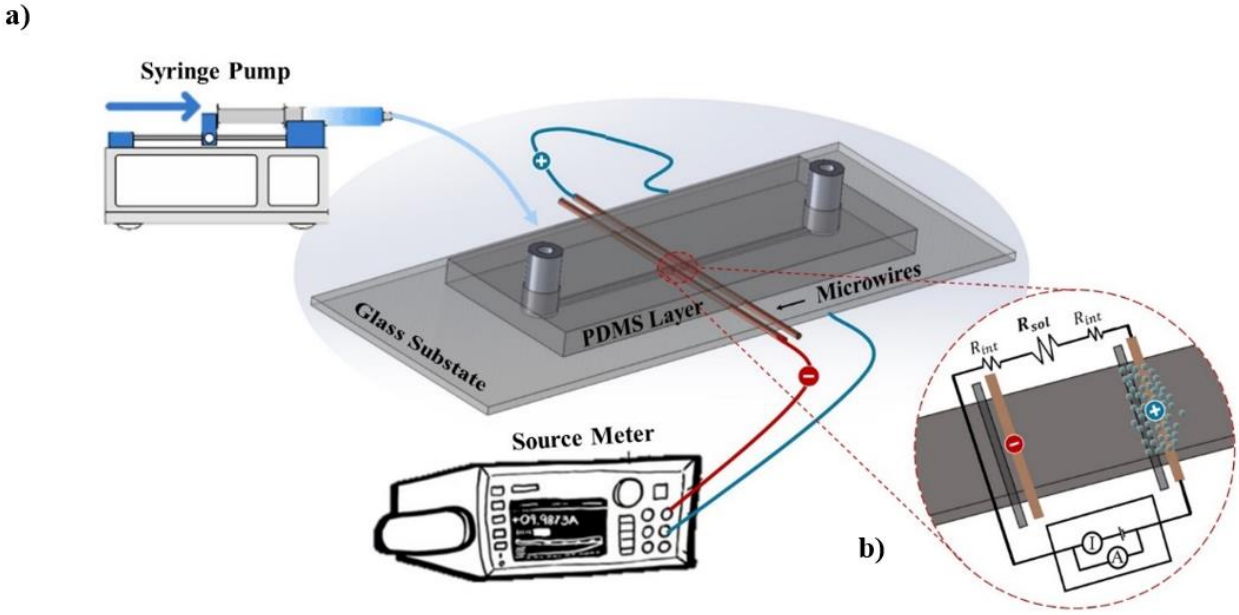

Fig. 3-2: The schematic of the experimental setup; **a)** including the microfluidic sensor, a source meter, and a syringe pump. The microfluidic sensor was made of a single layer PDMS containing two copper wires and the network of microchannels, plasma bonded to a glass substrate; **b)** the electrophoretic accumulation of microplastics at the anode as an electric field is formed between the microwires.

3.1.3 Microfluidic Sensor Fabrication

The fabrication process of the microfluidic sensor involved replicating a layer of PDMS, which encompassed the microchannel network, onto plastic master molds created through 3D printing (Objet260-Connex, Stratasys, USA). The PDMS base and curing agent were combined in a 10:1 ratio (Fig. 3-3a (i)), degassed in a vacuum chamber for 10 minutes (Fig. 3-3a (ii)), and then poured over the 3D-printed mold (Fig. 3-3a (iii)). The inlet and outlet tubes were positioned at opposite ends of the main microchannel on the master mold. The PDMS mixture, free of air bubbles, was cast over the 3D-printed molds and subsequently cured in an oven at 75°C for a duration of 2 hours (Fig. 3-3a (iv)). Following the curing process, the PDMS layer was carefully peeled off from the molds, and copper microwires were inserted into the designated channels on the PDMS layer, ensuring they were oriented perpendicular to the main microchannel (Fig. 3-3a (v)). To finalize the assembly, the PDMS layer containing the inlet and outlet tubes along with the embedded microwires was securely bonded to a glass substrate using plasma bonding (30 seconds at 900 mTorr) (Fig. 3-3a (vi)). The final output sensor is depicted in Fig. 3-3b.

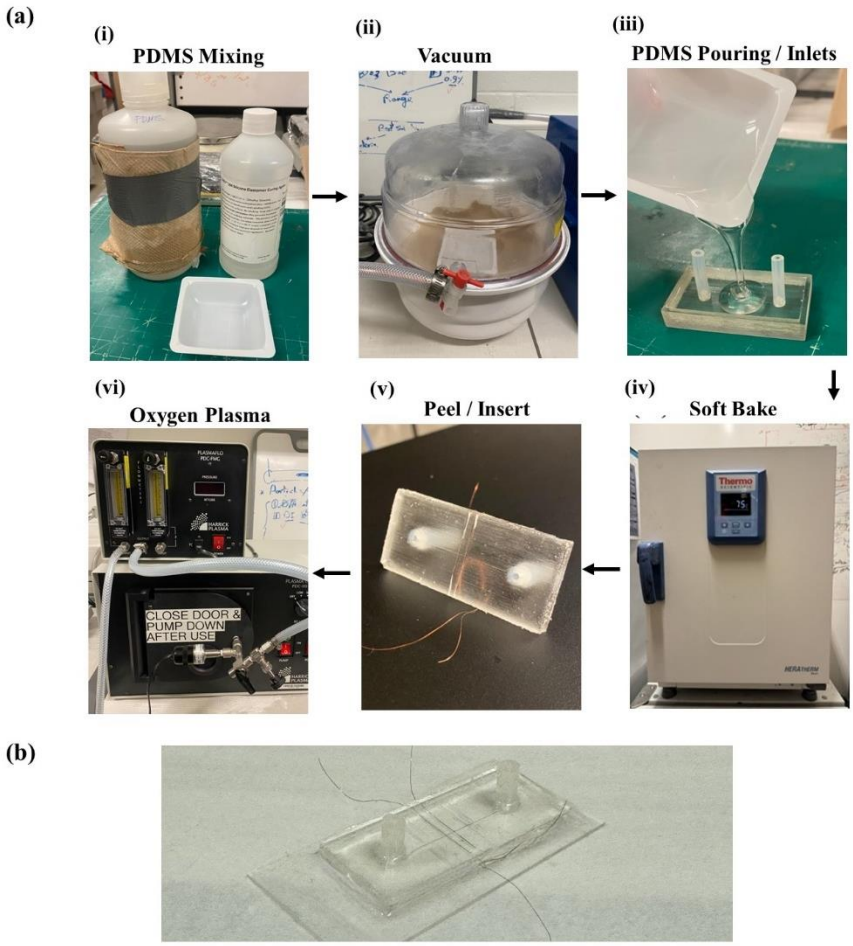

Fig. 3-3: The fabrication process for the microfluidic sensor**; a)** The complete fabrication process from i) PDMS mixing, ii) vacuuming the PDMS to eliminate bubbles, iii) PDMS pouring into master mold, iv) soft baking to cure the mold, v) peeling off the cured PDMS layer and inserting the microwires, vi) oxygen plasma treatment and bonding the PDMS layer onto the glass substrate; **b)** Fabricated microfluidic sensor

The microfluidic chip depicted in Fig. 3-3b comprises a primary microchannel responsible for conveying the fluid sample (32 mm length, 200 µm width, and 150 µm height). It also includes inlet and outlet tubes, a glass substrate, and two 90 µm-diameter copper wires positioned within

designated microchannels, oriented perpendicular to the fluid-conveying channel with 2 mm interwire gap. The height of the designated channels for microwires was designed to be 120 µm, ensuring that the microwires were positioned at the center of the fluidic microchannel, with 30 µm clearance above and below the wire. These dimensions for the sensor were kept the same as the sensor fabricated by Zabihihesari et al. [35], which was previously used to detect microplastics in DI water using a similar working principle. The parameters were initially kept the same to leverage an already established design that has proven effective in similar application, further ensuring consistency in sensor performance while extending its application to saline water conditions.

3.1.4 Sample Preparation

Polystyrene microplastics (1µm) were purchased from Spherotech Inc. were originally suspended in a carrier buffer consisting of DI water, 0.02% sodium azide, and other ingredients with unknown concentrations, rendering it electrically conductive. Hence it was crucial to remove the carrier buffer to avoid unknown interference with the detection process. Furthermore, to avoid the interference of salt with the centrifugal separation process, initial dilution in salty water was bypassed. Instead, we opted to dilute them in DI water, then centrifuged the mixture to eliminate the supernatant and the carrier buffer, following which saline water was introduced. This approach safeguarded the effectiveness of the separation and the reliability of the detection.

To achieve varying concentrations of microplastics as intended (Fig. 3-4a), we first removed the original carrier buffer by centrifuging the suspensions at 4200 rpm for 10 minutes. This process caused the microplastics to settle at the bottom of 10 ml centrifuge tubes. We then replaced 90%

of the supernatant with DI water, repeating this step three times (Fig. 3-4b), to ensure the effective removal of the carrier buffer and prepare the samples for accurate concentration adjustments. Various concentrations of NaCl (300, 650, 1000 ppm) were prepared in DI water to produce electrolytes with distinct levels of conductivity, all within the range of freshwater conductivity. To ensure that the tested NaCl concentrations fall within the range of freshwater conductivity, the conductivity of the samples was measured using a Cond 3310 conductivity meter (WTW, Xylem, Weilheim, Germany).

To create a uniform microplastic suspension in salty water, DI water was replaced by NaCl solution with a known conductivity (Fig. 3-4c). The blank NaCl solution, with the same concentration of salt and conductivity level was used as the control. The dilutions of microplastics and salt were ensured to be homogenous in the solution by using a vortex mixer (3200 rpm) followed by a 2 min ultrasonication (Fig. 3-4d). The resultant microplastic suspension and the blank salty water were tested to distinguish the effects of NaCl and microplastic concentrations on microplastic accumulation and electrical resistance drop in the sensor.

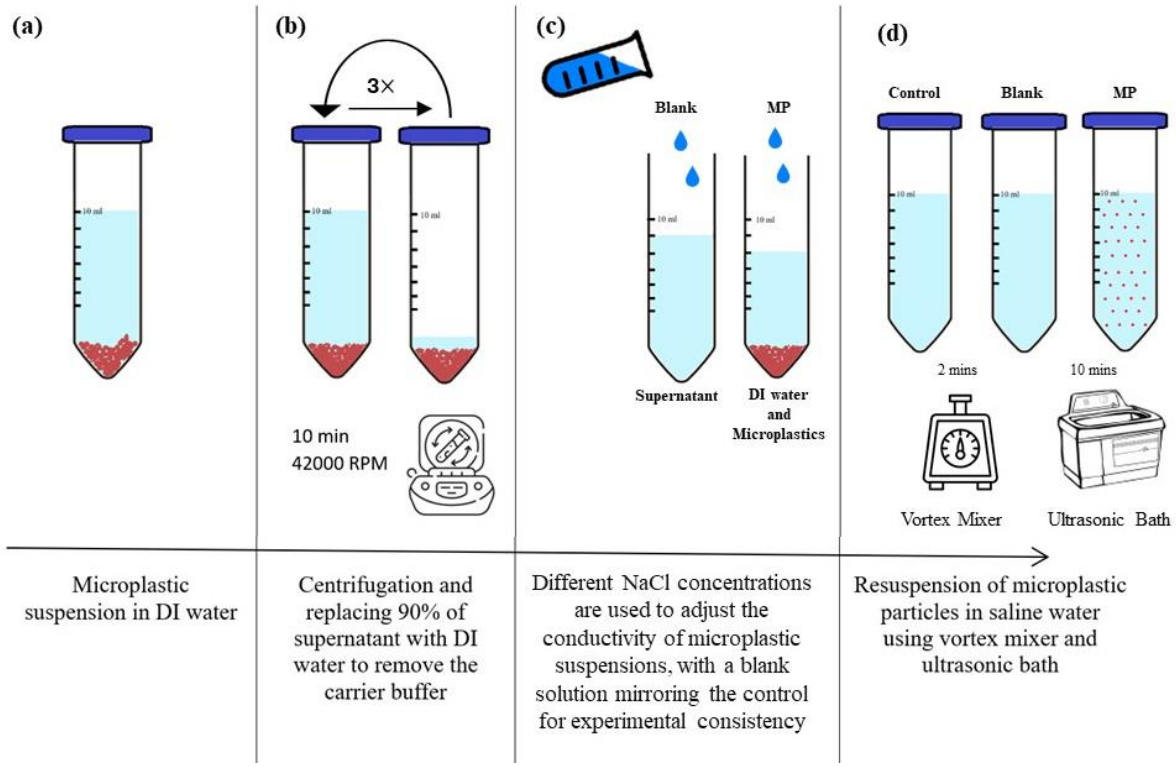

Fig. 3-4: Microplastic and blank sample preparation prior to testing in the microfluidic sensor.

3.1.4 Experimental Procedure

The terminal and ground microbridge wires of the microfluidic device were connected to the DC source-meter as depicted in Fig. 3-2. The source-meter was used to apply a current across the microwires and measure the resultant voltage. Operating on the electrophoresis principle (eq. 3-3), an electric current was applied through the microwires which induced an electric field in the interwire gap of the microfluidic chip. This induced electric field (eq. 3-2) exerted an electrophoretic force on charged microplastics flowing into the microchannel. Negatively charged microplastics tended to accumulate around the positive electrode (anode). The flow rate for introducing the sample through the sensor was configured to be 0.2 ml/min.

In the first set of experiments in Chapter 3, to keep consistent methodology with our prior work on detecting microplastics in DI water [35], sweep current was employed, incrementing from 10 nA to 1 μA in 10 nA steps, with a time interval of 0.5 s between each step. Then, as an alternative method to simplify the operation of the device, a constant current approach was developed and tested which will be discussed in Chapter 4. After each current application and voltage measurement, the electrical resistance was determined by dividing the voltage by the current, and the resulting values were plotted over time. Initially, the control solution was introduced into the sensor, undergoing a duration of 10 minutes comprising ten sweeps, each lasting 60 seconds. Then, the blank solution, possessing the same NaCl concentration and no microplastics, was subjected to an identical procedure in the same sensor. Finally, the solution with microplastics was introduced into the sensor, an electrical current was applied for 10 minutes, and the resultant aggregation of microplastics near the cathode and anode was visually captured through microscopic imaging, using a fluorescent microscope (Leica DM IL LED; Leica Microsystems).

3.1.5 Data Analysis

In each 60-second sweep current run of the experiment, a total of 100 voltage readings were collected. These readings, along with the applied current, were then utilized to calculate the electrical resistance at each step. It was observed that the resistance measurements displayed a high level of instability during the initial 30 seconds of each run, exhibiting a more transient response. Consequently, the latter half of the data set, specifically the final 50 readings (equivalent to the last 30 seconds of each sweep), was used to compute the average resistance for each 60-

second interval, as illustrated in Fig. 3-5. This approach ensured a stable and reliable resistance measurement for analysis.

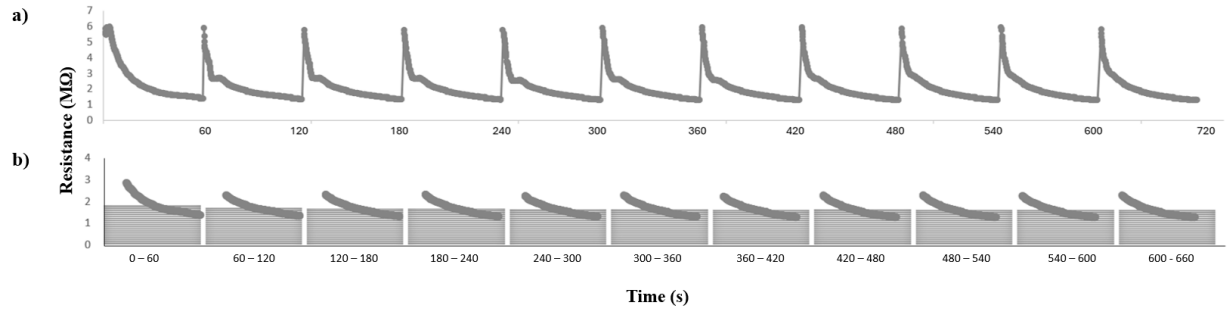

Fig. 3-5: Electrical resistance response for 25ppm microplastic suspension within 300 ppm NaCl solution**.** **a)** Electrical resistance response as 60-secound sweep current is applied; **b)** Average electrical resistance, calculated using the final 50 data points from each sweep.

The average electrical resistances of both the blank (R_{Blank}) and the microplastic solutions (R_{MP}) were normalized against the average electrical resistance of the control solution ($R_{Control}$) resulting in R^*_{Blank} and R^*_{MP} for the blank and the microplastic solutions, respectively. Subsequently, the absolute normalized resistance reduction due to the accumulation of microplastics around the anode was computed as indicated in eq. 3-6.

$$\frac{\Delta R}{R} = \left| \frac{R^*_{MP} - R^*_{Blank}}{R^*_{Blank}} \right| \tag{3-6}$$

In this study, significance determinations were made using the Mann-Whitney U test, a non-parametric statistical approach that does not assume a normal distribution of the data. The

calculated p-value from this test quantifies the probability that the observed differences between groups could occur by chance under the null hypothesis of no difference. A p-value below the conventional threshold of 0.05 was considered indicative of statistically significant differences. Specifically, p-values were denoted to demonstrate a certain significance level as follows; * $p < 0.05$, ** $p < 0.01$, *** $p < 0.001$, implying that the observed disparity is likely due to microplastics rather than uncertainty.

3.2 Microfluidic Sensor Simplification and Improvement

This section will discuss the simplification and improvement steps applied for the microfluidic sensor as proposed in objective 2 of the thesis. Additionally, the underlying revised circuit of the sensor will be discussed. The results will be presented in Chapter 5.

3.2.1 Simplification of experimental procedure

3.2.1.1 Sample Preparation

To stay consistent with the published method of microplastic detection in DI water [35], at the initial stages of investigation in Chapter …, we prepared three types of water samples, i.e., blank, base, and microplastics solutions. However, in studies reported in Chapter …, we streamlined the process by using only two samples: blank and microplastics. Initially, we aimed to eliminate the supernatant solution in which the microplastics were suspended to avoid any interference from the 0.02% sodium azide carrier buffer. However, since our focus in this thesis shifted to detecting

microplastics in saline water, the presence of the sodium azide carrier buffer did not significantly affect the conductivity of the solution. As seen in Fig. 3-6, the conductivity levels remain consistent across different saline concentrations, regardless of the addition of the buffer.

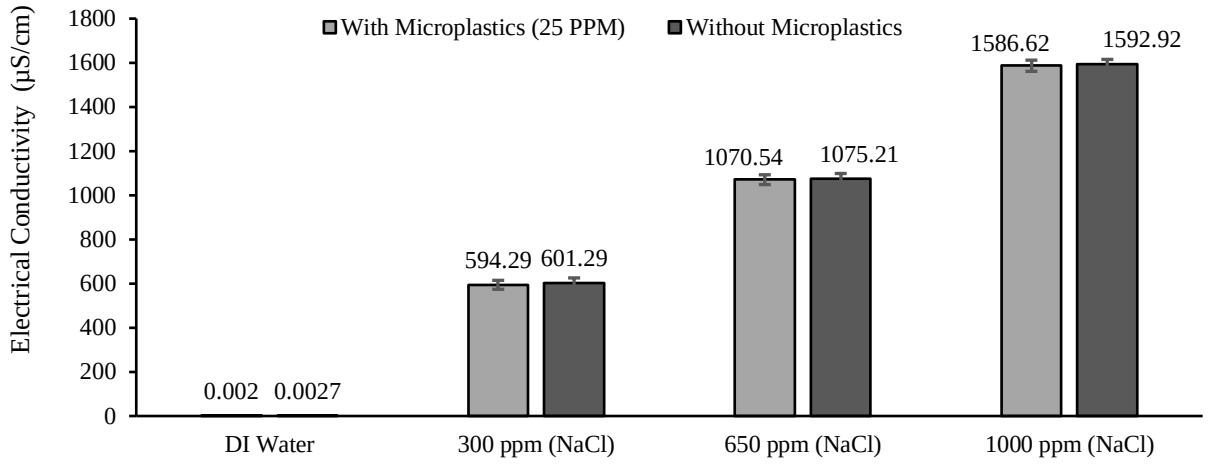

Fig. 3-6: Comparison of electrical conductivity across various NaCl concentrations for two solutions: one containing 1µm Polystyrene microplastics (25 ppm) with a buffer solution (Sodium azide (0.02%)) and the other without microplastics or buffer, at the same salinity levels.

To prepare the samples, we first created a concentrated NaCl solution by dissolving NaCl in deionized (DI) water to achieve a concentration of 10,000 ppm. This stock solution was then used to prepare the required saline solutions by mixing it with pure DI water. Specifically, we diluted the 10,000 ppm NaCl solution to achieve the desired concentrations of 300 ppm, 650 ppm, and 1000 ppm by calculating the appropriate volumes needed for each target concentration. This method proved to be more efficient than weighing the salt and preparing each NaCl concentration individually.

The microplastics samples were prepared by suspending the microplastics directly into the prepared saline solutions. The blank samples were prepared using the same NaCl solutions without microplastics. This approach ensured consistent conductivity levels across all samples, allowing for accurate assessment of the sensor's performance in detecting microplastics in saline environments. By maintaining consistent sample preparation techniques and materials, we ensured reliable comparisons between the blank and microplastics solutions, focusing on the sensor's detection capabilities.

3.2.1.2 Constant Current Operation

In previous experiments conducted, a sweep current method was employed, incrementing from 10 nA to 1 μA in 10 nA steps, to induce an electric field between the microwires. However, a transition from using a sweep current to applying a constant current of 1 μA was made to enhance the sensor's efficacy. This shift aimed to stabilize and strengthen the electric field between the microwires, thereby amplifying the electrophoretic force that accumulates microplastics around the anode. By implementing a constant current, we aimed to reduce the variability and improve the consistency of microplastic detection, ensuring more reliable sensor performance across different salinity levels. Notably the materials used, and the sensor fabrication process were kept constant, with the only changes being the applied current and moving to a simpler sample preparation technique, ensuring that the observed improvements in sensor performance were solely attributable to the transition to a constant current.

The experimental setup remained the same as discussed for sweep current. It included the microfluidic chip, a syringe pump (Series 210P; KDS Legato™ KD Scientific) for flow rate control, and a source meter (Model 2410; Keithley, USA) to apply a constant current and measure voltage. Initially, the blank solution was introduced into the sensor, followed by the solution containing the microplastic suspension. The flow rate for the samples through the sensor was set to 0.2 ml/min. A constant current of 1 μA was applied to the microwires using the source-meter to induce an electric field in the interwire gap. The negatively charged microplastics accumulated around the positive electrode (anode) under the influence of the electrophoretic force. The source meter was used to measure the electrical voltage across the copper microwires. The electrical resistance was determined by dividing the voltage by the current and plotted over 10 minutes time. Initially, there was some deviation in the output voltage readings due to sensor drift or the time required for the voltage to stabilize. To address this, we implemented a moving point average technique to smooth the data and identify the stabilization point. We calculated the moving point average for different time intervals (3, 6, 12, 24, 48, and 96 seconds) and plotted these averages on the same graph (Fig. 3-7). The point at which all moving averages converged was identified as the plateau point, indicating that the sensor's output had stabilized.

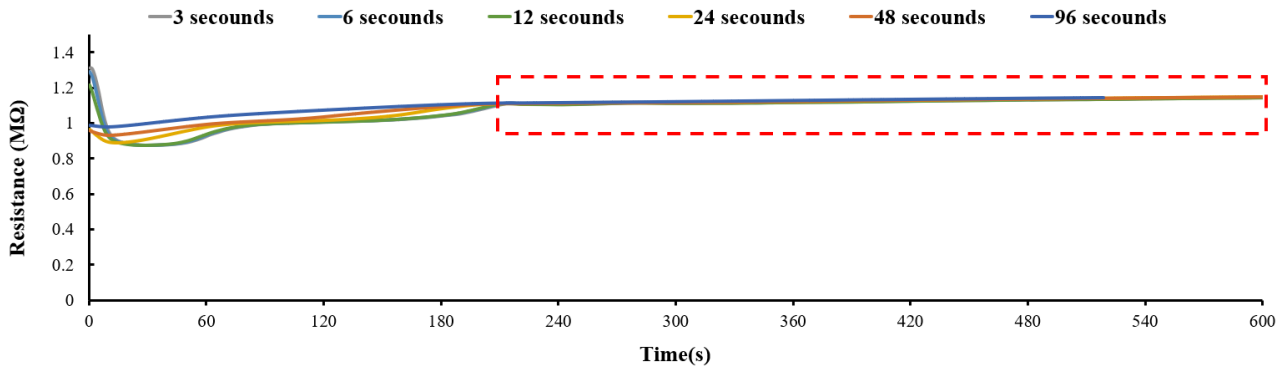

Fig. 3-7: Moving average of the resistance over time for 1µm polystyrene microplastics concentration of 25 ppm in a 300 ppm NaCl concentration solution, obtained to identify the plateau region in the measurement. The red dotted square highlights the area where the resistance stabilizes, indicating the plateau.

After identifying the plateau point, we calculated the average of the voltage readings from this point onward to represent the stable output of the sensor. This average resistance value was used for subsequent comparisons between the blank (R_{Blank}) and microplastic (R_{MP}) solutions. The difference in electrical resistance between these two solutions provided a direct measure of the sensor's response to the presence of microplastics. The reduction in electrical resistance due to the accumulation of microplastics around the anode was normalized using the following formula:

$$\Delta R = \frac{R_{Blank} - R_{MP}}{R_{Blank}} \tag{3-7}$$

This calculation highlighted the change in resistance attributable to the presence of microplastics, providing a quantitative measure of the sensor's performance. Significance determinations were

made using the Mann-Whitney U test, a non-parametric statistical approach that does not assume a normal distribution of the data. This was already discussed above in section 3.1.5.

3.2.2 Electrical Measurement Improvements

3.2.2.1 Implementing Wheatstone Bridge

A Wheatstone bridge was added to improve the accuracy and stability of the sensor measurements by compensating for variations and noise in the sensor output. It enhances sensor performance by amplifying small resistance changes, such as those caused by microplastic accumulation, while minimizing noise and external variations. This results in improved precision and stability, making the sensor more reliable for detecting microplastics under varying conditions.

Previously, a Keithley Instruments Model 2410 DC source-meter was used in the experimental setup to apply a current to the sensor and measure the changes in voltage. In the updated setup, a KORAD KD3005D digital-control DC power supply was used to apply a constant voltage across point A and C of the Wheatstone bridge, while the resulting voltage difference was measured across points B and D using the source-meter (Fig. 3-8). The Wheatstone bridge circuit is constructed using high-precision resistors (0.1% tolerance), enhanced the sensitivity of the measurements by providing a differential output that was less susceptible to noise and fluctuations. The Wheatstone bridge consisted of four resistors arranged in a diamond configuration: two fixed resistors (R_1 and R_3), one variable resistor (R_2), and the sensing resistor (R_S of the microfluidic device) whose resistance changes due to microplastic accumulation.

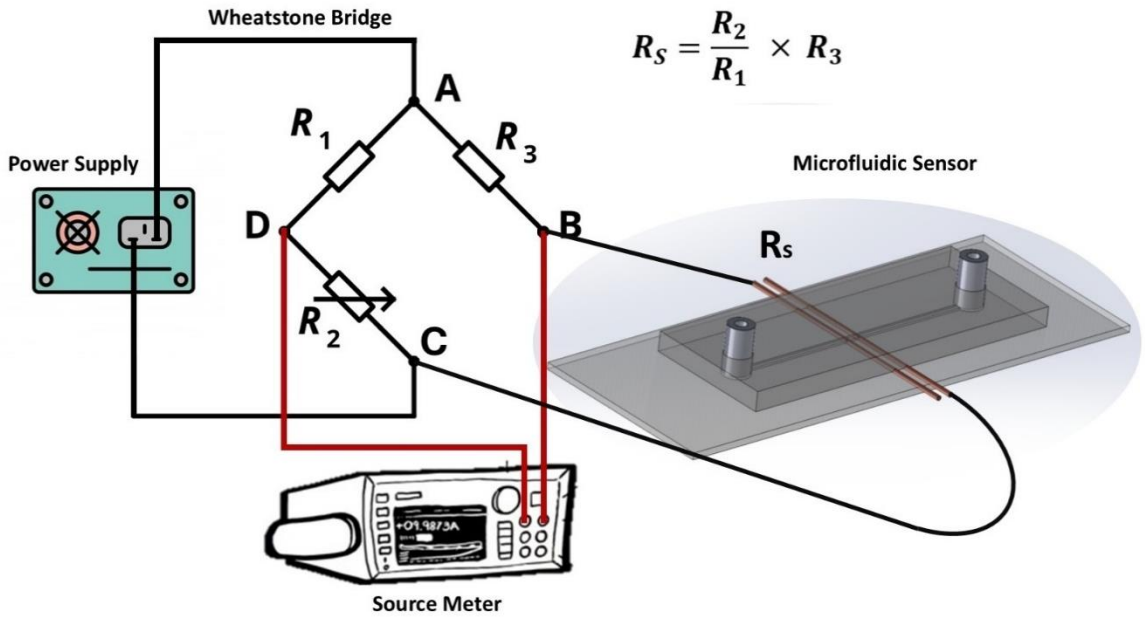

Fig. 3-8: Implementation of the Wheatstone bridge for microplastic detection; The bridge comprises four resistors: two fixed resistors (R_1 and R_3, a variable resistor R_2, and the sensing resistor (R_S) integrated as the microfluidic sensor

The Wheatstone bridge is balanced when the ratio of the resistances in one branch is equal to the ratio in the other branch. Mathematically, this balance is represented as:

$$R_s = \frac{R_2}{R_1} \times R_3 \tag{3-8}$$

A constant DC power supply is connected across the bridge (A → C) to provide a stable input voltage (V_{in}). When the bridge is balanced, the voltage difference between the midpoints (D → B) of the bridge (V_{out}) is zero, indicating that the resistances in the circuit are equal. This balanced condition allows for the detection of any changes in resistance due to microplastic accumulation.

The updated setup, illustrated in Fig. 3-9, included the original components—a microfluidic sensor, a Keithley Instruments Model 2410 DC source-meter, a Legato 110 syringe pump from KD Scientific, a Leica DMIL LED inverted fluorescence microscope, and a computer with KickStart software—along with the newly added Wheatstone bridge and a KORAD KD3005D digital-control DC power supply.

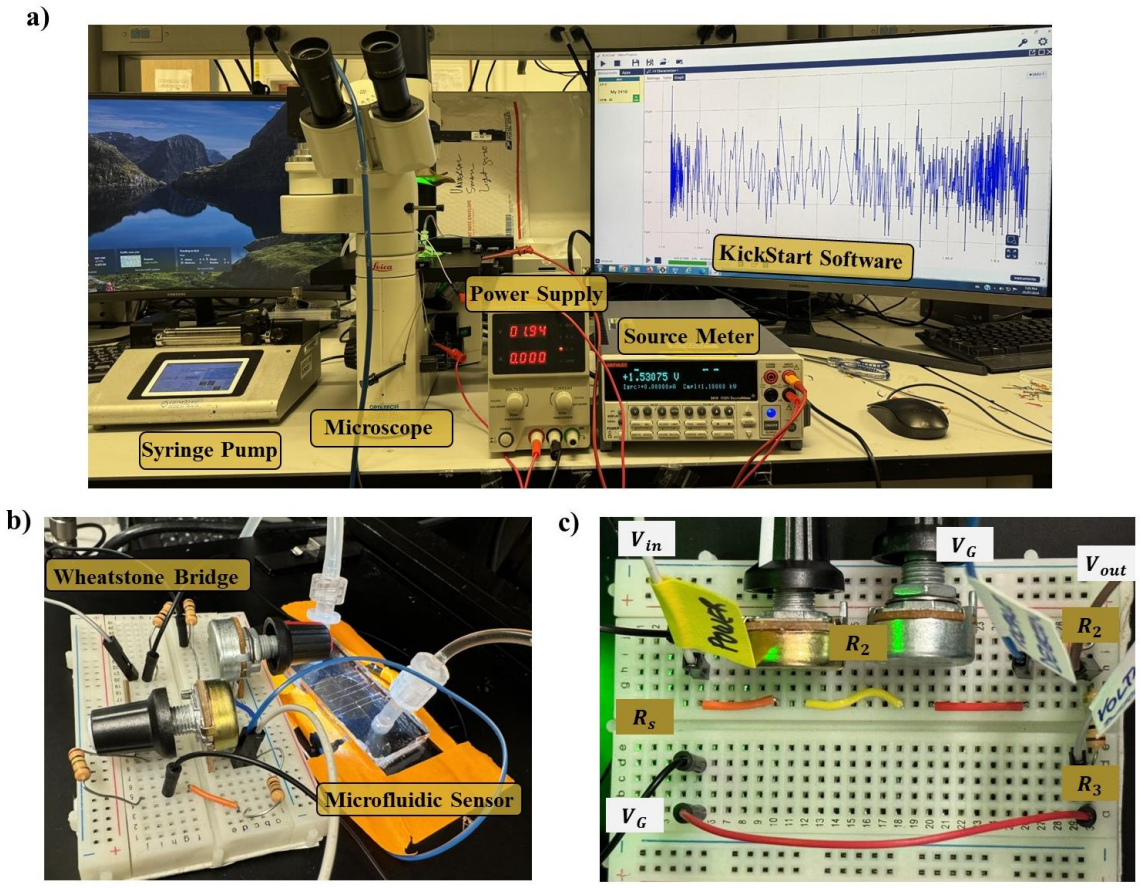

Fig. 3-9: Experimental setup for the Wheatstone bridge configuration; **a)** the overall setup includes a syringe pump for sample delivery, a microscope, a power supply for providing constant DC voltage, a

source meter for voltage measurements, and KickStart software for data visualization and analysis; **b)** closer view of the microfluidic sensor connected to a Wheatstone bridge circuit.

Despite the addition of the Wheatstone bridge, the sensor fabrication procedure, as well as its dimensions and specifications, remained unchanged. The microfluidic chip still featured a primary microchannel (32 mm length, 200 μm width, and 150 μm height), inlet and outlet tubes, a glass substrate, and two 90 μm-diameter copper wires positioned within designated microchannels. The careful design and consistent fabrication process ensured that the sensor's performance characteristics were maintained, while the updated setup with the Wheatstone bridge provided an improved platform for accurate and reliable measurements.

Initially, when using constant current without Wheatstone bridge, two samples were prepared: one containing microplastics and one blank. This setup allowed for comparison of the change in resistance between the blank and the microplastic sample. However, with the implementation of the Wheatstone bridge, the circuit can now be quickly balanced when the MP suspension is injected into the sensor, eliminating the need for a blank solution. In this process, the microplastic suspension is injected into the sensor, and the variable resistance R_2 is adjusted to balance the circuit resulting in $V_{out} = 0$. Any change in the output voltage after balancing are solely due to the accumulation of microplastics. The relationship between V_{out} and the resistance in the bridge is expressed as:

$$V_{out} = \left(\frac{R_2}{R_1+R_2} - \frac{R_S}{R_3+R_S}\right) V_{in} \tag{3-9}$$

Where, V_{in} represents the input voltage from the DC power supply, R_1 , R_2 , R_3 are known resistances and R_S is the resistance affected by the microplastic accumulation.

For data analysis, the output voltage was measured over a 10-minute run for the microplastic suspension (Fig. 3-10a). The experiment was repeated on three different sensors, and the changes in voltage were graphed (Fig. 3-10b). The sensor response was then average at each measured interval (0.5 seconds), and a 10-point moving average was computed (Fig.3-10c). Additionally, the change in voltage was measured over 60-second intervals for the complete 10-minute run (Fig.3-10d). The average resistance for each 60-second interval was calculated, capturing the change in resistance due to microplastic accumulation over time. These average resistances were then compared for different NaCl concentrations (300 ppm, 650 ppm, 1000 ppm) and microplastic concentrations (1 ppm, 5 ppm, 25 ppm). The recorded V_{out} values were analyzed to determine the extent of resistance change in R_S. As microplastics accumulated, R_S increased, resulting in measurable changes in V_{out}, which were used to quantify both the concentration and rate of microplastic accumulation in the microfluidic channel.

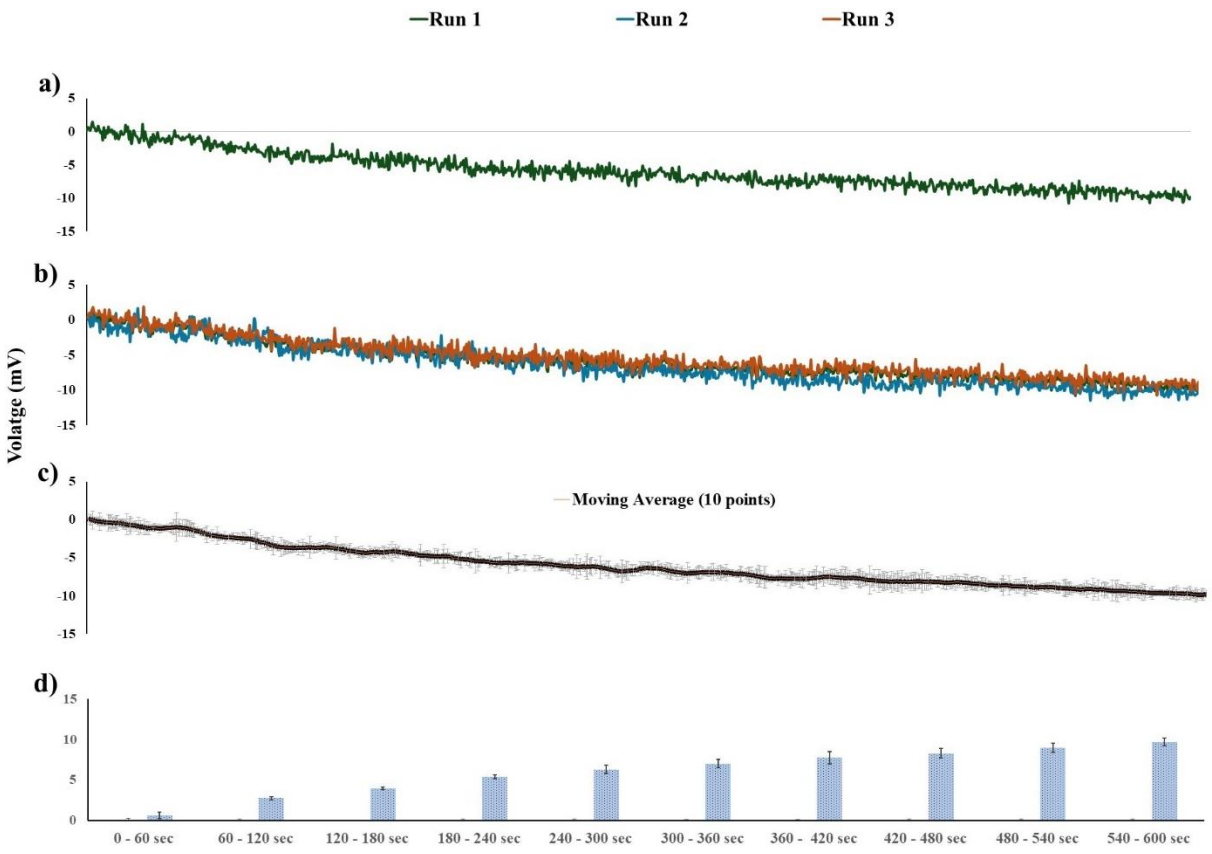

Fig. 3-10: Data analysis process for measuring the change in voltage using the Wheatstone bridge. **a)** The initial change in voltage for the microplastic suspended solution balanced at t=0; **b)** The resultant change in voltage due to microplastic accumulation, measured across three different fabricated sensors; **c)** The moving average (10-point) for the voltage change at each time step across all three runs; **d)** the average change in voltage over each 60-second interval throughout the complete 10 min run.

3.2.2.2 Microwires MXene Functionalization for Affinity to Microplastics

As reviewed in section 2.3, MXene, with its unique 2D design, has demonstrated remarkable capabilities in extracting and entrapping microplastics from water [71,79]. This approach has been specifically implemented in our microfluidic sensor design to enhance the accumulation of microplastics at the anode. We hypothesize that this increased accumulation of microplastics will amplify the magnitude of the output electrical signal, improving the sensor's sensitivity and detection capabilities.

The microwire coting process was carried out in two steps, following the method demonstrated by Coa et al.[80], first, preparation of the $Ti3C_2T_x$ and saline solution, and second, the preparation of copper microwires to be coated by $Ti3C_2T_x$ solution. Acetone, ethanol, acetic acid, (3-Mercaptopropyl) triethoxysilane (>98%), and Ti3C2Tx were obtained from Sigma Aldrich. All chemicals were of analytical grade and were used as received. Ethanol, distilled water, and (3-Mercaptopropyl) triethoxysilane were mixed in a beaker in a volume ratio of 90:6:4. The mixture was then ultrasonicated for 10 minutes. Afterward, acetic acid was added to the solution to adjust the pH to 4. The resulting mixture was allowed to hydrolyze in a water bath at 25 °C for 48 hours. Subsequently, 1 mL of Ti3C2Tx (at concentrations of 0.5 mg/mL) was added to the hydrolyzed solution with mechanical stirring for 15 minutes to form the Ti3C2Tx/silane solution as observed in Fig. 3-11

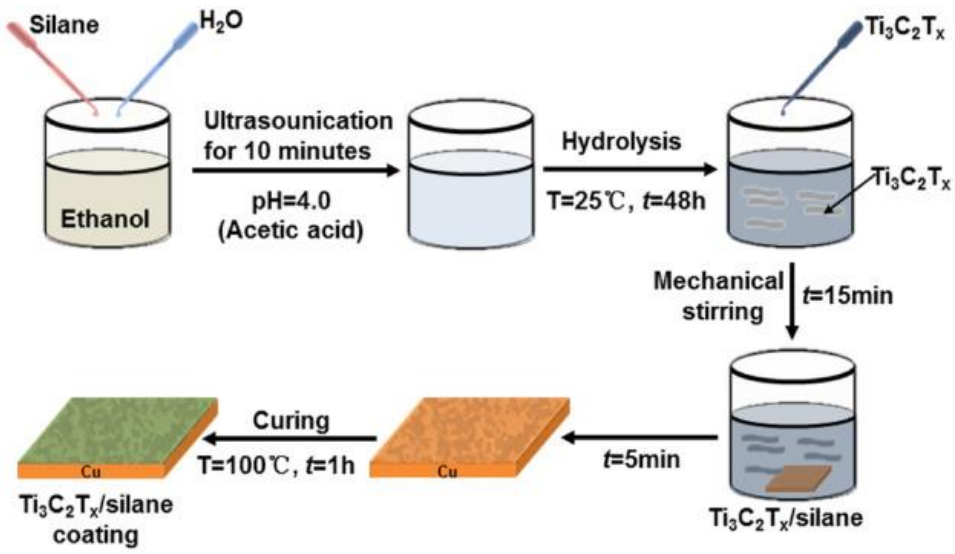

Fig. 3-11: The process of coating copper with Ti3C2Tx / silane composite [80]. Figure reprinted with permission of Elsevier

The copper microwire were carefully abraded using sandpaper with grits of 2000 very gently. After abrasion, the microwire was sequentially cleaned by ultrasonication in acetone, ethanol, and then distilled water for 5 minutes each, and then dried with air. The cleaned Cu microwire was then immersed in the Ti3C2Tx /silane solution at room temperature for 10 minutes. Finally, the samples were cured in an oven at 100 °C for 1 hours.

3.3 Numerical Model: Design, Governing Principles, and Boundary Conditions

A 2D numerical model was created in COMSOL Multiphysics based on the experimental setup of the sensor. The primary role of this model was to replicate the fluid dynamics and electric field interactions within the microfluidic sensor, providing a deeper understanding of how the electrophoretic force influences the accumulation of microplastics at the anode. This simulation was essential for visualizing the sensor's behavior under varying conditions, such as changes in salinity. Once the numerical model was constructed, it was verified and validated against experimental measurements using saline solution. The validation process ensured the accuracy of the model in reflecting real-world conditions. After validation, the model was employed to investigate the working mechanism of the electrophoretic force, offering insights into the precise conditions under which microplastics accumulate at the anode. The model demonstrated that this accumulation was driven solely by the electrophoretic force, ruling out other potential causes like clogging or physical blockage in the microfluidic channel. The parameters used in this study, along with their respective units, are summarized in the table below.

Table 3-1: Parameters utilized in the numerical model along with their symbols, descriptions, and units.

Symbol	Description	Units	Symbol	Description	Units
A	Microchannel cross-section area	m^2	Q_i	Current source	A/m^3
h	Height (along the y-axis)	m	c_{MP}	microplastic concentration	ppm
j	Current density	A/m^2	F_c	Faraday's constant	C/mol
L	Microchannel length (along the x-axis)	m	C_p	Specific heat capacity	J/kg·K
C_{mp}	Microplastic charge	$m^2/s \cdot V$	J_e	External current density	A/m^2
c_{NaCl}	NaCl concentration	ppm	F_{ep}	Electrophoretic force	N/m^3
p	Pressure	N/m^2	κ	Specific conductance	S/m
Re	Reynolds number	-	V	Electrical potential	V
w	Width (along the z-axis)	m	E	Electric field	V/m
g	Gravity	m/s^2	T	Temperature	K
D_h	Hydraulic diameter	m	u	Mean velocity	m/s
j_e	External current source	A/m^2	$\vec{u}$	Velocity vector	m/s
Λ	Molar conductivity	$S/cm^2 \cdot mol$	ζ	Zeta potential	mV
μ	Viscosity	Pa·s	J_i	Diffusive flux	$Mol/cm^2.s$
ρ	Density	Kg/m^3	u_p	Particle velocity	m/s
ρ_{el}	Electrical resistivity	Ohm·m	V_g	volume of the object	m^3
σ	Electrical conductivity	S/m	σ_p	Microplastic surface charge	C/m^2

3.3.1 Governing Equations

The simulation model was based on the physics of fluid dynamics, electric fields, diffusion of diluted species, and particle tracking. To improve convergence, we first calculated the fluid flow

and electric potential within the microchannel. Subsequently, we developed and executed the studies for diluted species transport and particle tracking.

In this study, the flow regime is identified as laminar, with the Reynolds number, Re (eq. 3-10) falling between 16<Re<64.

$$Re = \frac{\rho u D_h}{\mu} \tag{3-10}$$

The hydraulic diameter for the channel was obtained from the following equation (eq. 3-13):

$$D_h = 4\frac{cross-sectional\ area}{wetted\ perimeter} = \frac{2wh}{(w+h)} \tag{3-13}$$

The ratio of microplastic particle diameter to the hydraulic diameter was considered to justify the insignificance of the inertial forces under the given flow conditions. The ratio was calculated to be 0.0058 which indicates that the particle diameter is very small compared to the channel hydraulic diameter. For inertial forces to be considered significant, the ratio of particle diameter to channel hydraulic diameter should be larger than 0.07 [81].

The simplified forms of the Navier-Stokes equation (eq. 3-11) and the incompressible non-Newtonian continuity equation (eq. 3-12) were applied to analyze the electrolyte flow under steady-state conditions.

$$\rho(\vec{u}.\nabla)\vec{u} = \nabla\left(-pl + \mu(\nabla\vec{u} + (\nabla\vec{u})^T)\right) + \vec{F} \tag{3-11}$$

$$\nabla.(\rho\vec{u}) = 0 \tag{3-12}$$

The equation describes the steady-state flow of a non-Newtonian fluid. Here, ρ represents fluid density, $\vec{u}$ is the velocity vector, and $(\vec{u}.\nabla)\vec{u}$ accounts for momentum transport within the fluid. The term $\nabla(-pl)$ is the pressure gradient, driving the flow, while $\mu(\nabla\vec{u} + (\nabla\vec{u})^T)$ represents the viscous stress, and $\vec{F}$ accounts for any external forces acting on the fluid. Together, these terms describe how the fluid moves and deforms under different forces.

Initially, the simulation focused solely on the electrolyte sample containing sodium and chloride ions, without the introduction of microplastics. The electrolyte flows consistently through the microchannel. When an electric field is applied between the wires, the ions move towards the electrodes with opposite charges, forming an electric double layer.

$$\nabla.(\vec{j}) = -\nabla.(\sigma\nabla V - \overrightarrow{J_e})d = Q_j w \tag{3-14}$$

The electric field and the resulting current, which passes from the terminal to the ground electrode through the conductive electrolyte, are governed by the steady-state charge conservation equation (eq. 3-14). All parameters used in the equations are described in Table 3-1. To analyze the diffusion, and ionic migration of dissolved NaCl ions, mass conservation equation (eq. 3-15) was utilized. The process of diffusion is described by Fick's law.

$$\frac{\partial c_i}{\partial t} + \nabla.(\overrightarrow{J_i}) + \vec{u}.c_i = R_i \tag{3-15}$$

Fick's law, as expressed in the given equation, governs the transport of species i in a medium through a combination of diffusion, convection, and reaction processes. The term $\frac{\partial c_i}{\partial t}$ represents the time rate of change of the concentration of species i, indicating how its concentration varies over time. The second term, $\nabla.(\vec{J_i})$, describes the spatial distribution of the diffusive flux which quantifies how species i spreads out in space due to concentration gradients. The third term, $\vec{u}.c_i$ decrides the convective transport of species i due to the bulk motion of the fluid with velocity vector, carrying the substance along. Lastly, R_i represents any chemical reactions that produce or consume species i, either adding to or subtracting from its concentration.

The electrical resistance, between the parallel copper microwires was considered to be dependent on the sample's electrical resistivity, along with the geometrical characteristics of the channel, as outlined in equation (eq. 3-16).

$$\mathrm{R} = \rho_{\mathrm{el}} \frac{g}{hw} \tag{3-16}$$

All parameters used in the equations are described in Table 3-1. Experimental data was used to calculate the conductivity of the electrolyte at different concentrations of NaCl. Various samples with different NaCl concentrations were diluted in deionized water, and a conductivity meter was used to measure the resulting conductivity. When plotted on a graph (Fig. 3-12), the data points revealed a trend line, establishing a relationship between NaCl concentration and electrolyte conductivity. The resulting linear relationship (eq. 3-17) was used to determine the conductivity of the solution based on the NaCl concentration for the numerical simulation.

$$\sigma = 0.0017(c_{NaCl}) + 0.0396 \quad (3\text{-}17)$$

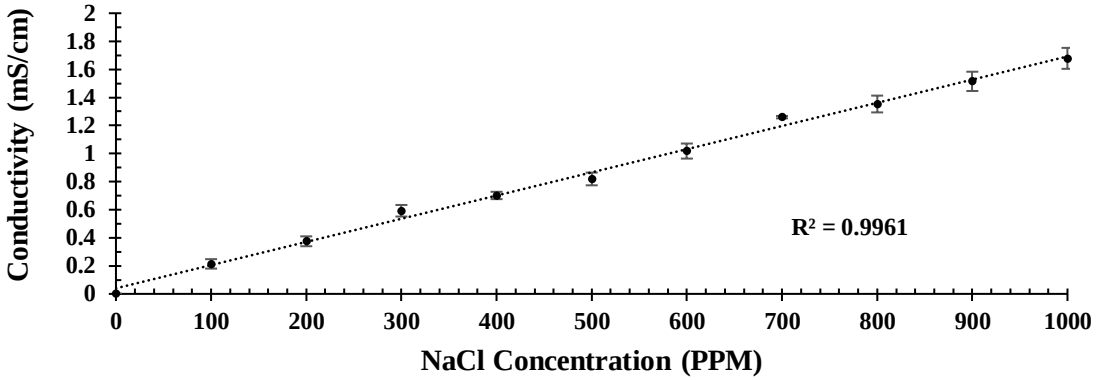

Fig. 3-12: Electrical conductivity range of water samples based on their NaCl concentration, with results obtained at room temperature. The linear relationship is described by the equation y = 0.0017x+0.0396. N=3 independent trials.

To simulate the accumulation of microplastics within the sensor, we employed a combination of fundamental equations governing particle motion. These equations were essential in accurately predicting the behavior of microplastics as they interacted with the fluid flow and the sensor surfaces. Newton's second law (eq. 3-18) was used to describe the motion of microplastic particles. By considering the mass of the particles and the total forces acting upon them, we could determine their velocities and trajectories within the fluid. This law is fundamental in understanding how microplastics move in response to various forces within the microchannel.

$$m\frac{du}{dt} = F_{total} \quad (3\text{-}18)$$

The total forces (F_{total}) acting on the microplastics include several components as seen in eq. 3-19:

$$F_{total} = F_{drag} + F_{gravity} + F_{buoyancy} + F_{EP} \quad (3\text{-}19)$$

The drag force equation (eq. 3-20) was crucial for modeling the resistance experienced by microplastics as they moved through the fluid. This force, which depends on the relative velocity between the fluid and the particles, the fluid density, and the particle's cross-sectional area, helped us understand how microplastics slow down and accumulate within the sensor. Due to the steady nature of the flow in our system, history forces like the Basset force are neglected, allowing us to focus solely on the immediate forces acting on the microplastics as they move through the fluid.

$$F_{drag} = \frac{1}{2}\rho C_D A|u - u_p|(u - u_p) \quad (3\text{-}20)$$

All parameters used in the equations are described in Table 3-1. The drag coefficient C_D plays a central role in calculating the drag force. Its value varies with the flow conditions, particularly the Reynolds number, and can be calculated (eq. 3-21) for 1 < Re < 1000 or looked up in empirical tables for different shapes and flow regime.

$$C_D = \frac{24}{Re} + \frac{6}{1\sqrt{Re}} + 0.4 \quad (3\text{-}21)$$

Gravity (eq. 3-22) and buoyancy (eq. 3-23) forces were considered to account for the vertical movement of microplastic particles within the fluid. The gravitational force drives the particles

downward, while the buoyancy force, which is dependent on the fluid density and the volume of the particles, acts in the opposite direction. Balancing these forces was essential to accurately simulate the vertical distribution and accumulation of microplastics within the sensor.

$$F_{gravity} = mg \tag{3-22}$$

$$F_{buoyancy} = -\rho V_g g \tag{3-23}$$

Additionally, the electrophoretic force (eq. 3-24) was incorporated to account for the movement of charged microplastic particles in response to the applied electric field. This force plays a significant role in driving the microplastics toward the electrodes. Understanding this interaction was vital for accurately predicting the accumulation patterns within the sensor.

$$F_{EP} = 6\pi\epsilon\delta aE \tag{3-24}$$

3.3.2 Boundary Conditions

The boundary conditions for the 2D model were established to align with the experimental setup and ensure precise simulation outcomes. In this simulation, the x-axis represents the flow direction, the y-axis the transverse direction, and the z-axis the vertical direction. A fully developed flow profile with a constant flow rate of 0.2 mL/min was implemented in the x-direction. The corresponding velocity was calculated based on the channel's cross-sectional area and applied as the inlet boundary condition. This assumption was based on the longer channel length of the actual

devices compared to the numerical model, justifying the fully developed flow. In the y-axis direction, the velocity was set to zero, and a no-slip boundary condition was applied throughout the microchannel, including the walls and wires. At the channel outlet, a static gauge pressure of zero ($p=0$) was assumed to simulate an open boundary, allowing the flow to exit naturally.

For the electrical boundary conditions, the two copper microwires were used as electrodes to measure the resistance in the salinity sensor. A constant DC current was applied at the terminal of 1 μA, with the ground electrode maintained at zero voltage ($V=0$). Additionally, the PDMS walls were treated as insulated, with no current density ($J=0$) present.

The dynamic viscosity of the solution is crucial in this type of simulation because it affects the fluid flow and, consequently, the distribution and migration of ions under an electric field. Previous studies have shown that adding 10,000 ppm of salt to water at 25°C results in a 0.7% increase in dynamic viscosity and a 2% increase in density [82]. However, for our simulations, which used salt concentrations ranging from 300 to 1000 ppm, these changes were minimal and could be safely neglected. Therefore, we assumed a dynamic viscosity of $\mu=8.90\times10^{-4}$ Pa.s and a density of $\rho=1000$ kg/m³ for the water in our numerical analyses. This assumption simplified the model without significantly affecting the accuracy of the results.

Chapter 4: Preliminary Results and Discussion[1]

As outlined in the methods section, microplastics were suspended in saline waters with varying salt levels from 0 ppm to 1000 ppm NaCl. The resulting solutions exhibited conductivities in the range of 0 to 1.67±0.07 mS/cm comparable to the conductivity of freshwater. Establishing the correlation between NaCl concentration and the resultant conductivity is vital to achieve the correct conductivity of freshwater, which, as discussed later, significantly affects the sensor's ability to detect charged microplastics. This experimentation directly supports **Objective 1**, which aims to characterize the sensor parameters, such as sensitivity and detection limits, under different saline conditions and microplastic concentrations.

4.1 Electrical and optical microplastic detection in salty water

Here, we investigated the potential of a DC electrical microfluidic sensor for qualitative and quantitative detection of microplastics through their electrophoretic accumulation on the electrode surface in a saline solution containing 300 ppm NaCl. The experiment involved measuring the electrical resistance of the NaCl solution ($R_{control}$), followed by a blank solution with the same concentration of salt (R_{Blank}), and then a 25 ppm microplastic suspension in 300 ppm NaCl solution (R_{MP}). Results are shown in Fig. 4-1.

[1] A manuscript based on this chapter has been submitted to IEEE Sensors Journal

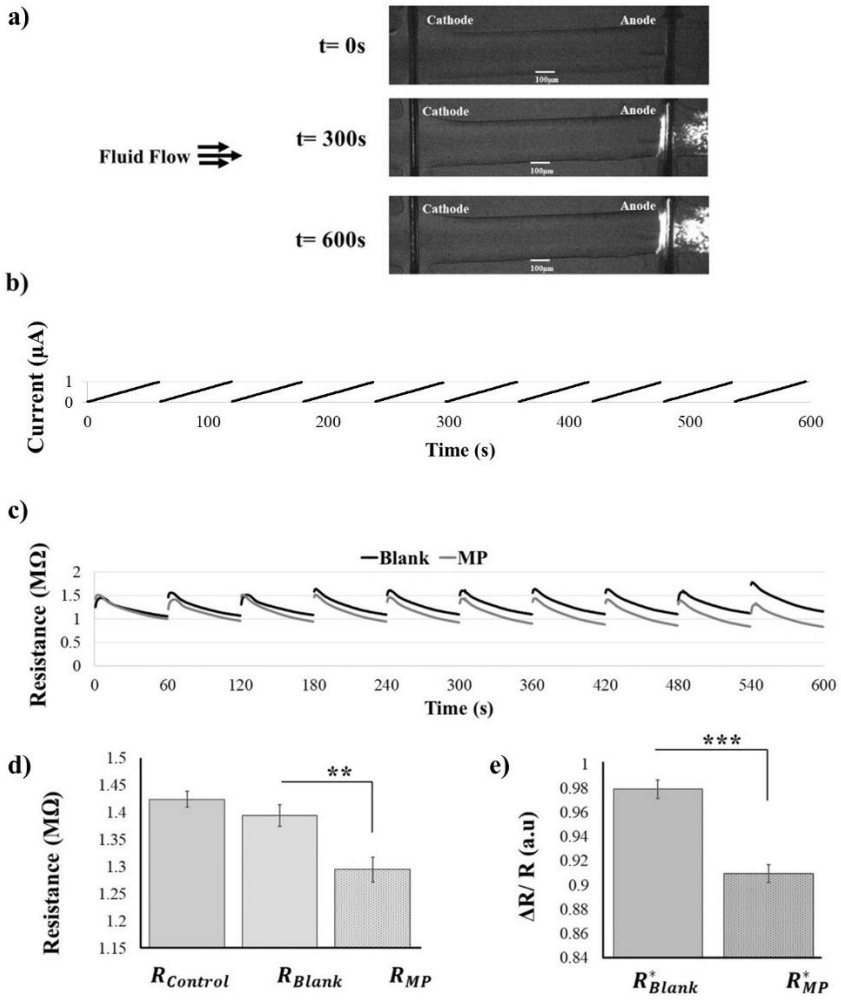

Fig. 4-1: Microplastics electrophoretic accumulation and detection in solutions containing 300ppm NaCl and 25ppm microplastics**. a)** Microplastic accumulation at the anode at different time intervals; **b)** Applied electrical current from 10 nA to 1 μA in 10 nA steps, with a time interval of 0.5 s between each step; **c)** Resultant electrical resistance for blank solution (R_{Blank}) and microplastic suspension (R_{MP}) as cycles of 60 s sweep current were applied; **d)** The average electrical resistances of control, blank, and microplastic suspensions; **e)** The normalized electrical resistance for the blank solution and microplastic suspension with respect to the control solution; Error bars are standard deviations (SD); **: $p < 0.01$, ***: $p < 0.001$; N = 10 in three independent trials.

Optically, microplastic accumulation was clearly visible at the anode (Fig. 4-1a) at different time intervals (t = 0, 300, and 600 s). This accumulation resulted from the electrophoretic movement and concentration of the particles under the influence of the applied sweep current. It is important to highlight that the flow direction was from the cathode towards the anode. Fig. 4-1a depicts a significant intensity of microplastics at the inner side of the anode that faces the cathode. This is attributed to the higher electric field intensity at this location which exerts a stronger force on the particles, leading to their enhanced accumulation in this area. The accumulation of microplastics at the bottom of the microchannel following the anode was a result of the electrophoretic force counteracting the hydrodynamic flow of the microplastics. This counteraction slowed them down, leading to sedimentation.

The migration of microplastics toward the positively charged anode is not only visually apparent but also corresponds to a significant change in the measured resistance. This pattern emerges from the microplastics gathering at the anode over time, revealing the interplay between particle accumulation and electrical resistance dynamics. As a sweep current is applied from 10 nA to 1 μA in 10 nA steps (Fig. 4-1b), an electric field is established between the microwires. This causes the microplastics to accumulate, resulting in a consistent decline in resistance over the duration of the experiment (600s) was noted for samples containing microplastics (R_{MP}), in contrast to the blank samples (R_{Blank}), as illustrated in Fig. 4-1c.

The immediate decrease in resistance over each 60-second sweep current interval (Fig. 4-1c) could be explained by the accumulation of ions around the electrode, which was then 'washed away' as a new sweep started, allowing for a clear distinction in resistance measurements between the

sweeps. The salt ions are much smaller and more mobile compared to the microplastics, allowing them to quickly re-distribute in the fluid when the electric field is removed or applied during each new sweep. They are also more responsive to changes in the electric field due to their charge-to-mass ratio. In contrast, microplastics are larger, less mobile, hence becoming trapped at or near the electrode surface, preventing them from being 'washed away' as readily as ions when the sweep current started over. Therefore, they gradually resulted in an overall resistance drop between the electrodes.

The three average resistances for each sample (R_{Contol}, R_{Blank}, R_{MP}) are shown in Fig. 4-1d. We observed a significant decrease in the resistance of the microplastic suspension (R_{MP}) compared to the blank solution (R_{Blank}). Additionally, a slight decrease in electrical resistance between the control solution ($R_{Control}$) and R_{Blank} was noted. This reduction highlights the influence of the supernatant left in the blank solution post-centrifugation. Consequently, to achieve more accurate results, we normalized the electrical resistance of both the blank solution and the microplastic suspension relative to the control solution, leading to R^*_{Blank} and R^*_{MP} (Fig. 4-1e), characterized by eq. 3-6. The normalized resistance experienced a statistically significant decrease, going from 0.98 in the blank solution to 0.90 in the solution containing 25ppm of suspended microplastics, as shown in Fig. 4-1e (Mann–Whitney U test, p-value < 0.001).

A positive correlation is observed between the accumulation of microplastics at the anode and the reduction in electrical resistance within the microfluidic system. This effect is shown by a decrease in resistance when a current is applied, highlighting the sensor's ability to distinguish between samples with and without microplastics. The enhancement of electrical current flow is due to the

accumulation of microplastics under the applied electrophoretic force. This force causes the microplastics to align or gather at the electrode, thereby altering the electrical dynamics of the system. Although microplastics are typically non-conductive, they interact with the ionic environment of the medium. Their surfaces carry a charge that attracts counter-ions from the solution, forming a conductive double layer around each microplastic particle. This conductive layer decreases the overall insulating properties of the microplastics, effectively lowering the electrical resistance of the system. Additionally, the formation of these conductive layers reduces the effective distance between the two electrodes, further contributing to the decrease in resistance. Consequently, this interaction enhances the sensor's sensitivity to the presence of microplastics, as the reduction in resistance indicates their accumulation.

4.2 Effect of salt concentration on microplastic detection

The influence of salt concentration on the accumulation and detection of 1μm PS microplastics was also investigated in this section. While maintaining a constant microplastic concentration of 25 ppm, the salt concentration in the solution was altered to understand its impact on detection efficiency. It was observed that as the NaCl concentration was increased from 300 ppm to 1000 ppm, there was a notable decrease in the accumulation of microplastics around the anode (Fig. 4-2a). Correspondingly, a decrease in the normalized electrical resistance drop (ΔR/R) was also recorded, indicating that higher salt concentrations adversely affect the sensor's ability to detect microplastics (Fig. 4-2b).

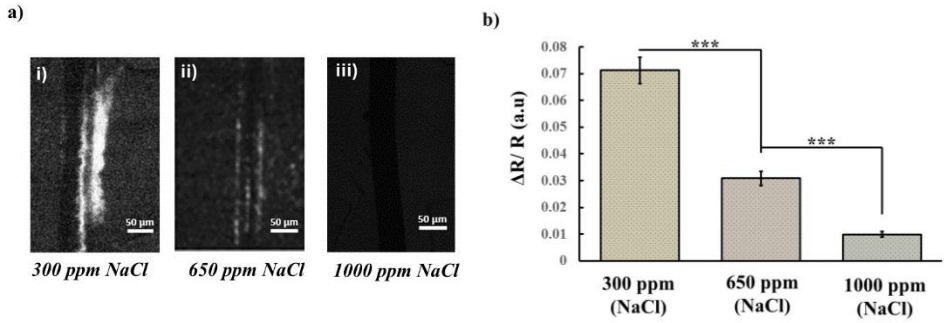

Fig. 4-2: Effect of salt concentration on 1µm PS microplastic (25 ppm) accumulation and the electrical resistance. **a)** Microplastic accumulation at the anode for i) 300ppm, ii) 650ppm and iii)1000ppm NaCl; **b)** Normalized resistance drop at different salt concentrations; ***: P < 0.001; N=10 with 3 independent trials.

Fig. 4-2b presents a significant decline in the normalized resistance drop which diminishes significantly with escalating salt concentrations. Specifically, an increase in NaCl concentration from 300 ppm to 650 ppm corresponds to a decrease in $\frac{\Delta R}{R}$ from 0.072 to 0.031 (56.9%). Further elevation of NaCl concentration from 650 ppm to 1000 ppm leads to an additional reduction in the normalized resistance drop, bringing it down to 0.007. This is equivalent to 86% decrease in $\frac{\Delta R}{R}$ upon increasing the NaCl concentration from 300 ppm to 1000 ppm. Both transitions are statistically significant, as evidenced by Mann–Whitney U test results with p-values less than 0.001. This reduction is due to a weaker electric field between the sensor's electrodes at higher NaCl concentrations, as explained by (eq. 3-2). Concurrently, the electrical double layer is enhanced (eq. 3-4), leading to a decreased zeta potential for charged microplastic particles at higher salt concentrations. This, in turn, diminishes the electrophoretic force on the microplastics (eq. 3-3), resulting in a lower accumulation of microplastics around the anode at increased salt

concentrations. Consequently, there is a significant drop in the sensor's sensitivity to microplastics with higher ionic strength in the solution. This is further investigated in section 4.3.

When compared to existing literature, our study introduces a cost-effective approach utilizing a DC electrical microfluidic sensor for the detection of microplastics in saline environments, where traditional methods struggle. While previous studies have mostly focused on detection of microplastics in DI water [22,76], we extend the application to varying saline concentration, which more accurately represent real-world conditions. For instance studies using resistive pulse sensor (RPS) in KCl-diluted solution have shown an inverted response at lower ionic strengths but primarily focused on concentrations similar to seawater conductivity (3727.5 ppm KCL) [63]. Our results, however, emphasize the challenges in detecting microplastics at freshwater conductivity levels, where the lower ionic strength significantly affects sensor sensitivity. These findings highlight the limitations of previous approaches when applied to freshwater environments and underscore the importance of optimizing sensor parameters for low-salinity conditions. By detecting microplastics in solutions with salt concentrations as low as 300 ppm, our study bridges the gap in the literature, providing new insights into microplastic detection at lower salinities, which has significant implications for environmental monitoring in freshwater systems.

4.3 Effect of microplastic concentration on detection

The sensitivity of the sensor to varying 1µm PS microplastic concentrations, from 1 to 25 ppm, was examined across a range of salt concentrations from 300 to 1000 ppm to explore the sensor's

detection capabilities. At the lower spectrum of salt concentrations, notably at 300 ppm and 650 ppm, there was a visible escalation in the accumulation of microplastics at the anode. This accumulation directly increased with the rise in microplastic concentrations, as shown in Fig. 4-3a(i) and a(ii). However, the microplastic accumulation at 1000 ppm salt was visually insignificant for samples containing 5 and 25 ppm microplastics (Fig. 4-3a(iii)). Consequently, a lower microplastic concentration of 1 ppm at 1000 ppm salt was not tested.

For samples containing 300 ppm NaCl in Fig. 4-3b, a positive correlation was observed between the microplastic concentration and normalized electrical resistance drop. $\frac{\Delta R}{R}$ significantly increased by 86.7% upon increasing microplastic concentration from 1 ppm to 25 ppm. As the concentration of microplastics increases, they form larger networks within the sensor that improve electrical conduction. This leads to a greater decrease in measured resistance, as the microplastics more effectively lower the system's overall resistance. The existence of a statistically significant difference in the sensor's response to varying microplastic concentrations suggests that the sensor remains sensitive at 300 ppm salt concentration.

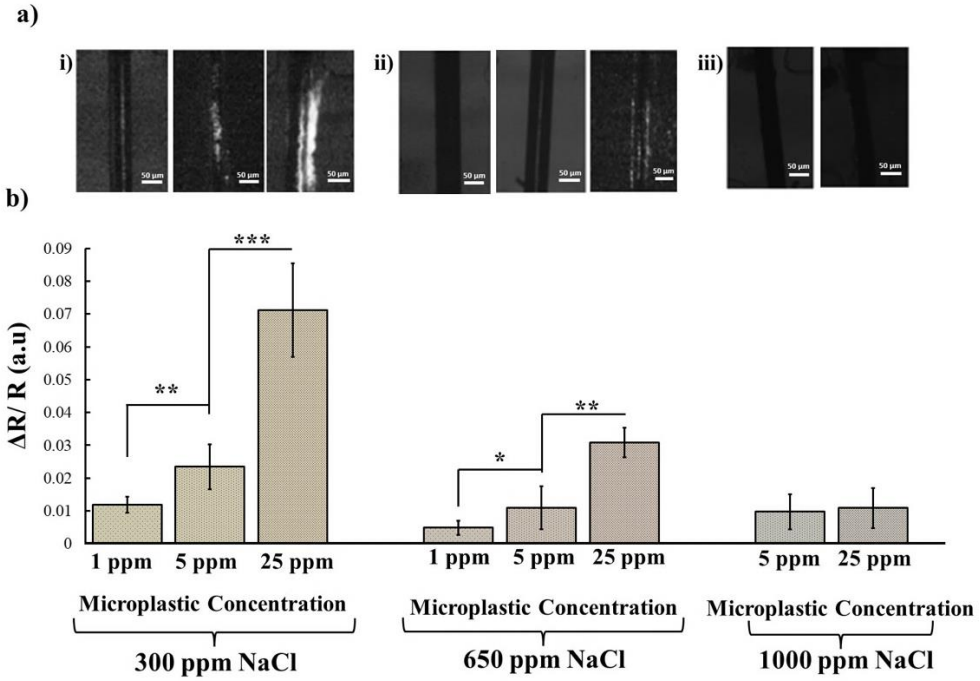

Fig. 4-3: The sensor's response to 1µm PS microplastic concentrations (1-25 ppm) at varying salt levels (300-1000 ppm). **a)** Microplastic accumulation around the anode; **b)** Normalized resistance drops due to microplastic accumulation; *: $P < 0.05$, **: $P < 0.01$, ***: $P < 0.001$; N=10 with 3 independent trials.

Increasing the salt concentration to 650 ppm decreased the sensor response towards microplastic concentration. Nonetheless, the sensor still could differentiate between three distinct microplastic concentrations, with $\frac{\Delta R}{R}$ increasing by 87.8% as the microplastic concentration increased from 1 to 25 ppm. However, the significance level (indicated by the asterisk) at 650 ppm salinity was lower compared to the 300 ppm salt level. A subsequent increase in salt concentration to 1000 ppm led to an insignificant difference in $\frac{\Delta R}{R}$ values between 5 and 25 ppm microplastics, rendering experiments at 1 ppm unnecessary.

The effect of microplastic concentration on sensor response is further documented in Table 4-1, which presents the percentage reduction in the resistance for various microplastic concentrations suspended in different salt levels.

Table 4-1: Percentage drop between R^*_{Blank} and R^*_{MP} for various microplastics concentrations at varying salt levels. Table reprinted with permission of IEEE

	1 ppm (microplastic)	**5 ppm** (microplastic)	**25ppm** (microplastic)
300 ppm (NaCl)	*0.96%*	*2.12%*	*7.24%*
650 ppm (NaCl)	*0.38%*	*1.14%*	*3.1%*
1000 ppm (NaCl)		*0.76%*	*0.79%*

* ***P < 0.05*** ** ***P < 0.01*** *** ***P < 0.001***

Notably, at 300 ppm NaCl, the percentage change in between the blank and the 1 ppm microplastic solutions was 0.96%, which increased to 7.24% for a 25 ppm microplastic concentration, highlighting the sensor's capability to detect and quantify higher concentrations of microplastics effectively. However, as the salt concentration increased to 650 ppm and beyond, there is a clear trend of diminishing sensor response, with the resistance change for 25 ppm microplastics dropping to 3.1% and 0.79% in samples containing 650 ppm and 1000 ppm NaCl, respectively. These data not only validate the sensor's capacity to recognise and quantify microplastics across a gradient of concentrations but also its susceptibility to the confounding effects of high salt levels.

4.4 Improving detection in highly saline freshwater

At 1000 ppm NaCl, the sensor's ability to detect 1µm PS microplastics optically or electrically is significantly compromised when a sweep current of 0 - 1 µA was used, as shown in Fig. 4-4.

Therefore, we explored the effects of increasing the sweep current range to 0 - 5 µA on the sensor's ability to detect microplastics. This increase in current was intended to increase the electric field strength between microwires, thereby enhancing the electrophoretic force on microplastics, as described by (eq. 3-3) and (eq. 3-4).

Fig. 4-4 illustrates the outcomes of this modification on the applied current for microplastic concentrations of 5 ppm and 25 ppm suspended in salty water with a NaCl concentration of 1000 ppm. Fig. 4-4a(i) shows the microplastic accumulation at a sweep current of 0 - 1 µA, while Fig. 4-4a(ii) displays the accumulation when the current range is increased to 0 - 5 µA. The images present a clear visual confirmation of increased microplastic accumulation at the anode under the higher current. As expected, with an increase in the electric field, the electrophoretic force should correspondingly increase, driving more microplastics towards the anode.

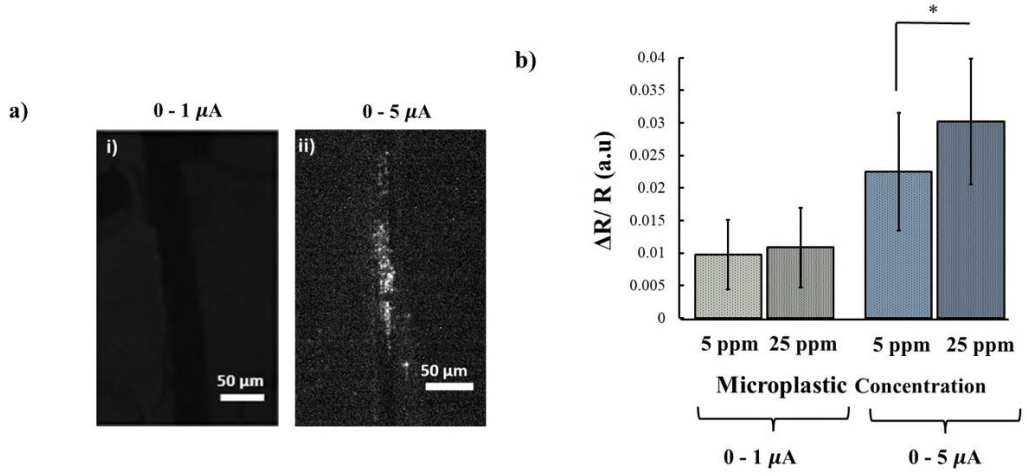

Fig. 4-4: The impact of increasing the sweep current on microplastic detection in 1000 ppm NaCl saline waters. **a)** Accumulation of microplastics around the anode in i) 0-1 µA and ii) 0-5 µA current sweep

ranges; **b)** Normalized resistance drop illustrating the sensor's response to the increased current; *: P < 0.05; N=10 with 3 independent trials.

A more pronounced normalized resistance drop with the increased current was observed (Fig. 4-4b), indicating a stronger electrophoretic force in action. Upon increasing the sweep current range, $\frac{\Delta R}{R}$ increased by 65.9% for 5 ppm microplastic suspensions and 72.2% for 25 ppm microplastic suspensions, respectively. These signal enhancements demonstrate that the sensor can more significantly detect the presence of microplastics at higher current inputs. However, the statistical significance between the two microplastic concentration levels remained moderate, with a p-value of 0.042. This indicates that while the sensor can detect microplastics, it struggles to accurately quantify the different concentrations within the tested range (5-25 ppm) at 1000 ppm NaCl concentration. Therefore, while there is a detectable increase in microplastic accumulation at the anode and a corresponding decrease in resistance with a higher current, the sensor's sensitivity requires further optimization to effectively quantify microplastics at high salinity levels.

These results align with Thesis Objective 1, which focuses on characterizing the sensor's parameters, specifically, its sensitivity and detection limits under different saline conditions (300, 650, and 1000 ppm NaCl) and microplastic concentrations (1, 5, and 10 ppm). Chapter 5 will address Objectives 2 and 3, which focus on optimizing the sensor's electrical and optical performance across the complete range of freshwater salinity and evaluating its ability to detect microplastics of varying sizes.

Chapter 5: Sensor Optimization and Performance Enhancement for Improved Microplastic Detection

The motivation behind this chapter stems from the need to improve the accuracy and efficiency of microplastic detection in water, especially in high-salinity environments where traditional methods often fall short. Previous experiments using sweep current revealed several limitations, such as transient effects and challenges in consistently detecting microplastics due to fluctuating electric fields. This chapter addresses **objectives 2 and 3**, focusing on optimizing the sensor's electrical response and enhancing its optical performance for effective detection of microplastics across varying salinity levels (Objective 2). Additionally, the sensor's capability to detect microplastics of different sizes is evaluated to ensure comprehensive monitoring (Objective 3).

In Section 5.1, the application of constant current is explored to stabilize the electric field and enhance electrophoretic accumulation of microplastics, leading to a more consistent detection signal. The effects of sample salt concentration and microplastic concentration are also analyzed, showcasing the method's effectiveness in challenging conditions. Section 5.2 presents the numerical analysis of the sensor's performance, focusing on domain and mesh independency, model verification, and validation. Finally, Section 5.3 investigates enhancements to sensor sensitivity using a Wheatstone bridge configuration and MXene-coated microwires, examining their impact on improving detection capabilities, especially for larger microplastic particles. The findings demonstrate significant improvements in signal strength and accuracy, contributing to more reliable microplastic detection.

5.1 Application of constant current

The implementation of a constant current in our experiments was aimed at mitigating the transient effects observed during the sweep current method presented in Chapter 4. By applying a steady current across the sensor of (1μA), the electric field within the microfluidic device remained constant, thereby reducing the initial fluctuations in voltage that were previously encountered. Further, the sample preparation was simplified to just using a blank solution (R_{Blank}) and a microplastic suspended solution (R_{MP}), eliminating the need for the previously used base solution (R_{Base}), as explained in section 3.2.

The constant electric field induced by the steady current created a uniform electrophoretic force, which is directly proportional to the strength of the electric field and the charge on the microplastics (eq. 3-3). As the negatively charged microplastics moved through the fluid in the microchannel, they were consistently drawn toward the positive electrode (anode) due to this force. As seen in Fig. 5-1a, the steady electric field facilitated a more rapid and pronounced accumulation of microplastics near the anode compared to the sweep current method, where the fluctuating electric field led to intermittent accumulation. The continuous application of the electric field ensured that this force remained active throughout the entire experimental run, leading to a sustained and enhanced accumulation of microplastics at the anode as seen in Fig. 5-1a.

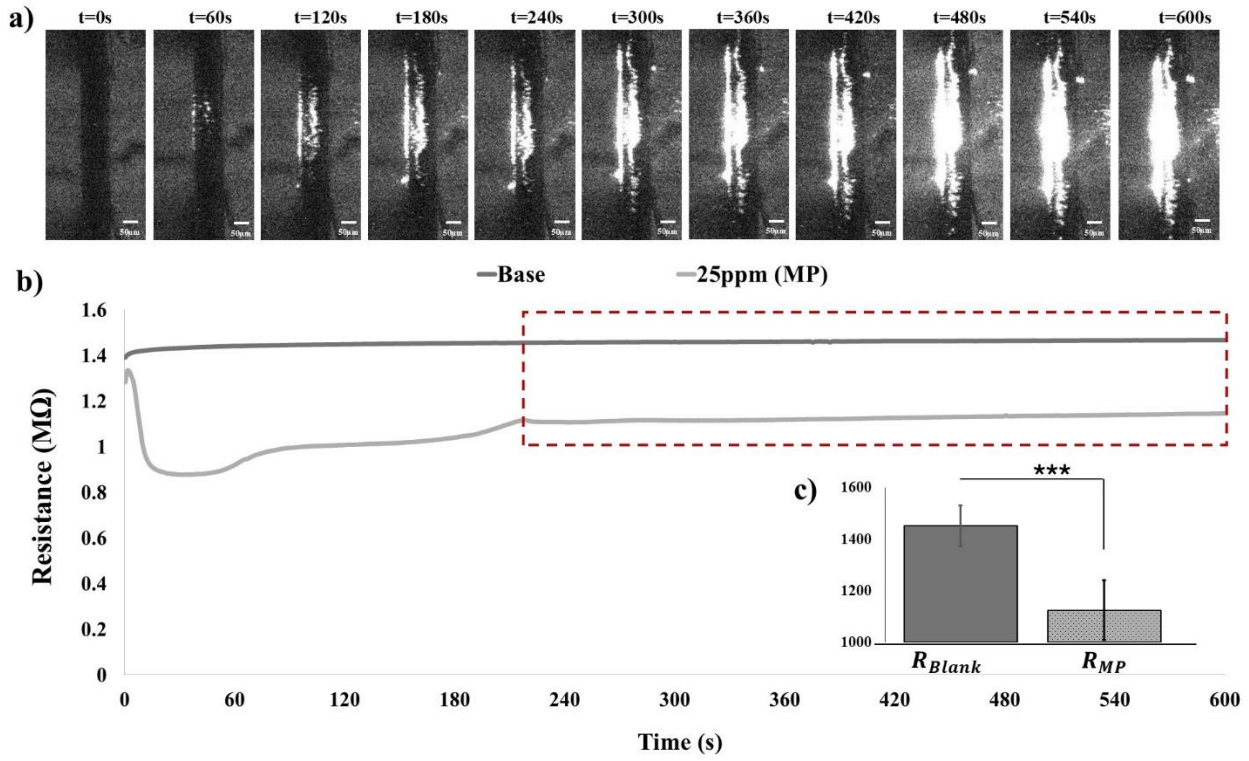

Fig. 5-1: Electrophoretic accumulation of microplastics leading to detection in solutions containing 300ppm NaCl and 25ppm microplastics (1µm). a) Microplastic accumulation at the anode throughout the 10 min experimental run; b) Electrical resistance response for blank solution (R_{Blank}) and microplastic suspension (R_{MP}) as constant current (1µA) was applied, the dashed boxed region represents the plateau resistances; c) The average electrical resistances of the blank, and microplastic suspensions; Error bars are standard deviations (SD); **: $p < 0.001$, 3 independent trials.

The ability to maintain a constant electrophoretic force ensured that the microplastics were consistently attracted and accumulated at the electrode surfaces, resulting in a change in electrical resistance (Fig. 5-1b). Switching to a constant current was crucial for achieving a plateau in the sensor's response, where the output voltage stabilized after the initial transient phase. By averaging the electrical resistance over this stabilized region, a significant change was observed between the

blank solution and the microplastic-suspended solution. The average resistance dropped from 1.45 MΩ to 1.12 MΩ, with a p-value of 0.000781 and three-start significance indicated by the asterisk when the experiments were repeated three times (Fig. 5-1c). However, while this change was statistically significant, it was not notably more pronounced within the 10-minute experimental window compared to the results obtained with the sweep current. This highlighted the need for further optimization of the sensor to enhance its detection capabilities. The transition to constant current did improve overall stability by reducing initial fluctuations, but the lack of substantial improvement in signal sensitivity compared to the sweep current method suggests that further refinements are necessary.

5.1.2 Effect of sample salt concentration on microplastic detection using constant current

We hypothesized that the electrolyte concentration will play a crucial role in the sensor's ability to detect microplastics under constant current conditions, as previously established for the sweep current tests. Similar to the results obtained with sweep current, the accumulation of microplastics diminished as the NaCl concentration increased from 300 ppm to 1000 ppm (Fig.5-2a). This reduction in microplastic accumulation at higher NaCl concentrations is primarily attributed to the decrease in the electric potential and electrophoretic force across the sensor.

While the overall trend of diminished accumulation with increasing salt concentration remained the same when using constant current, there was a notable improvement in microplastic accumulation compared to the sweep current method at the same salinity levels. Optically, the

results were significantly enhanced when transitioning from sweep to constant current, as the uninterrupted electric field provided a stronger and more consistent electrophoretic force. At the highest NaCl concentration of 1000 ppm, which presented the greatest challenge for microplastic detection, the use of sweep current proved ineffective, as no accumulation was observed at the anode (Fig. 5-2a(iii). However, under the same conditions, switching to constant current resulted in significant microplastic accumulation at the anode, a result that was not achieved with sweep current (Fig. 5-2a(vi)). Furthermore, even at lower NaCl concentrations, such as 300 ppm (Fig. 5-2a(i,iv)). and 650 ppm (Fig. 5-2a(ii,v)), microplastic accumulation was notably higher when using constant current. These findings clearly demonstrate the superiority of the constant current approach in overcoming the detection challenges associated with high salinity environments.

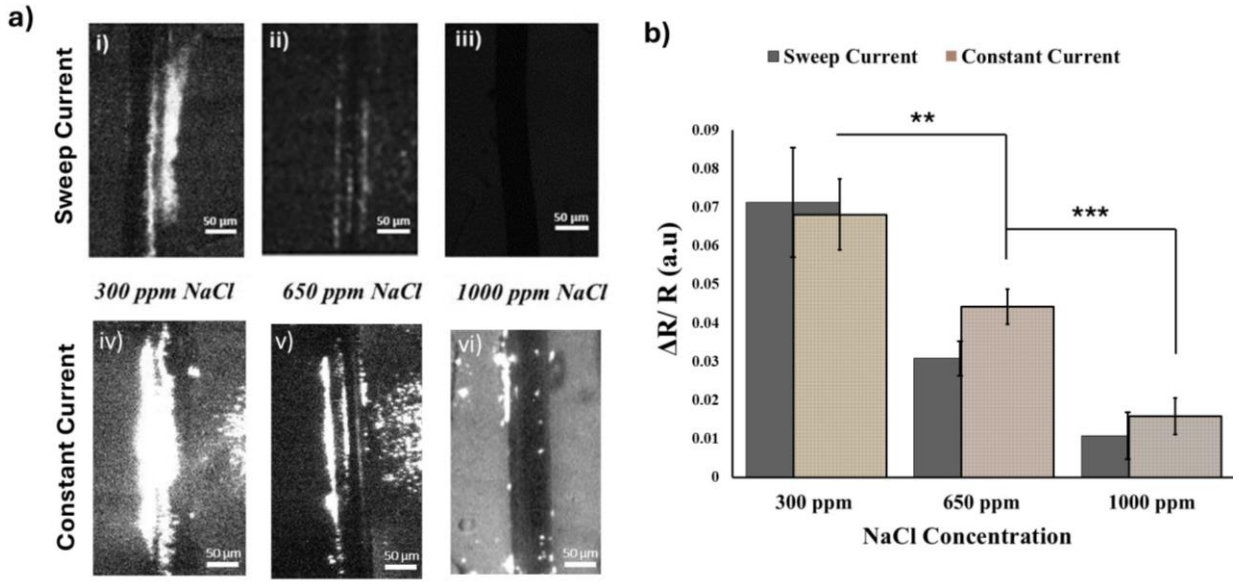

Fig. 5-2: Effect of salt concentration on microplastic (25 ppm) accumulation and the electrical resistance. a) Microplastic accumulation at the anode for i) 300ppm, ii) 650ppm and iii)1000ppm NaCl for sweep current application, and for iv) 300ppm, v) 650ppm, vi) 1000ppm for constant current application; b)

Normalized resistance drop at different salt concentrations for both sweep and constant current applications; **: $P < 0.01$, ***: $P < 0.001$; 3 independent trials.

The electrical response of the sensor was not significantly influenced whether sweep or constant current was applied. Although the constant current experiments yielded a slightly stronger normalized resistance drop compared to the sweep current counterparts, the results remained statistically indifferent between the two methods (Fig. 5-2b). As the salinity of the solution containing microplastics increased from 300 ppm to 1000 ppm, there was a noticeable decrease in the drop in electrical resistance. However, the difference in the normalized electrical resistance drop between the sweep and constant current methods was not statistically significant, with the Mann–Whitney U test yielding p-values greater than 0.05 for all NaCl concentrations tested. The smallest p-value occurred at 650 ppm NaCl, with a value of 0.0571, indicating that the difference between the methods was still not statistically significant. This suggests that while constant current improved optical detection, it did not significantly affect the electrical response compared to sweep current with varying salt concentration.

While the constant current method did improve optical detection by enhancing the accumulation of microplastics at the anode, a lack of significant variation in electrical resistance compared to the sweep current method was observed. This could be due to uneven or incomplete coverage of the microwire by the microplastics. Although more microplastics are being captured, they are not distributed evenly and completely along the surface of the wire to affect its electrical charge transfer capability significantly.

5.1.3 Influence of microplastic concentration on detection capabilities using constant current

The concentration of microplastics in the solution had a significant influence on both the optical and electrical detection capabilities of the sensor regardless of the characteristics of the applied current. Across all NaCl concentrations tested (300 ppm, 650 ppm, and 1000 ppm), the accumulation of microplastics at the anode increased with higher microplastic concentrations. Electrically, the sensor's response—represented by the normalized change in electrical resistance (ΔR/R)—followed a similar pattern of that using sweep current as seen in Fig. 5-3.

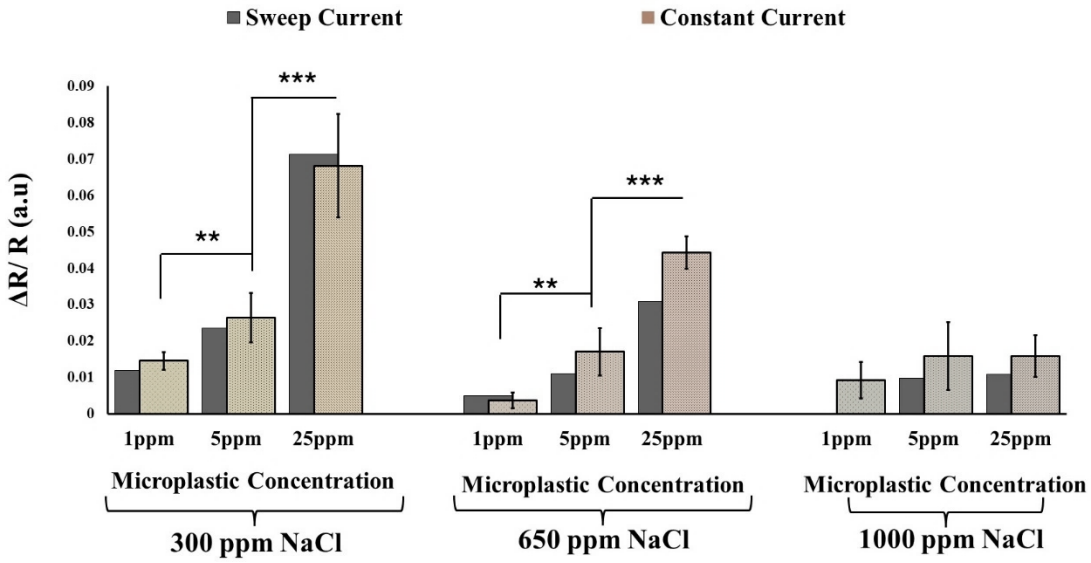

Fig. 5-3: Comparison of normalized electrical resistance drop (ΔR/R) between sweep current and constant current at various NaCl concentrations (300 ppm, 650 ppm, and 1000 ppm) and different microplastic concentrations (1 ppm, 5 ppm, and 25 ppm). *: $P < 0.05$, **: $P < 0.01$, ***: $P < 0.001$;. 3 independent trials.

At 300 ppm NaCl, the change in electrical resistance increased as the microplastic concentration increased from 1 ppm to 25 ppm. This trend continued at 650 ppm NaCl, with a more pronounced increase in $\Delta R/R$ between the 1 ppm and 5 ppm microplastic concentrations when using constant current (Fig. 5-3). Notably, the statistical significance of this difference increased to $p < 0.01$ (two stars), indicating a significant improvement in sensitivity at this concentration. However, the overall trend remained consistent, with higher microplastic concentrations resulting in a greater reduction in resistance.

At 1000 ppm NaCl, the sensor exhibited reduced sensitivity, as the electrical response to increasing microplastic concentrations was less pronounced. While the difference between 1 ppm and 5 ppm microplastic concentrations was still observable, the effect of further increasing the concentration to 25 ppm was diminished. This behavior suggests that at higher salinity levels, the detection capability of the sensor is hindered, possibly due to the reduced electrophoretic force acting on the microplastics as ionic strength increases.

While the constant current method significantly improved optical detection and showed promise at lower salinity levels, the reduced sensitivity at higher NaCl concentrations, particularly at 1000 ppm, highlighted a key limitation in the sensor's ability to effectively detect microplastics. As the salinity increases, the electrophoretic force acting on the microplastics weakens, resulting in diminished accumulation and a less pronounced electrical response. This behavior raises important questions about the underlying mechanisms that inhibit microplastic detection in high-salinity environments.

To address these challenges and gain deeper insight into the factors affecting microplastic accumulation, a numerical analysis was conducted. The next section (Section 5.2) presents a detailed exploration of the sensor's performance through numerical modeling. By simulating the behavior of microplastics within the sensor under varying salt concentrations, this analysis helps us better understand the reasons behind the reduced accumulation at higher NaCl levels. Additionally, it provides a foundation for optimizing the sensor design and enhancing detection capabilities, especially in challenging environments with elevated salinity, such as the 1000 ppm case discussed earlier.

5.2 Numerical analysis of the sensor

To validate the sensor's response and ensure that the observed accumulation was due to electrophoretic effects on the microplastics, a 2D numerical model was developed. The choice of a 2D model was made to simplify the complex geometry while capturing the essential physics of the electrophoretic accumulation of microplastics. The 2D numerical model was first developed, verified, and validated before being applied in a parametric study to determine the relationship between electrolyte concentration and microplastic accumulation. This subsection will first review the model's domain and mesh independence, followed by the verification and validation process of the 2D model.

5.2.1 Domain independency

To minimize the computational load in the numerical model, the channel length along the x-axis was set to a smaller value than the actual experimental sensor's length of 20 mm (Fig. 5-4a). To verify that this adjustment would not affect the outcomes, a series of simulations were conducted to evaluate the influence of varying channel lengths. The study involved decreasing the channel length from 20 mm to 2 mm and analyzing the velocity magnitude (Fig.5-4b) along the x-axis and the electric field (Fig.5-4c), measured along a vertical line in the y-axis. The results indicated that reducing the channel length had a negligible impact on the numerical results, including velocity magnitude and electric field. Consequently, a channel length of 2 mm was selected for the numerical simulations.

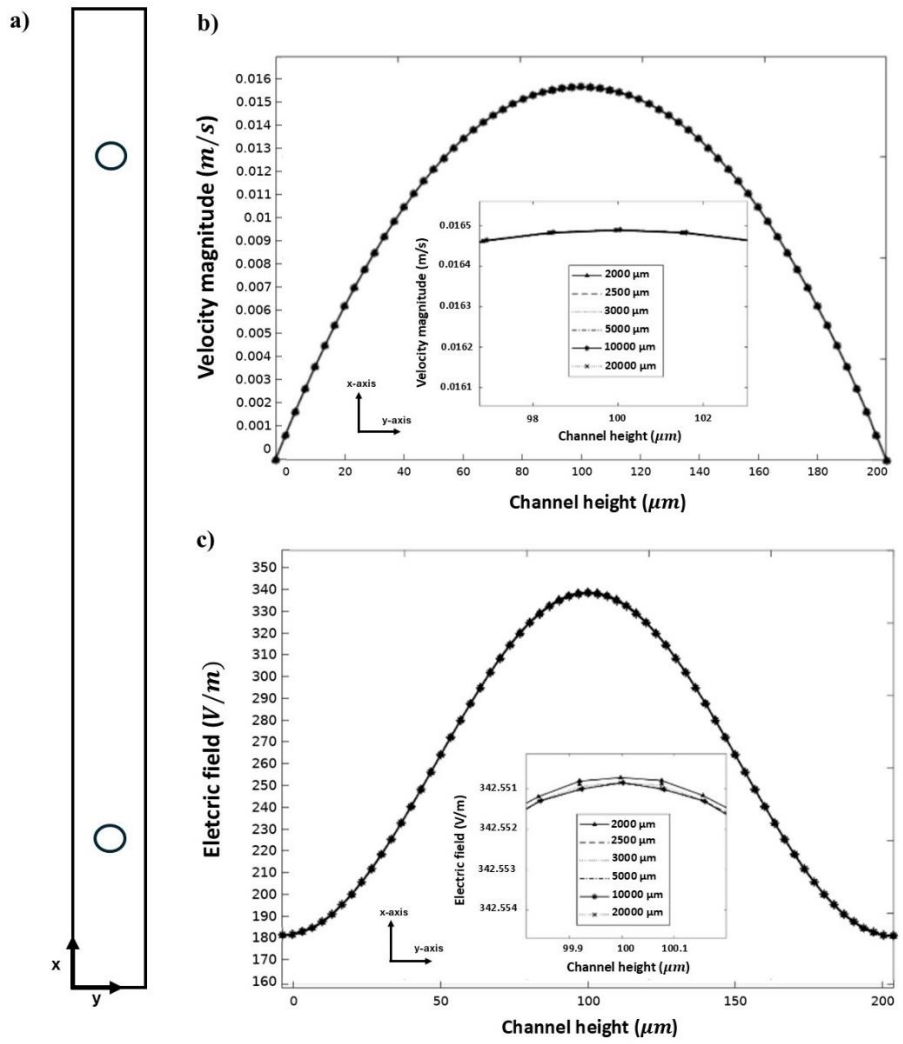

Fig. 5-4: Domain independence study of the primary sensor model. **a)** simple channel geometry used; **b)** Velocity magnitude in the x-direction and **(c)** electric field along the y axis, representing the channel height, are plotted. Microchannel lengths of 20, 10, 5, 3, 2.5, and 2 mm were investigated, as indicated in the legend.

5.2.2 Mesh independency

A user-controlled mesh was employed for the 2D model to ensure optimal control over element distribution. A free quad-style mesh was selected due to the relatively simple geometry of the straight channel. To capture the areas of greatest interest, the mesh was refined closer to the channel walls and around the electrodes, as these regions are expected to experience the highest velocity gradients and the most significant changes in the electric field (Fig. 5-5). Specifically, the boundary layers were carefully meshed to account for the interactions near the channel walls and the electrode surfaces. This refinement is crucial, particularly when running the particle tracking module, as the microplastics are expected to accumulate near the electrode, where electrophoretic forces are strongest.

The mesh independency was assessed by simulating the primary sensor's geometry under six different meshing conditions, with mesh elements ranging from 12,506 to over half a million and element sizes from 10 μm to 0.024 μm. As the number of elements increased, the overall mesh quality improved significantly. Initially, with 12,506 elements (Fig. 5-5a), the mesh quality was relatively low, with a minimum quality of 0.2462 and an average quality of 0.6121. After refining the mesh to 584,002 elements (Fig. 5-5b), the minimum quality improved to 0.5931, and the average quality increased to 0.9643. This improvement in mesh quality contributed to more accurate simulations, as higher quality meshes better resolve the geometry and physics of the sensor.

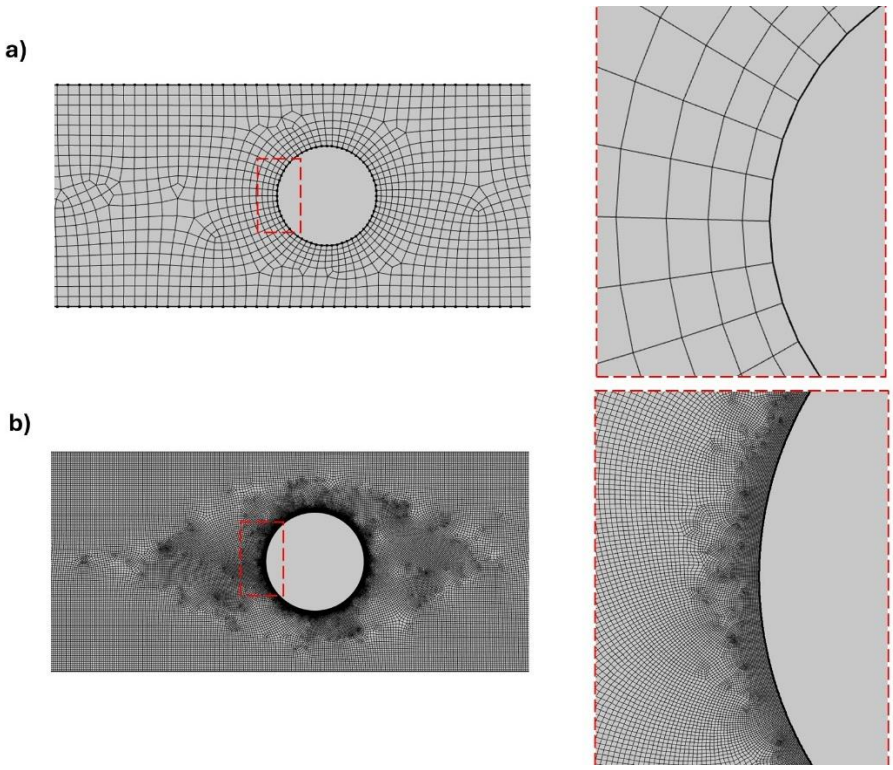

Fig. 5-5: Mesh configuration at two levels of refinement. **a)** Coarse mesh with 12,506 elements showing a simpler, less detailed discretization of the geometry**; b)** Finer mesh with 584,002 elements, providing greater accuracy and detail around the circular electrode. The red dashed boxes highlight the refined regions near the anode boundary, emphasizing the difference in mesh density between the two configurations.

The increase in mesh elements was focused particularly on refining the areas near the boundary conditions, especially around the electrodes where the electric field and velocity gradients are most significant (Fig.5-5). To achieve this, corner refinements and boundary layer refinements were applied, ensuring a smoother transition of mesh elements. A stretching factor of 1.05 was used for boundary layers to maintain a gradual element size increase while capturing the sharp gradients

effectively. These refinements ensured accurate resolution of the physical properties near the electrodes, which are critical for simulating the electric field and fluid behavior in the sensor.

To evaluate the impact of various mesh configurations, the electric field and velocity magnitude along the x-axis at the certain cut points was examined (Fig. 5-6a). These cut points were strategically selected along the channel where the most significant deviations in velocity and electric field were expected to occur. The initial configuration, which utilized 12,506 mesh elements, exhibited a significant deviation in velocity field compared to the other configurations, rendering it unreliable for accurate results and thus, it was excluded from further consideration.
The remaining configurations, which utilized more refine meshing in critical areas appeared similar at first glance. However, detailed analysis, including magnified views in Fig. 5-5b and Fig. 5-5c, revealed subtle differences. It was determined that increasing the number of mesh elements beyond 170,898 to 584,002 resulted in a maximum deviation of 0.09% in the maximum electric field strength (V/m), confirming that this configuration provided a balance between accuracy and computational efficiency. Therefore, the mesh configuration with 170,898 elements was chosen for the study.

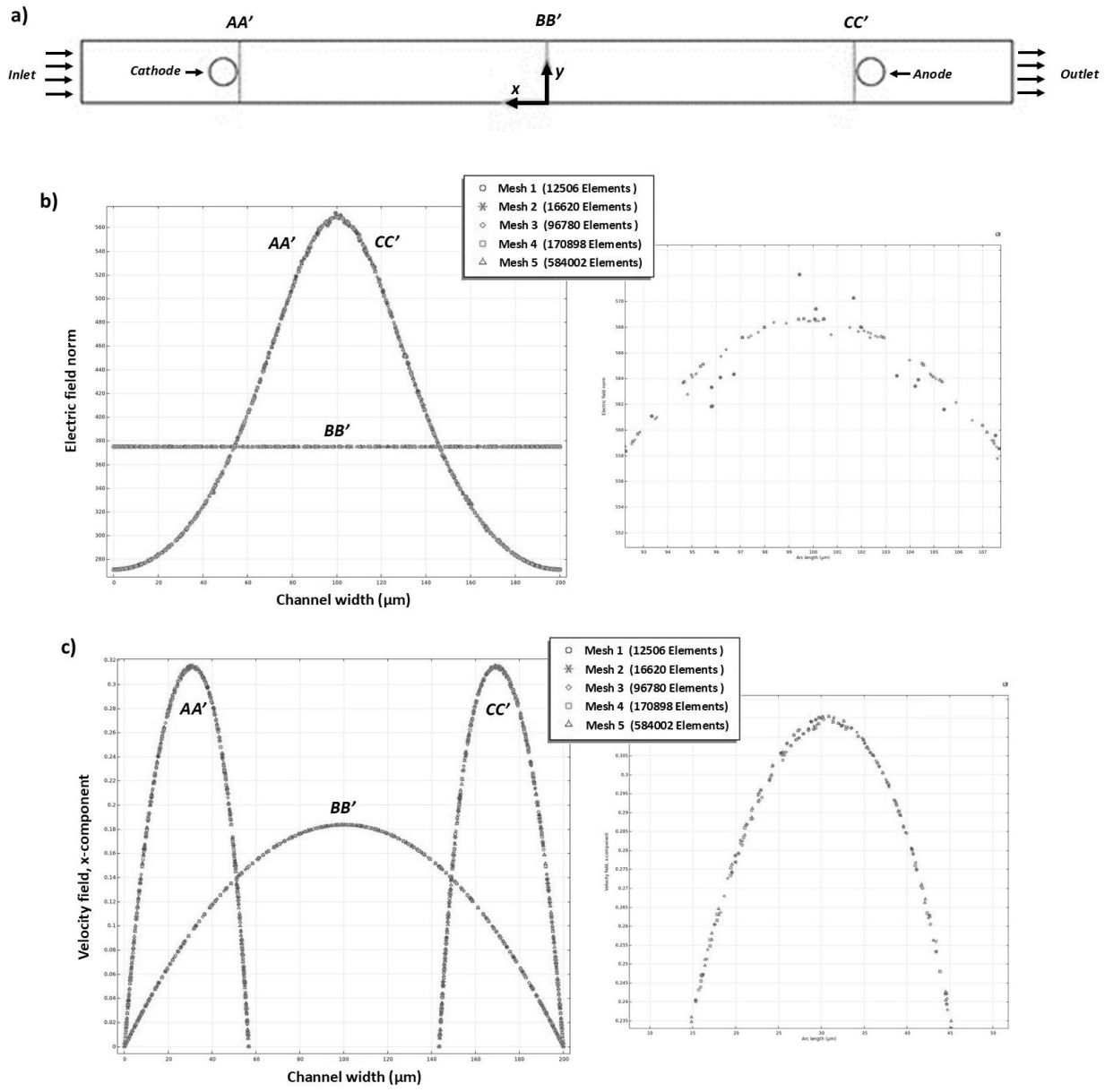

Fig. 5-6: Mesh independency of the primary sensor model. **a)** Diagram showing the cutlines AA', BB', and CC' across the channel, where data was analyzed along for mesh independency; **b)** Electric field norm across the channel width at different mesh densities, comparing results for five mesh configurations; **c)** Velocity field (x-component) across the channel width for the same five mesh configurations, showing mesh refinement impact on velocity calculations

5.2.3 Model Verification

To verify the model, several fundamental physical phenomena were analyzed using our numerical method. The fluid flow was first examined, confirming that it exhibited a parabolic pattern through the microfluidic channel, which is consistent with expected behavior. As the salt concentration increased, the electrolyte conductivity also increased, leading to a corresponding reduction in the electric field strength, as illustrated in Fig. 5-7. The electric field was computed along three different cutlines positioned along the channel length (Fig. 5-7a) for each salinity concentration (300 ppm, 650 ppm, and 1000 ppm).

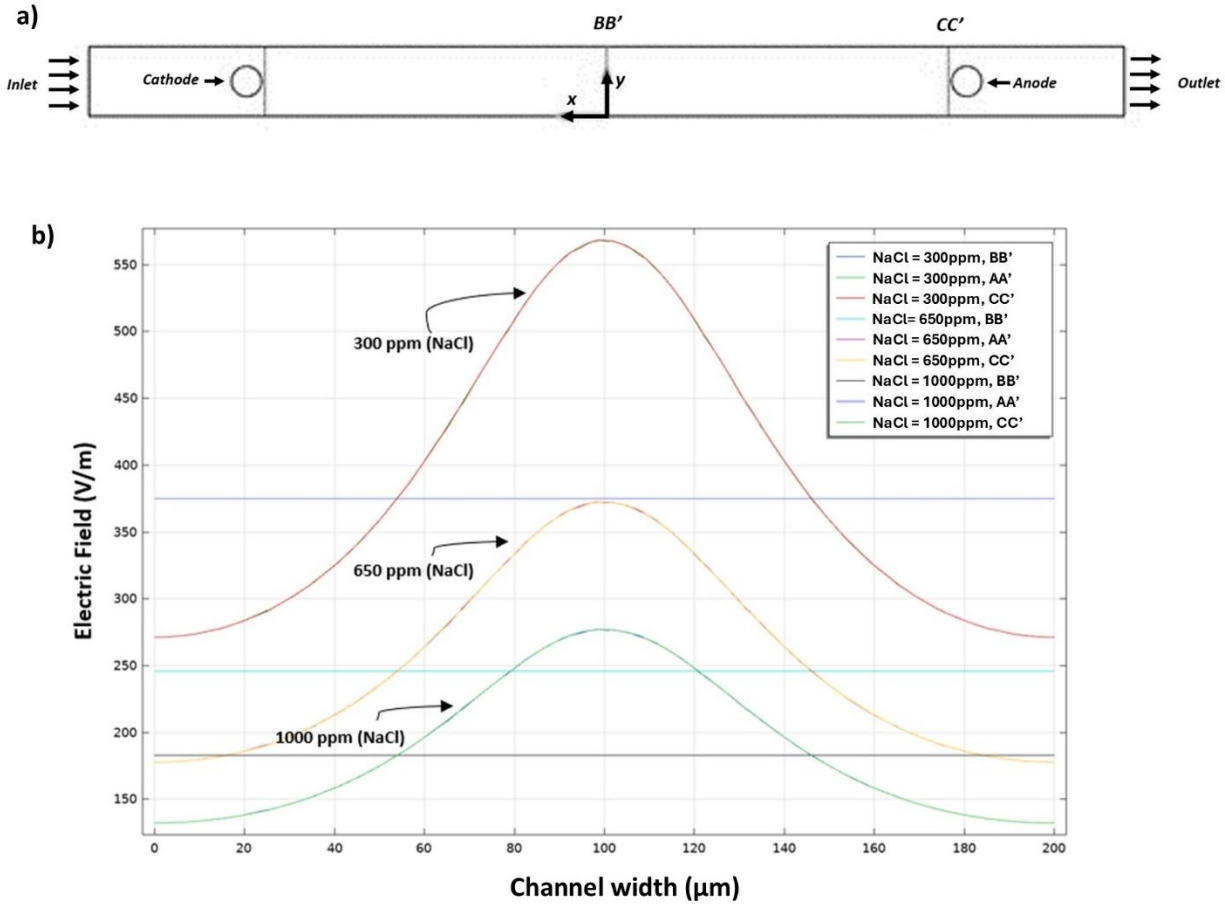

Fig. 5-7: Change in the electric field strength at; **a)** Diagram showing the cutlines AA', BB', and CC' across the channel, where data was analyzed along for mesh independency; **b)** Variation in the electric field strength along the channel width with changing NaCl concentration.

As expected, the electric field distribution near the electrodes exhibited a parabolic shape, with the field strength peaking near the electrode surfaces. In contrast, the electric field in the center of the channel remained relatively uniform, with significant variations primarily observed along the channel width. These observations helped validate the accuracy of the model in simulating the sensor's operating conditions. These results validated the model's ability to accurately simulate the sensor's electric field distribution under operating conditions. Additionally, the electric potential was observed to decrease progressively from its initial value at the terminal (anode) to zero at the ground (cathode), consistent with theoretical expectations (Fig. 5-8).

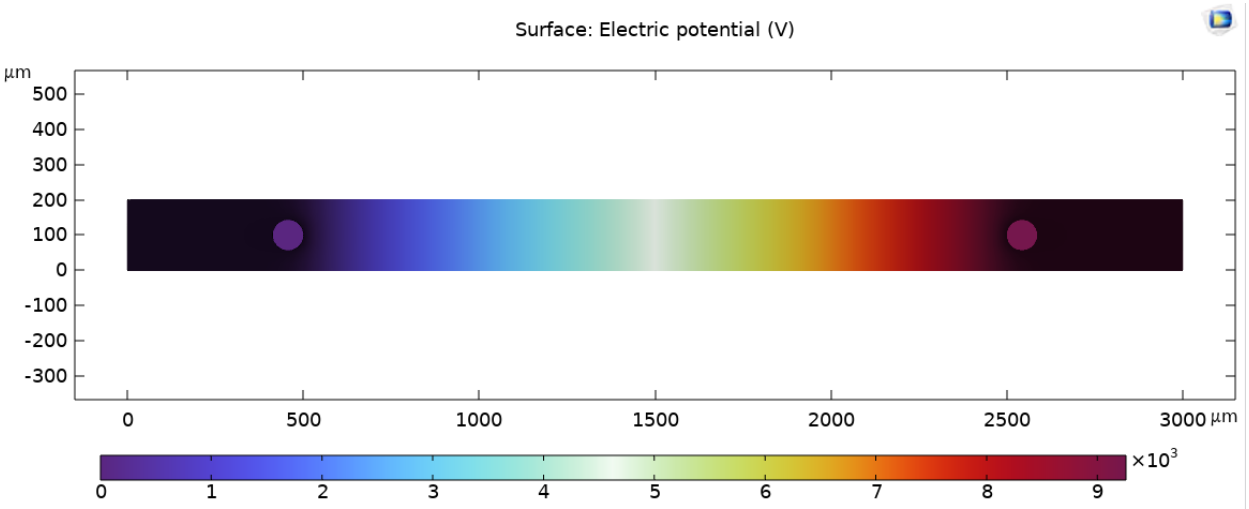

Fig. 5-8: The electric potential gradient between the anode and cathode

Further analysis reveled ion migration within the channel, with Na+ and Cl- ions accumulating around the ground and terminal electrodes due to the potential differences (Fig. 5-8). This ion accumulation became more pronounced at higher salt concentrations (Fig. 5-9), where increased ionic strength led to greater charge accumulation. The fluid flow in the channel induced convection, which dispersed these accumulated ions around the electrodes, reducing the concentration of free ions available for current transfer. These observations aligned with the underlying physics of ion migration and confirmed the model's accuracy in capturing the behavior of the system under different salinity conditions.

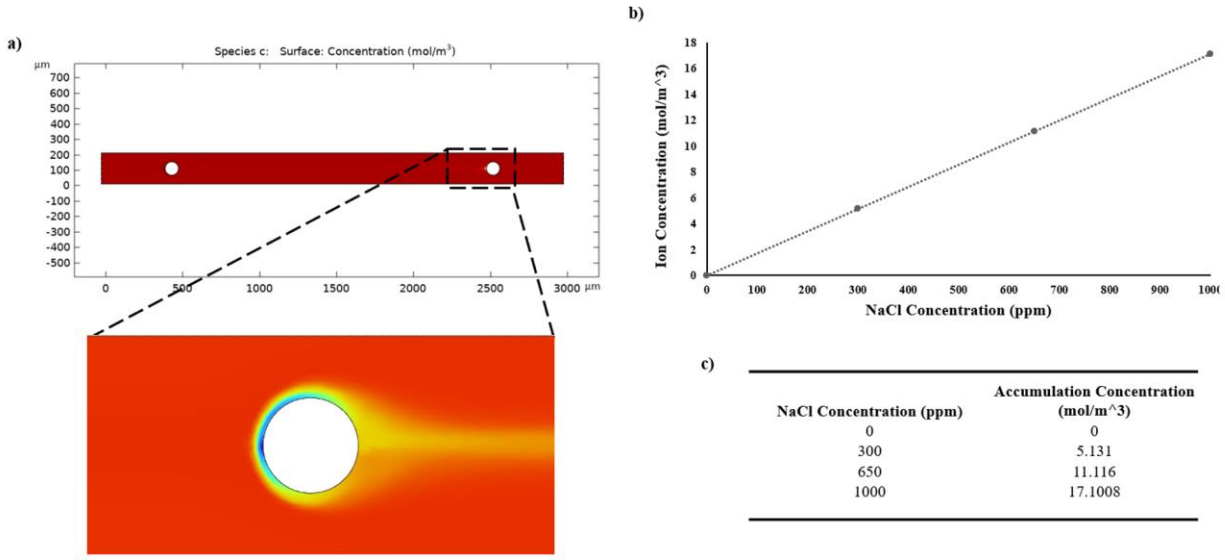

c)

NaCl Concentration (ppm)	Accumulation Concentration (mol/m^3)
0	0
300	5.131
650	11.116
1000	17.1008

Fig. 5-9: a) Accumulation of ions at the opposing terminal wire; **b)** A linear increase in ion concentration observed with increasing NaCl concentration; **c)** Ion concentration corresponding to various NaCl concentrations.

5.2.4 Model Validation

The numerical model was validated by comparing its results with experimental resistance values obtained from the sensor. Fig. 5-10 presents the mean electrical resistance values recorded in both the numerical and experimental studies, within the freshwater range of 300-1000 ppm NaCl concentration, corresponding to resistivities of 1.43 to 0.71 MΩ. As anticipated, the simulation results exhibited a perfectly linear relationship (R^2=1). However, discrepancies between the experimental and simulated datasets were observed, with differences of 5.75%, 12.54%, and 8.93% for 300 ppm, 650 ppm, and 1000 ppm NaCl concentrations, respectively.

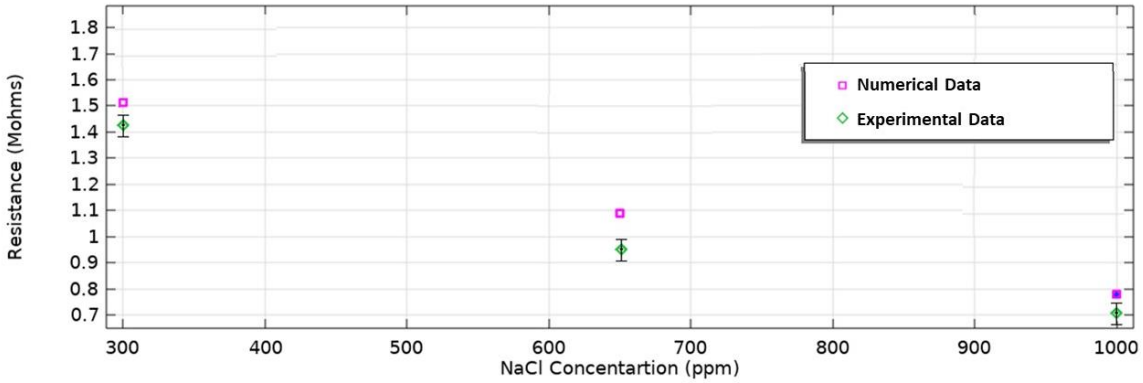

	300 ppm (NaCl)	650 ppm (NaCl)	1000 ppm (NaCl)
Experimental Resistance (M Ω)	1.42614809	0.952852846	0.709718523
Analytical Resistance (M Ω)	1.5130	1.0895	0.7793
Relative Error $\frac{R_A - R_E}{R_A}$	5.75 %	12.54%	8.93%

Fig. 5-10: Numerical simulation results compared to the experimentally measured resistance.

These discrepancies are primarily due to the simulation's inability to account for imperfections like slight irregularities in the microchannel geometry, minor inaccuracies in channel dimensions,

misalignment of the microwires, or the presence of small air pockets. Variations in temperature and impurities in the experimental samples could further influence the results. Despite these differences, the percentage deviations are within an acceptable range for this type of sensor analysis, given the complexity of real-world factors that are difficult to fully simulate.

5.2.5 Electrophoretic Accumulation of Microplastics

The numerical method was employed to investigate the electrophoretic accumulation of microplastics under varying electrolyte concentrations, with a particular focus on the highest concentration of NaCl, 1000 ppm. This concentration represents a challenging environment for electrophoretic accumulation due to the elevated ion density within the solution as seen in Fig. 5-9, which was also observed experimental (Fig. 5-2a (iii, vi)).

Initially the numerical model was used to simulate the behaviour of microplastics in absence of the electrophoretic force, providing foundational understanding of their movement (Fig. 5-11a). The objective was to observe the natural behaviour of the particles, solely under the influence of the fluid flow and without any applied electric field. As expected, the microplastics moved through the channel in response to the velocity field, following the flow direction without any additional forces acting upon them. This provided the baseline results for comparison.

Following this initial simulation, the electrophoretic force was introduced to examine its impact on the microplastics' behavior. It is important to note that the electric field, laminar flow and the transport of diluted species models were computed under steady-state conditions, however, the

movement of the microplastics was simulated using a transient particle tracking model, which captures the dynamic and time-dependent behavior of the microplastics as they responded to the electric field. The electrophoretic force is heavily influenced by the conductivity of the solution (eq.3-3). Without any NaCl dilution within the sample, the electric field within the channel remained strong. As a result, the electrophoretic force was highly effective in directing the movement of microplastics. As expected, the simulation showed that majority of the negatively charged microplastics were directed toward and accumulated at the positive anode, as they came in contact with the induced electric field, confirming the sensor's ability to effectively concentrate microplastics under ideal, low-ionic-strength conditions (Fig. 5-11b).

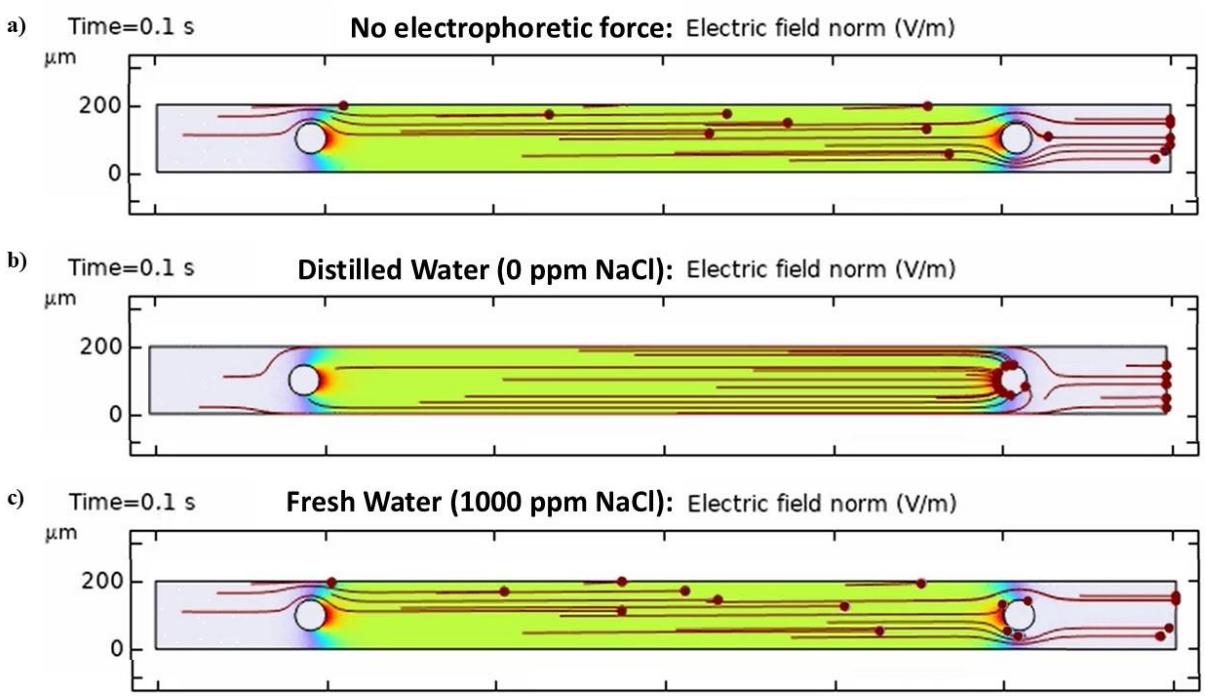

Fig. 5-11: Microplastic tracking within the channel: **a)** Microplastic movement without applied electrophoretic force; **b)** Microplastic movement and accumulation under electrophoretic force in distilled water; **c)** Microplastic movement and accumulation under electrophoretic force in 1000 ppm NaCl solution.

The simulation was then applied to a 1000 ppm NaCl concentration, which, as shown by previous experimental results, led to minimal accumulation (Fig. 4-2a) and an insignificant electric response (Fig. 4-2b). This simulation aimed to determine whether, by maintaining consistent experimental conditions, electrophoretic accumulation of microplastics could still be achieved at this high concentration. The high NaCl concentration resulted in a significant decrease in the electric field strength within the channel, which in turn reduced the electrophoretic force available to drive microplastic accumulation (eq.3-3). Consequently, while some accumulation of microplastics was observed, it was far less pronounced than in the scenarios without NaCl (Fig. 5-11c). Upon increasing the NaCl concentration from 0 ppm to 1000 ppm, the number of microplastics accumulated at the anode dropped, representing a 60% decrease in accumulation over the span of 0.1 seconds. This lower level of accumulation aligns with our experimental findings, supporting that increasing salt concentration diminishes microplastic accumulation due to the weakened electric field (eq.3-2) and the formation of a double layer around the particles (eq.3-4).

When transitioning from distilled water to freshwater with a 1000 ppm NaCl concentration, the time required for microplastics to accumulate at the anode increased significantly. In the case of distilled water, where the solution was free of ions, the particles reached the anode in just 0.00634 seconds due to the strong electrophoretic force acting on them as seen in Fig. 5-12a.

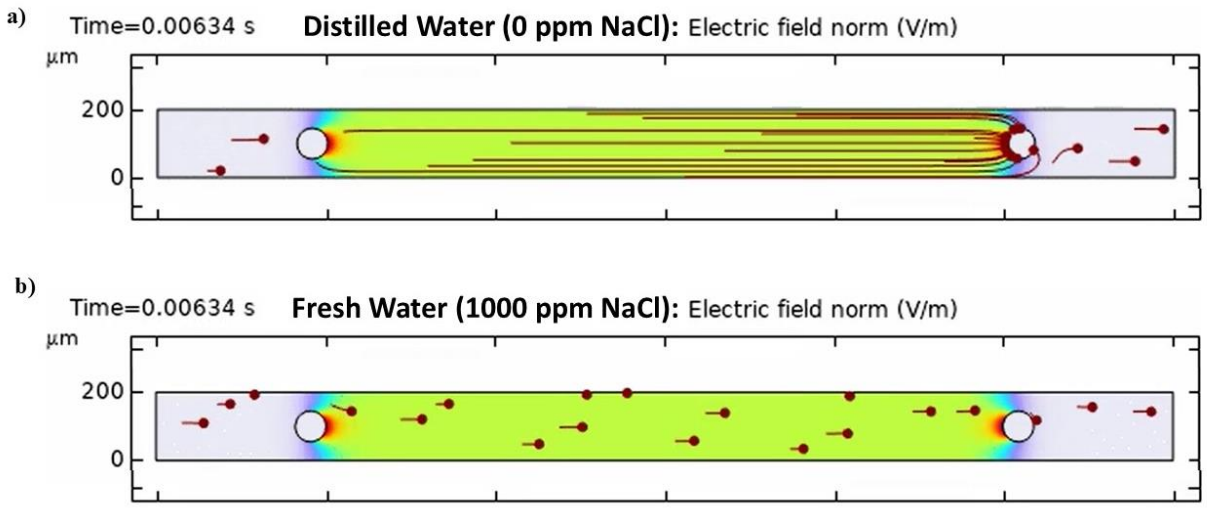

Fig. 5-12: Accumulation of microplastics at t=0.00634 seconds for **a)** distilled water condition and **b)** 1000 ppm NaCl concentration solution.

With the introduction of ions in the 1000 ppm NaCl solution, the accumulation process slowed considerably (Fig. 5-12b). The particles moved toward the anode at a much slower rate, with the furthest microplastics taking 0.048 seconds to reach the anode. This represents a nearly 7.6-fold increase in the time required for accumulation, highlighting the significant impact of ionic strength on the electrophoretic process.

The numerical simulations provided valuable insights into the behavior of microplastics under varying electrolyte concentrations and highlighted the significant influence of ionic strength on electrophoretic accumulation. In low-ionic-strength conditions, such as distilled water, the simulations showed rapid and effective accumulation of microplastics at the anode, closely mirroring the strong electric field in the channel. However, as the NaCl concentration increased to 1000 ppm, the simulations revealed a substantial reduction in electric field strength, resulting in a

dramatic slowdown in microplastic accumulation and a decrease in particle concentration at the anode. These findings align closely with the experimental results, where diminished microplastic accumulation and weaker electrical signals were noted at higher salinity levels. The numerical model confirmed that the primary factors contributing to reduced sensor performance in high-salinity environments were the decreased electrophoretic force and the formation of a double layer around the microplastics, which reduced their effective movement (Fig. 5-11 and Fig. 5-12). The consistency between the numerical simulations and experimental data strengthens the conclusion that further optimization of the sensor is required to overcome the challenges posed by elevated salinity, particularly for freshwater monitoring applications with high salt concentrations. The model can be used in the future to perform this optimization with respect to the design of the microfluidic device.

5.3 Enhancing Sensor Sensitivity

In the earlier sections of this chapter, two key limitations were identified in the detection of microplastics: the reduced sensitivity of the sensor at higher salt concentrations, particularly at 1000 ppm NaCl, and the instability of the electrical signal when using traditional detection methods such as sweep current and constant current. To address these issues, two solutions were explored: the implementation of a Wheatstone bridge and the functionalization of the microwires with MXene. The Wheatstone bridge was introduced to isolate and amplify small voltage changes caused by microplastic accumulation, reducing noise and improving measurement precision. This approach aimed to improve sensitivity, particularly in high-salinity environments where detection becomes more difficult. Additionally, MXene—a 2D material known for its high affinity to

microplastics—was applied to the microwires to enhance microplastic accumulation. This functionalization was expected to improve the overall detection efficiency by increasing the density of microplastics accumulated at the anode and thereby amplifying the sensor's electrical response.

5.3.1 Implementing Wheatstone Bridge

The Wheatstone bridge shown in Figures 3-8 and 3-9 was implemented to improve the precision of voltage measurements by isolating small changes in resistance caused by microplastic accumulation. Initially, the bridge was balanced with a constant voltage, ensuring a stable baseline. As microplastics accumulated around the anode, the resistance shifts, resulting in a measurable voltage change across the bridge as discussed in section 3.2.2.1. This setup minimizes signal fluctuations and noise, allowing for more accurate detection of microplastics by focusing solely on the small voltage changes, rather than the overall resistance, enhancing measurement accuracy in saline environments particularly at high salt levels (e.g., 1000 ppm NaCl) where the sweep and constant current techniques previously showed lack of sensitivity.

After implementing the Wheatstone bridge, microplastics were observed to accumulate at the anode due to the induced electrophoretic force, which is a result of the negative surface charge on the microplastics interacting with the applied electric field. This accumulation was tracked optically and through changes in the electrical signal for a period of 10 minutes, keeping the experimental conditions constant. As the microplastics began to accumulate, a noticeable change in the output voltage (V_{out}) in the Wheatstone bridge was detected. To ensure accuracy, this voltage

change was averaged over 60-second intervals, allowing for a more precise observation of how the accumulation progressed over time, as explained in section 3.2.2. Different concentrations of NaCl (300, 650, and 1000 ppm) and microplastic suspensions (1, 5, and 25 ppm) were compared to a base solution, and the obtained data in Fig. 5-13 showed a clear, consistent relationship between increased microplastic concentration and changes in the electrical signal.

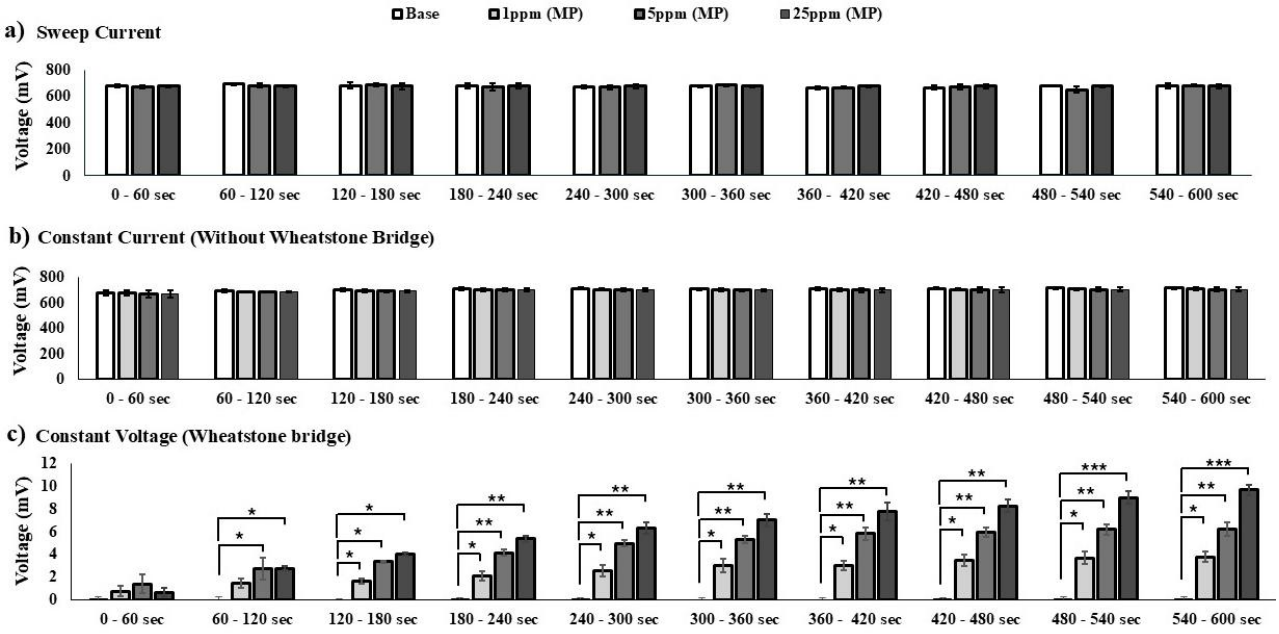

Fig. 5-13: Comparison of voltage response across different detection methods and microplastic concentrations at 1000 ppm NaCl concentration. **(a)** Sweep current: the average voltage remains stable for all runs with and without microplastics, indicating minimal change in the signal using sweep current. **(b)** Constant Current: Similar to the sweep current results, the voltage shows little variation across time intervals for different microplastic concentrations, suggesting that the constant current method without the Wheatstone bridge does not significantly enhance the detection signal. **(c)** Constant Voltage (Wheatstone Bridge): The implementation of the Wheatstone bridge shows a clear voltage increase over time as

microplastic concentration increases. Statistical significance is denoted by *: $P < 0.05$, **: $P < 0.01$, ***: $P < 0.001$. 3 independent trials.

The results confirmed a direct correlation between microplastic accumulation and the change in electrical signal, as seen in prior experiments. However, the use of the Wheatstone bridge markedly enhanced the sensitivity of the measurements. Unlike the setups using a simple electrical sweep (Fig. 5-13a) or constant (Fig. 5-13b) current, the Wheatstone bridge amplified the signal output (Fig. 5-13c), resulting in a more robust and detectable voltage change. This enhancement allowed for more precise measurements across varying salinity and microplastic concentrations, especially at higher conductivity levels where the signal from traditional methods became inconsistent. By isolating small voltage changes caused by microplastic accumulation, the Wheatstone bridge effectively minimized noise and stabilized the output signal.

The Wheatstone bridge's ability to isolate and measure only the small voltage shifts, rather than total resistance, reduced the noise inherent in previous methods. This significantly improved the signal-to-noise ratio, particularly at lower microplastic concentrations. The results demonstrated that the enhanced electrical signal output provided by the Wheatstone bridge not only improved the reliability of the sensor but also enabled more accurate detection of microplastics in challenging saline environments. For instance, at a 1000 ppm NaCl concentration and 1 ppm microplastic concentration, the voltage change using the sweep current method ranged from 677.9 mV to 675.4 mV. Similarly, the constant current method without the Wheatstone bridge showed a voltage drop from 716.8 mV to 706.4 mV, but both methods had high error bars, around 20 mV, for both the base and microplastic runs. In contrast, using the Wheatstone bridge, the voltage change was far

more pronounced, from 0.023 mV to 6.233 mV, with a much smaller error bar of around 0.5 mV. This significant reduction in noise and greater voltage difference clearly demonstrates the Wheatstone bridge's superior sensitivity and accuracy. These improvements are especially important in high-salinity environments like 1000 ppm NaCl, where conventional methods struggle due to fluctuations and high error margins. The enhanced performance of the Wheatstone bridge allows for more accurate detection of microplastics, making it a critical improvement for monitoring in challenging saline environments.

5.3.1.1 Effect of salinity concentration

Building on the enhanced detection capabilities introduced by the Wheatstone bridge, it was essential to examine how varying salinity levels affected the sensor's performance. Since the salinity of freshwater typically falls within the range of 300 to 1000 ppm NaCl, this study focused on evaluating microplastic detection within this salt concentration range. In this experiment, NaCl concentrations of 300 ppm, 650 ppm, and 1000 ppm were tested to observe how salinity affected the accumulation of microplastics and the subsequent change in the output voltage (V_{out}). The Wheatstone bridge was initially balanced to establish a stable baseline, and then the voltage change was measured as microplastics accumulated at the anode over a 10-minute period. Results are shown in Fig. 5-14.

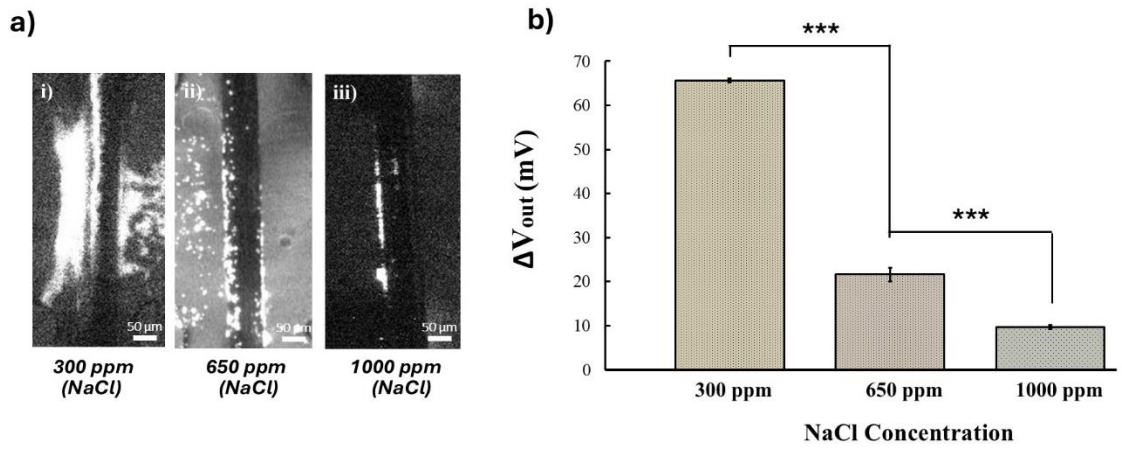

Fig. 5-14: Effect of salt concentration on microplastic (25 ppm) accumulation and the electrical resistance measured over the last 60 seconds of the 10 min run using a Wheatstone bridge configuration. **a)** Microplastic accumulation at the anode for i) 300ppm, ii) 650ppm and iii)1000ppm NaCl; **b)** Normalized resistance drop at different salt concentrations; ***: $P < 0.001$; 3 independent trials.

As expected, the increase in NaCl concentration led to a noticeable reduction in microplastic accumulation (Fig.5-14a). This reduction is consistent with previous experiments conducted without the Wheatstone bridge, where higher salinity levels caused a decrease in electrophoretic force. The higher ionic strength in more saline solutions screened the surface charge of the microplastics, which reduced their migration toward the anode. At the highest concentration of 1000 ppm (Fig.5-14a(iii)), this screening effect was most pronounced, resulting in minimal microplastic accumulation.

The diminished accumulation of microplastics at higher salinity levels also led to a smaller voltage change ΔV_{out} within the Wheatstone bridge (Fig.5-14b). While the bridge remained sensitive enough to detect changes in microplastic concentration, the voltage difference was significantly

less at 1000 ppm (9.68 mV) compared to 300 ppm (65.68 mV) or 650 ppm (21.62 mV). This decrease in V_{out} is directly correlated with the reduced accumulation, as fewer microplastics near the anode result in a smaller change in resistance. Notably, the statistical analysis of the voltage changes revealed that the differences between the microplastic concentrations at each NaCl level were highly significant, with $p < 0.001$, resulting in a 3-star significance level (***). This further reinforces the effectiveness of the Wheatstone bridge in distinguishing between different microplastic concentrations even when the accumulation is reduced due to higher salinity. It should be noted that detection of microplastics with the sweep current and constant current (without Wheatstone bridge) methods at 1000 ppm NaCl was not possible as shown in Fig. 5-13.

5.3.1.2 Sensitivity and quantification across different microplastic concentrations

In this section, we examine the sensor's ability to detect and quantify various microplastic concentrations using the Wheatstone bridge, as shown in Fig. 5-15. The study investigated microplastic concentrations of 1 ppm, 5 ppm, and 25 ppm, across three different salinity levels (300 ppm, 650 ppm, and 1000 ppm NaCl). The results demonstrate that the Wheatstone bridge effectively differentiated between all tested microplastic concentrations, producing distinct and measurable voltage changes (ΔV_{out}) at each concentration level.

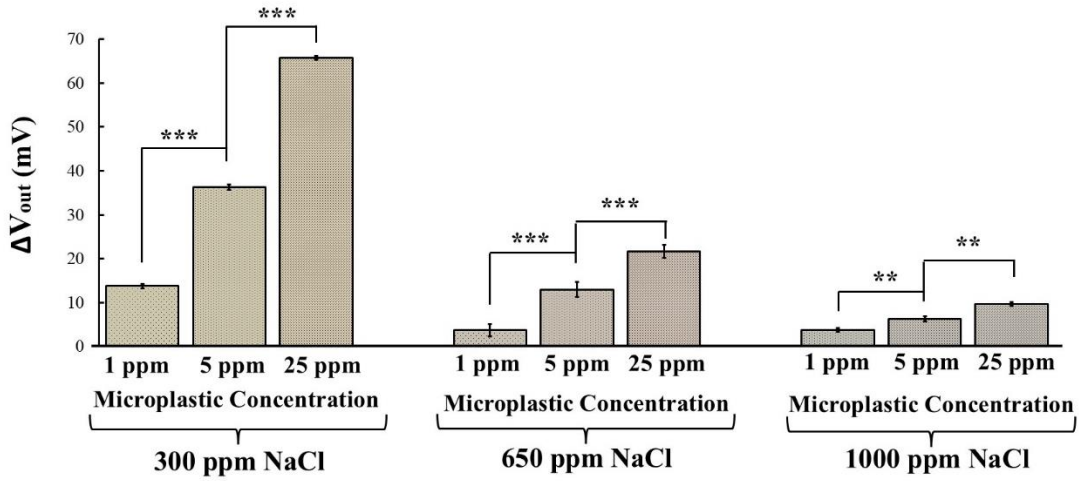

Fig. 5-15: Comparison of the change in Wheatstone bridge voltage at various NaCl concentrations (300 ppm, 650 ppm, and 1000 ppm) and different 1µm microplastic concentrations (1 ppm, 5 ppm, and 25 ppm) measured over the last 60 seconds of the 10 min run; **: P < 0.01, ***: P < 0.001; 3 independent trials.

As expected, the change in voltage increased with higher microplastic concentrations, showing a direct relationship between microplastic accumulation and the resulting electrical signal. For instance, at 300 ppm NaCl, V_{out} increased from 13.74 mV for 1 ppm to around 65.78 mV for 25 ppm. A similar trend was observed across all salinity concentrations, as show in Table 5-1. The change in voltage decreased as the NaCl concentration increases, or as the microplastic concentration decreased. This reduction in voltage is due to factors explained in section 5.3.1.1 (i.e., reduced electrophoretic force with increasing salinity).

Table 5-1: Voltage change in mV (V_{out}) between initial (t=0s) and final (t=600s) measurements for different microplastic concentrations across varying NaCl levels

	1 ppm (microplastic)	**5 ppm** (microplastic)	**25ppm** (microplastic)
300 ppm (NaCl)	13.74942	36.23366	65.67914
650 ppm (NaCl)	4.695439	12.98634	21.62311
1000 ppm (NaCl)	3.749423	6.233663	9.679143
P < 0.05	** ***P < 0.01***	*** ***P < 0.001***	

The ability of the Wheatstone bridge to distinguish between these microplastic concentrations is a significant improvement over previous method. In earlier experiments using either constant current or sweep current applications, we observed similar trends in voltage change with respect to microplastic concentration. However, the sensitivity of the Wheatstone bridge far exceeds that of the prior setups. The bridge amplified even the smallest differences in microplastic concentration, which were previously obscured by noise and large error bars, especially in higher salinity conditions.

One of the key improvements seen with the Wheatstone bridge is its ability to maintain sensitivity across a wide range of NaCl concentrations. Unlike prior methods, where error bars associated with resistance measurements made it challenging to accurately distinguish between different microplastic concentrations, the Wheatstone bridge significantly reduced measurement variability. This reduction in error allowed for clear separation between different microplastic concentrations, regardless of the NaCl concentration used in the experiment.

5.3.2 Microwires Functionalization for Affinity to Microplastics

To enhance microplastic accumulation at the anode, the microwires were functionalized with a coating of MXene (Ti_3C_2Tx), a 2D material known for its ability to trap and extract microplastics from aqueous environments [70,71]. MXenes porous, multilayered structure provides a large surface area that promotes the adsorption and entrapment of microplastics, thereby increasing the accumulation at the anode and amplifying the sensor's electrical output signal. The coating process followed a two-step method, as outlined in the methodology section (3.2.2.2). MXenes affinity for microplastics, as demonstrated in previous literature, is crucial for increasing the efficiency of microplastic detection by promoting targeted accumulation, which in turn enhances the sensor's electrical response.

The SEM images of both the uncoated and MXene-coated microwires can be seen in Fig. 5-16. This figure displays the uncoated copper wire (Fig. 5-16a), serving as a control, while Fig. 5-16b, shows the MXene-coated wire. The uncoated wire exhibits a smooth surface, in contrast to the coated wire, which displays a homogeneous and consistent MXene layer across the surface of the microwires. At higher magnification, the images reveal the multilayered structure of the MXene coating. This structure increases the surface area, potentially allowing for greater interaction with microplastics. This increased surface area is one of the key factors behind MXene's ability for trapping microplastics, as it provides more binding sites for microplastic particles to attach to the surface of the wire.

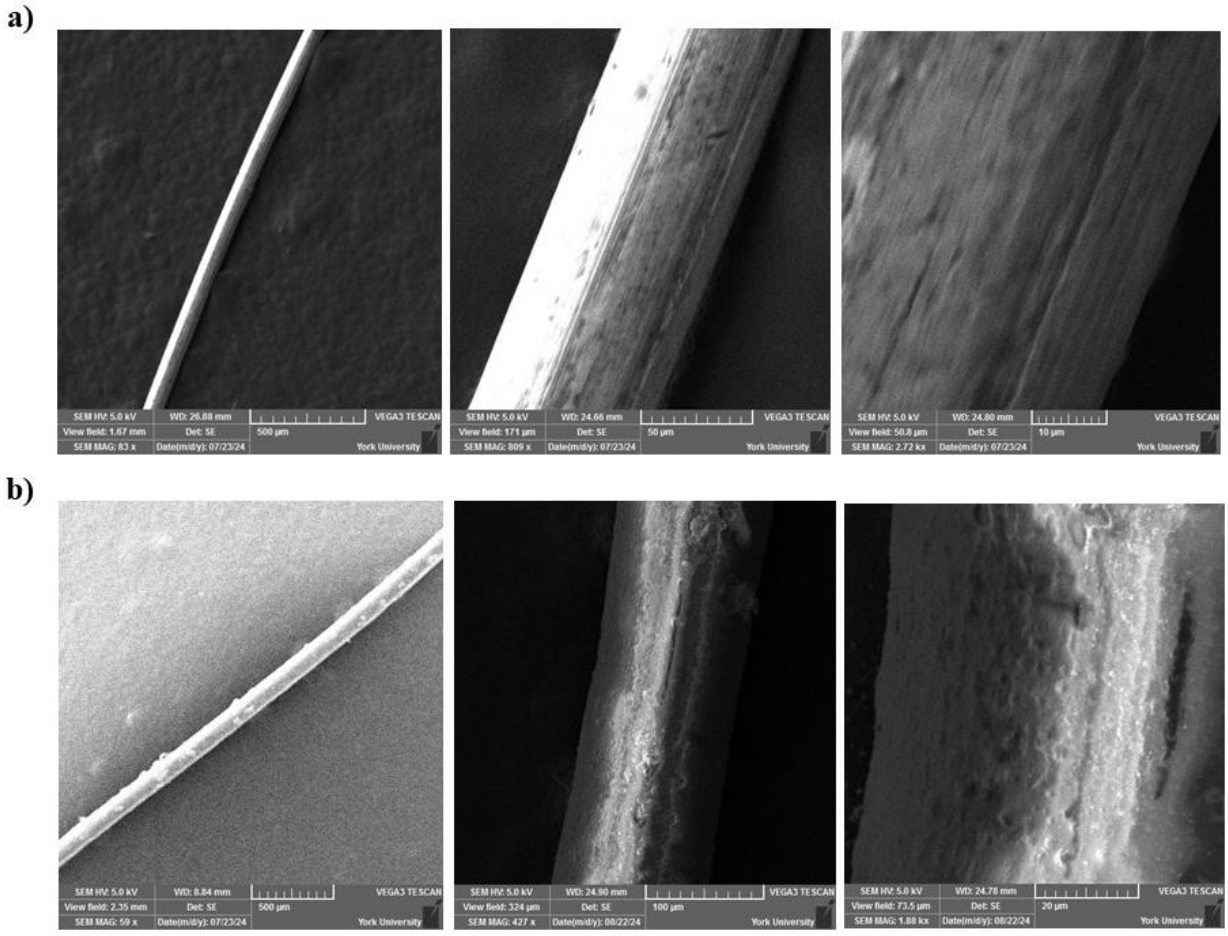

Fig. 5-16: SEM images of; **a)** Uncoated copper microwire; **b)** MXene coated copper wire at different magnifications.

The use of MXene-coated microwires led to significantly higher microplastic accumulation density compared to bare copper wires, as shown in Fig. 5-17. For this experiment, the NaCl concentration was set at 1000 ppm, and the microplastic concentration was 1 ppm. This specific combination was chosen as it represents a worst-case scenario, where the sensor typically performs the least effectively in capturing and detecting microplastics. Higher levels of salinity diminish the electrophoretic force, while lower microplastic concentrations result in weaker signals. MXene

was applied to the microwires to improve the sensor's performance under these challenging conditions.

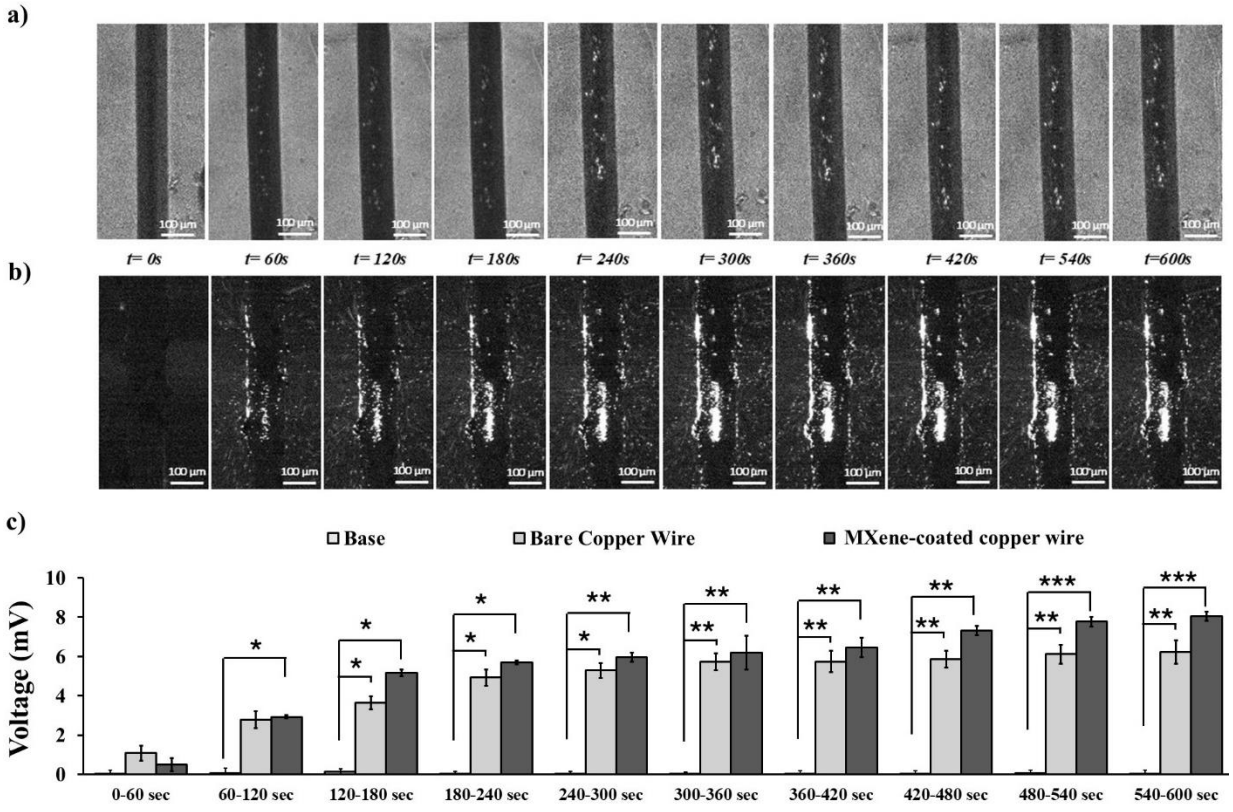

Fig. 5-17: Comparison of microplastic accumulation on bare copper wire and MXene coated microwire for 1000ppm NaCl concentration and 1ppm microplastics concentration; **a)** Time-lapse images of microplastic accumulation on the bare copper wire over 10 minutes; **b)** Time-lapse images of microplastic accumulation on the MXene-coated microwire over 10 minutes; **c)** Voltage change over time for base solution, bare copper wire, and MXene-coated microwire. *: $P < 0.05$, **: $P < 0.01$; 3 independent trials.

In Fig. 5-17a, which shows the time-lapse of microplastic accumulation on the bare copper wire, we observe a gradual increase in accumulation, but the overall density of microplastics on the

surface remains limited. In contrast, Fig. 5-17b presents the time-lapse images for the MXene-coated microwire. The accumulation begins earlier and at a much higher density, with a significant amount of microplastics visibly concentrated along the length of the microwire as time progresses. By the end of the 10-minute period, the MXene-coated microwire shows a much more pronounced accumulation of microplastics than the bare copper wire.

Additionally, Fig. 5-17c quantifies the corresponding voltage change (ΔV_{out}) over time. The MXene-coated microwire demonstrates a much larger voltage change compared to the bare copper wire, with a clear and statistically significant difference ($p < 0.05$, $p < 0.01$) in the output signal. Specifically, over the last 60 seconds of the run, the voltage change for the MXene-coated microwire was 8.045 mV, whereas for the bare copper wire, it was 6.22 mV, confirming that MXene was more effective in enhancing microplastic capture and improving the sensor's electrical response. Moreover, the MXene-coated microwire achieved microplastic accumulation much faster, which is reflected in the voltage change. By 120 seconds, the voltage change for MXene had already reached 5.15 mV, while the bare copper wire lagged behind at 3.64 mV. This faster voltage change indicates that MXene not only increases the overall accumulation but also accelerates the process, resulting in quicker and more sensitive detection of microplastics.

5.4 Effect of Microplastic Size

Following the successful detection and differentiation of varying microplastic concentrations (1ppm, 5ppm, 25ppm) in the freshwater salinity range (300-1000 ppm NaCl), we extended our investigation to assess the sensor's ability to detect and quantify microplastics based on particle

size. The focus here was to determine whether the sensor could distinguish between different sizes of polystyrene microplastics, specifically 1 µm, 5 µm, and 10 µm spherical particles. Given the findings from earlier experiments, we know that the sensor's performance decreases at higher salinity levels, particularly at 1000 ppm NaCl, due to the reduction in electrophoretic force and increased screening effect around the microplastics. This setting presents the most difficult conditions for detection, making it an ideal scenario to evaluate the sensor's sensitivity to size differences. Therefore, 1000 ppm NaCl was chosen as the target salinity for this analysis.

The results indicate a distinct difference in accumulation patterns based on microplastic size, with 1 µm (Fig.5-18a(i)) and 5 µm (Fig.5-18a(ii)) particles accumulating more effectively at the anode, while the accumulation of 10 µm particles (Fig.5-18a(iii)) was notably lower. This variation can be attributed to several factors related to particle dynamics within the microfluidic environment.

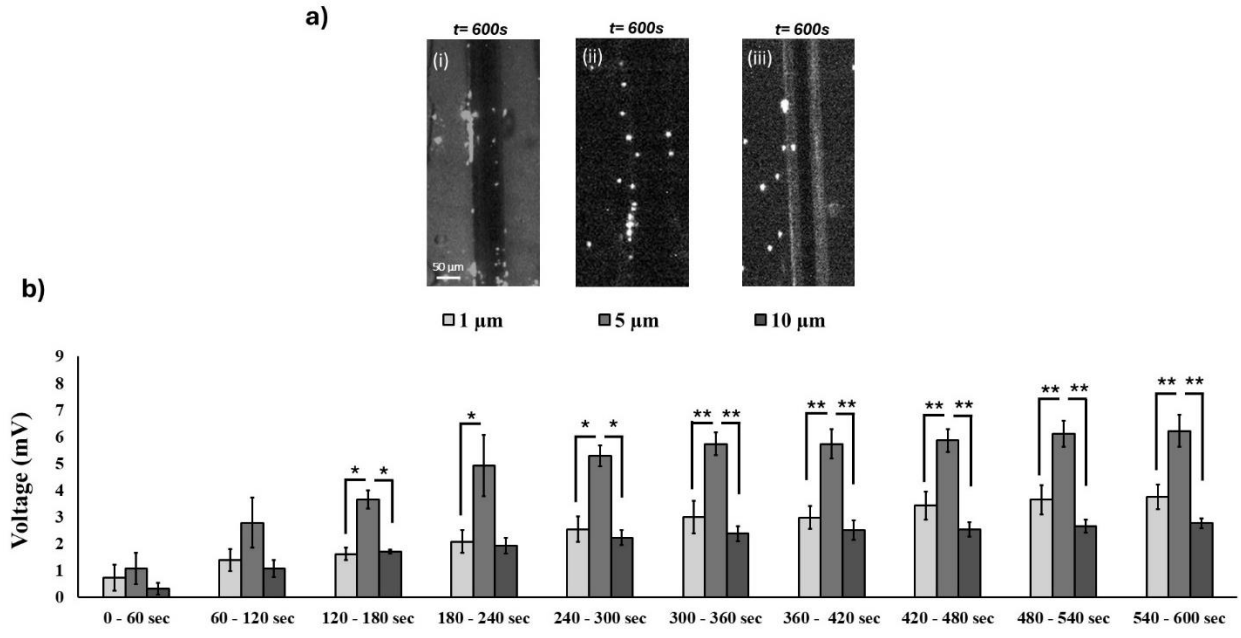

Fig. 5-18: Comparison of polystyrene microplastic sizes in saline solution of 1000ppm NaCl and 1ppm microplastic concentration; **a)** optical accumulation at the anode after 600s for i) 1 µm ii) 5 µm, and iii) 10 µm microplastic sizes; **b)** change in the output voltage for each particle size over the complete 10min run; *: $P < 0.05$, **: $P < 0.01$; 3 independent trials.

Firstly, the larger 10 µm particles experience greater hydrodynamic drag, which, combined with their higher inertia, makes them potentially less responsive to the electrophoretic force compared to smaller particles. Although the flow rate is sufficient to push these larger particles across the sensing zone, the interplay between drag, inertia, and the weaker relative influence of the electrophoretic force means that fewer 10 µm particles are directed toward the anode within the 10-minute timeframe. Additionally, during the experiment, it was observed that some of the 10 µm particles settle to the bottom of the channel and adhere to the sensor wall. This settling effect likely occurs due to the greater mass of the larger particles, which increases their tendency to sediment under gravity, especially in a laminar flow setting. Once these particles contact the channel wall, they are more likely to stick, further reducing their chances of reaching the anode.

Despite the observed differences in accumulation for the 1 µm, 5 µm, and 10 µm particles, the sensor was still able to detect the presence of each size effectively through changes in the output voltage (ΔV_{out}), as shown in Fig. 5-18b. However, differentiating between the 1 µm and 10 µm particles proved challenging, as the voltage drop for these two sizes was quite similar. This similarity in the electrical response suggests that the accumulation density of 1 µm and 10 µm particles, while differing visually, resulted in comparable resistive changes, likely due to the lower accumulation rate for the larger particles counterbalancing the higher accumulation density of the

smaller ones. In contrast, the 5 µm particles produced a more distinct and statistically significant change in voltage, showing a greater separation from both the 1 µm and 10 µm results. This enhanced statistical differentiation for the 5 µm particles indicates that this size may represent an optimal balance within the sensor's detection range, where both the electrophoretic force and particle response within the electric field are well-matched to achieve a clear and distinguishable signal.

5.4.1 Effect of microplastic size on enhanced sensor performance

To further investigate the sensor's ability to detect and quantify microplastic sizes, we explored the combined effects of MXene coating and the Wheatstone bridge configuration. Given that MXene has demonstrated significant potential in increasing microplastic accumulation due to its high surface area and affinity for microplastic particles, we aimed to determine if coating the anode with MXene could enhance the accumulation of larger 10 µm particles, which previously showed lower accumulation levels. By combining the MXene coating with the Wheatstone bridge setup, we sought to improve the sensor's signal response and its ability to differentiate between particle sizes. The MXene coating was specifically applied to the anode to leverage its porous structure and multilayered surface, which promotes microplastic entrapment. With the Wheatstone bridge configuration enhancing the sensitivity of the voltage measurement, this setup was designed to maximize accumulation and signal output, especially for the challenging 10 µm particles. This combination aimed to increase the detectability and statistical differentiation of each microplastic size (1 µm, 5 µm, and 10 µm), providing clearer quantification across sizes.

The MXene-coated microwire compared to the bare copper wire showed to increase the measure change in voltage (Fig.5-19), however the most significant improvement was observed for the 10 µm particles. Specifically, the change in voltage for the 1 µm particles increased from 3.75 mV with the bare copper wire to 4.63 mV with the MXene-coated wire, representing a 23.5% increase. Similarly, for the 5 µm particles, the voltage rose from 6.22 mV to 7.05 mV, corresponding to a 13.4% increase. The most pronounced improvement was observed with the 10 µm particles, where the voltage increased significantly from 2.77 mV to 4.27 mV, showing a 54.2% increase.

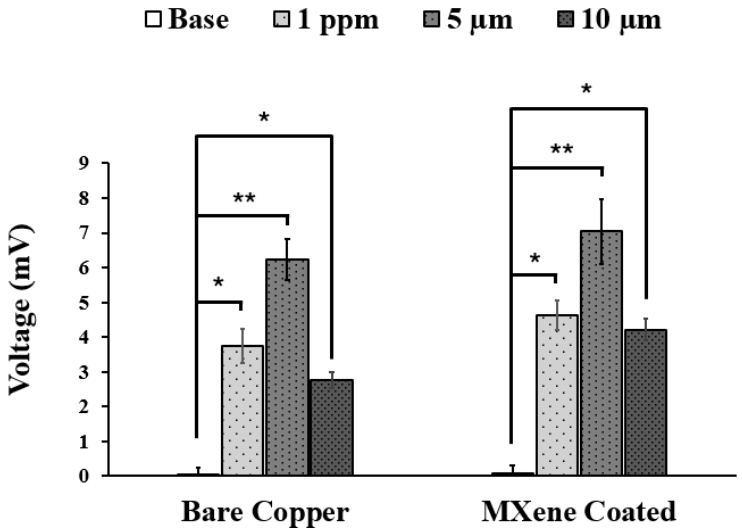

Fig. 5-19: Comparison of Wheatstone bridge voltage change (ΔV_{out}) over the last 60sec of the 10 min run for different microplastic sizes (1 µm, 5 µm, 10 µm) using bare copper and MXene-coated microwires; *: P < 0.05, **: P < 0.01; 3 independent trials.

Despite this improvement, statistical analysis revealed that the voltage changes for all microplastic sizes, including the 10 µm particles, were not significantly different when compared to the baseline voltage of the base solution. While the MXene coating did enhance the signal response, particularly

for the larger particles, these improvements were not large enough to reach statistical significance in comparison to the baseline. The use of MXene coating, as shown in Fig. 5-20, increased the voltage change and electrical output signal for all particle sizes (1 µm, 5 µm, and 10 µm) compared to the bare copper wire over the 10min run. However, despite this improvement in signal strength, the MXene coating did not enhance the sensor's ability to differentiate between particle sizes. In fact, the statistical difference between the 1 µm and 10 µm particles decreased as the voltage change increased for both sizes.

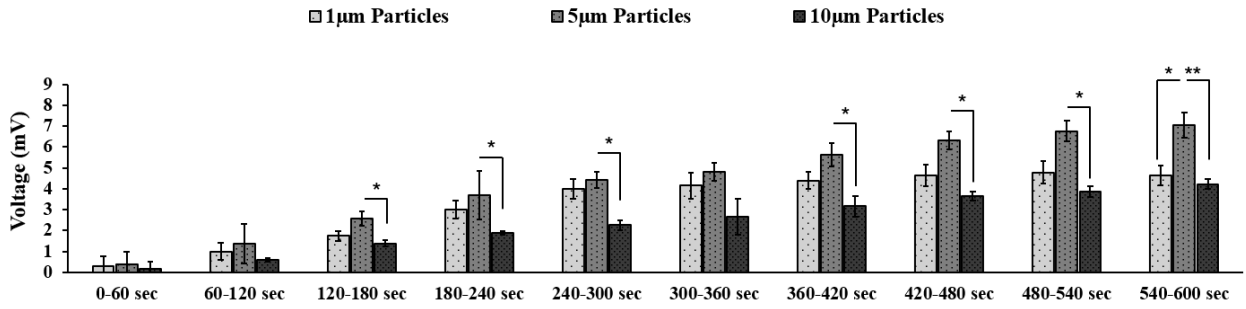

Fig. 5-20: Comparison of the change in output voltage for microplastic sizes in saline solution of 1000 ppm NaCl and 1ppm microplastic concentration; *: $P < 0.05$, **: $P < 0.01$; 3 independent trials.

Notably, after 300 seconds using the bare copper wire, a statistically significant 2-star ($p < 0.01$) difference was observed between the 1 µm and 5 µm particles, as well as between the 5 µm and 10 µm particles (Fig. 5-19). However, after the complete 10-minute run with the MXene-coated wire, the statistical difference between the 1 µm and 5 µm particles decreased to 1-star significance ($p < 0.05$), while the 5 µm and 10 µm particles maintained a 2-star significance ($p < 0.01$) (Fig. 5-20). While the MXene coating led to a notable increase in voltage for the 1 µm and 10 µm particles,

with both sizes showing improved signal output, the increased voltage response appeared to overlap, making it difficult to clearly quantify the particle sizes. The 5 µm particles still showed the most distinct voltage change and statistical differentiation, but the 1 µm and 10 µm particles became less distinguishable from one another after applying the MXene coating.

5.5 Limit of Detection and Sensitivity Zone

The integration of the Wheatstone bridge and MXene-coated microwires has enhanced the sensor's capability for quantitative detection of microplastics in saline freshwater environments. As shown in Fig. 5-21, the dose-response curve for the sensor at a NaCl concentration of 650 ppm exhibits logarithmic response over the entire concentration range of 0.1 ppm to 100 ppm for 1 µm polystyrene microplastics. The voltage change (ΔV_{out}) exhibits a power-law response, increasing steadily across the entire range of concentrations. The response is more pronounced at higher concentrations, reflecting the sensor's consistent performance.

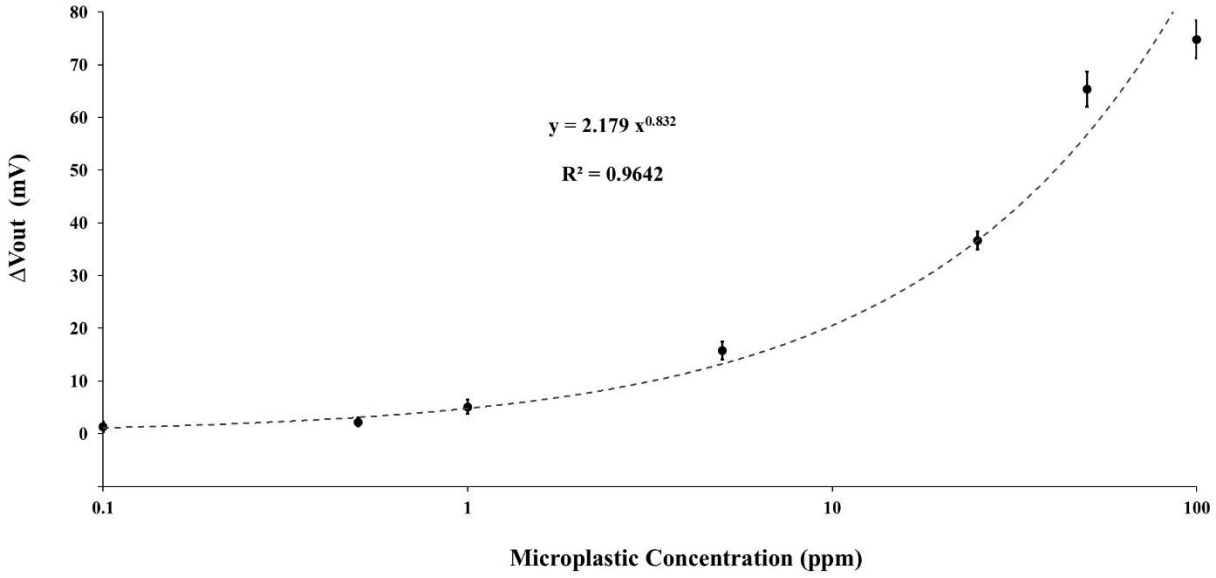

Fig. 5-21: Dose-response curve for sensor response (ΔV_{out}) as a function of 1µm polystyrene microplastic concentration (ppm) in the range of 0–100 ppm exhibiting a power-law behavior. The sensor response is modeled by the equation $y = 2.179.x^{0.832}$ with a high correlation ($R^2 = 0.962$). The curve illustrates the steady increase in response across the concentration range, with a diminishing rate of increase at higher concentrations

Several fitting functions were explored to model the dose-response data, including logarithmic and power-law equations. A power-law model ($y = 2.179.x^{0.832}$) was determined to provide the best fit, with a strong goodness-of-fit value ($R^2 = 0.962$), indicating excellent agreement between the model and the experimental data. This was significantly better than the logarithmic model, which showed noticeable deviations at multiple concentrations. The high R^2 value validates the choice of the power-law model as the most suitable representation of the sensor's response.

The power-law behavior highlights the sensor's capability to detect minimal but impactful levels of microplastic contamination while maintaining consistent performance across a broad range of concentrations. At concentrations below the limit of detection (LOD), the sensor's signal cannot be reliably distinguished from noise, making detection uncertain. In contrast, concentrations above the limit of quantification (LOQ) enable precise and accurate measurements, ensuring dependable quantification of microplastics. Using this sensitivity, along with the 3σ approach the signal corresponding to LOD (eq. 9) [54] and the 10σ approach for the signal corresponding to LOQ (eq. 10) [54], was calculated.

$$S_{\mathrm{LOD}} = S_{Blank} + (3 \times \sigma_{\mathrm{blank}}) \tag{9}$$

$$S_{\mathrm{LOQ}} = S_{Blank} + (10 \times \sigma_{\mathrm{blank}}) \tag{10}$$

These thresholds were substituted into the best-fit power model, yielding an **LOD of 0.825 ppm** and an **LOQ of 3.38 ppm**. This process ensures accurate determination of the sensor's detection limits.

The optimized sensor demonstrates the ability to detect and quantify microplastics at exceptionally low concentrations. Its high sensitivity and robust response enable precise monitoring of microplastic contamination in saline freshwater environments, particularly at trace levels. However, due to the sensor's power-law response, the rate of increase in signal diminishes at higher concentrations, indicating saturation.

Chapter 6: Thesis summary and future work

6.1 Thesis summary

This thesis presents the optimization and sensor enhancement of a microfluidic sensor designed to detect microplastics in saline water environments, addressing a significant gap in current environmental monitoring technologies. The research focused on three primary objectives: characterizing sensor performance, investigating the detection mechanisms, and optimizing sensor sensitivity under varying conditions of salinity and microplastic concentration. Through experimentation, the sensor's response was evaluated across a range of NaCl concentrations (0 to 1000 ppm) and microplastic suspensions (1 ppm to 25 ppm), revealing a direct correlation between microplastic accumulation and a drop in electrical resistance. Lower salt concentrations facilitated better sensor performance, while higher salinity weakened the electrophoretic force, leading to diminished detection sensitivity.

Detection was achieved both optically and through electrical measurements, with the electrophoretic accumulation of microplastics at the anode driving a measurable change in resistance. However, under high salinity conditions, the sensor struggled to maintain its sensitivity, necessitating further optimization. To improve its performance, the implementation of a constant current method stabilized the electric field, while the integration of a Wheatstone bridge significantly enhanced the ability to detect subtle voltage changes caused by microplastic accumulation. The functionalization of microwires with MXene further boosted microplastic capture, particularly in challenging conditions such as high salinity and low microplastic

concentrations. Despite these advancements, challenges remained, particularly in distinguishing between different microplastic sizes, which required further refinement.

In addition to experimental work, numerical modeling was employed to validate the sensor's behavior under different saline conditions, confirming the sensitivity drop at higher ionic strengths and providing insights into the microplastics electrophoretic behavior. Overall, this research contributes a cost-effective and scalable solution for detecting microplastics in freshwater environments, though future work is needed to enhance performance in higher salinity conditions and improve size differentiation for a wider range of particle types.

6.2 Limitations and recommendations for future research

The limitations of this study primarily revolve around the sensor's sensitivity in high salinity environments, especially at NaCl concentrations nearing 1000 ppm. Under these conditions, the electrophoretic force weakens significantly, reducing the microplastic accumulation around the anode and thus hindering the sensor's detection capability. Although improvements, such as the Wheatstone bridge configuration and MXene functionalization, helped enhance the sensor's performance, they were still challenged by high salt levels, leading to inconsistent results, particularly when detecting larger microplastic particles (e.g., 10 μm). These particles exhibited variable accumulation rates, and their corresponding electrical signals were less consistent, further highlighting the need for optimization.

Future research should address these limitations by refining the sensor design to increase its sensitivity in high-salinity conditions. One potential approach involves investigating alternative materials with stronger affinities for microplastics, such as advanced functional coatings or nanomaterials, to improve accumulation rates and detection. Additionally, expanding the sensor's range to detect smaller microplastic particles and improving its quantification accuracy across various particle sizes would increase its applicability in environmental monitoring.

Incorporating biological elements such as algae or bacterial colonies into the testing environment could also simulate more realistic water samples, as biological matter in natural water systems may influence microplastic behavior. This would provide insights into the sensor's robustness in detecting microplastics in complex, real-world conditions. Furthermore, introducing different types of microplastics, including variations in polymer composition (e.g., polyethylene, polypropylene) and shapes (e.g., spheres, fibers, fragments), could provide a comprehensive assessment of the sensor's capabilities and potential limitations in more diverse scenarios.

Moreover, enhancing sensor reproducibility and standardizing experimental protocols would ensure consistent results, especially when applied to real-world water systems. The integration of machine learning algorithms or advanced signal processing techniques could further refine the sensor's ability to differentiate between microplastic concentrations and sizes, even under noisy or fluctuating environmental conditions. Finally, conducting field tests in natural water bodies with varying salinity levels and organic matter content would offer valuable insights into the sensor's practical performance and scalability for environmental monitoring applications.

References

1. Fan J, Zou L, Duan T, Qin L, Qi Z, Jiaoxia Sun. Occurrence and distribution of microplastics in surface water and sediments in China's inland water systems: A critical review. *J Clean Prod*. 2022;331:129968. doi:10.1016/J.JCLEPRO.2021.129968

2. Cai Y;, Li C;, Zhao YA, et al. A Review of the Migration and Transformation of Microplastics in Inland Water Systems. *Int J Environ Res Public Heal 2022, Vol 19, Page 148*. 2021;19(1):148. doi:10.3390/IJERPH19010148

3. Wu M, Tang W, Wu S, Liu H, Yang C. Fate and effects of microplastics in wastewater treatment processes. *Sci Total Environ*. 2021;757:143902. doi:10.1016/J.SCITOTENV.2020.143902

4. Enfrin M, Dumée LF, Lee J. Nano/microplastics in water and wastewater treatment processes – Origin, impact and potential solutions. *Water Res*. 2019;161:621-638. doi:10.1016/J.WATRES.2019.06.049

5. Issac MN, Kandasubramanian B. Effect of microplastics in water and aquatic systems. *Environ Sci Pollut Res 2021 2816*. 2021;28(16):19544-19562. doi:10.1007/S11356-021-13184-2

6. Wei XF, Bohlén M, Lindblad C, Hedenqvist M, Hakonen A. Microplastics generated from a biodegradable plastic in freshwater and seawater. *Water Res*. 2021;198:117123. doi:10.1016/J.WATRES.2021.117123

7. Ugwu K, Herrera A, Gómez M. Microplastics in marine biota: A review. *Mar Pollut Bull*. 2021;169:112540. doi:10.1016/J.MARPOLBUL.2021.112540

8. Wang W, Ge J, Yu X. Bioavailability and toxicity of microplastics to fish species: A review. *Ecotoxicol Environ Saf*. 2020;189:109913. doi:10.1016/J.ECOENV.2019.109913

9. Thiele CJ, Hudson MD, Russell AE, Saluveer M, Sidaoui-Haddad G. Microplastics in fish and fishmeal: an emerging environmental challenge? *Sci Reports 2021 111*. 2021;11(1):1-12. doi:10.1038/s41598-021-81499-8

10. Godoy V, Blázquez G, Calero M, Quesada L, Martín-Lara MA. The potential of microplastics as carriers of metals. *Environ Pollut*. 2019;255:113363. doi:10.1016/J.ENVPOL.2019.113363

11. Scopetani C, Cincinelli A, Martellini T, et al. Ingested microplastic as a two-way transporter for PBDEs in Talitrus saltator. *Environ Res*. 2018;167:411-417. doi:10.1016/J.ENVRES.2018.07.030

12. Kwon JH, Kim JW, Pham TD, et al. Microplastics in Food: A Review on Analytical Methods and Challenges. *Int J Environ Res Public Heal 2020, Vol 17, Page 6710*. 2020;17(18):6710. doi:10.3390/IJERPH17186710

13. Egbeocha CO, Malek S, Emenike CU, Milow P. Feasting on microplastics: ingestion by and effects on marine organisms. *Aquat Biol*. 2018;27:93-106. doi:10.3354/AB00701

14. Cunha C, Lopes J, Paulo J, et al. The effect of microplastics pollution in microalgal biomass production: A biochemical study. *Water Res*. 2020;186:116370. doi:10.1016/J.WATRES.2020.116370

15. van der Meulen M, de Vriese L, Lee J, et al. Socio-economic impact of microplastics in the 2 Seas, Channel and France Manche Region. An initial risk assessment. Published online December 31, 2013. Accessed August 1, 2024. https://archimer.ifremer.fr/doc/00287/39834/

16. Prata JC, da Costa JP, Duarte AC, Rocha-Santos T. Methods for sampling and detection of microplastics in water and sediment: A critical review. *TrAC Trends Anal Chem*. 2019;110:150-159. doi:10.1016/J.TRAC.2018.10.029

17. Käppler A, Fischer D, Oberbeckmann S, et al. Analysis of environmental microplastics by vibrational microspectroscopy: FTIR, Raman or both? *Anal Bioanal Chem*. 2016;408(29):8377-8391. doi:10.1007/S00216-016-9956-3

18. Xu JL, Thomas K V., Luo Z, Gowen AA. FTIR and Raman imaging for microplastics analysis: State of the art, challenges and prospects. *TrAC Trends Anal Chem*. 2019;119:115629. doi:10.1016/J.TRAC.2019.115629

19. Araujo CF, Nolasco MM, Ribeiro AMP, Ribeiro-Claro PJA. Identification of microplastics

using Raman spectroscopy: Latest developments and future prospects. *Water Res*. 2018;142:426-440. doi:10.1016/J.WATRES.2018.05.060

20. Pollard M, Hunsicker E, Platt M. A Tunable Three-Dimensional Printed Microfluidic Resistive Pulse Sensor for the Characterization of Algae and Microplastics. *ACS Sensors*. 2020;5(8):2578-2586. doi:10.1021/acssensors.0c00987

21. Weatherall E, Willmott GR. Applications of tunable resistive pulse sensing. *Analyst*. 2015;140(10):3318-3334. doi:10.1039/C4AN02270J

22. Zabihihesari A, Khalili A, Farshchi-Heydari MJ, Eilaghi A, Rezai P. Simple microfluidic device for simultaneous extraction and detection of microplastics in water using DC electrical signal. *New J Chem*. 2023;47(19):9050-9060. doi:10.1039/D2NJ06268B

23. Pollard M, Maugi R, Platt M. Multi-resistive pulse sensor microfluidic device. *Analyst*. 2022;147(7):1417-1424. doi:10.1039/D2AN00128D

24. Lee M, Choi W, Lim G. Electrokinetic-assisted filtration for fast and highly efficient removal of microplastics from water. *Chem Eng J*. 2023;452:139152. doi:10.1016/J.CEJ.2022.139152

25. Thompson JR, Wilder LM, Crooks RM. Filtering and continuously separating microplastics from water using electric field gradients formed electrochemically in the absence of buffer. *Chem Sci*. 2021;12(41):13744-13755. doi:10.1039/D1SC03192A

26. Iri AH, Shahrah MHA, Ali AM, et al. Optical detection of microplastics in water. *Environ Sci Pollut Res*. 2021;28(45):63860-63866. doi:10.1007/S11356-021-12358-2/TABLES/1

27. Araujo CF, Nolasco MM, Ribeiro AMP, Ribeiro-Claro PJA. Identification of microplastics using Raman spectroscopy: Latest developments and future prospects. *Water Res*. 2018;142:426-440. doi:10.1016/J.WATRES.2018.05.060

28. Kaile N, Lindivat M, Elio J, Thuestad G, Crowley QG, Hoell IA. Preliminary Results From Detection of Microplastics in Liquid Samples Using Flow Cytometry. *Front Mar Sci*. 2020;7:552688. doi:10.3389/FMARS.2020.552688/BIBTEX

29. McKinnon KM. Flow Cytometry: An Overview. *Curr Protoc Immunol*. 2018;120(1):5.1.1-5.1.11. doi:10.1002/CPIM.40

30. Elsayed AA, Erfan M, Sabry YM, et al. A microfluidic chip enables fast analysis of water microplastics by optical spectroscopy. *Sci Reports 2021 111*. 2021;11(1):1-11. doi:10.1038/s41598-021-89960-4

31. Zhang Y, Zhang M, Fan Y. Assessment of microplastics using microfluidic approach. *Environ Geochem Health*. 2023;45(3):1045-1052. doi:10.1007/S10653-022-01262-4/FIGURES/7

32. Mesquita P, Gong L, Lin Y. A Low-Cost Microfluidic Method for Microplastics Identification: Towards Continuous Recognition. *Micromachines 2022, Vol 13, Page 499*. 2022;13(4):499. doi:10.3390/MI13040499

33. Pollard M. Design and development of a multifunctional fluidic sensor platform for particle and cellular characterisation utilising resistive pulse sensing. Published online May 21, 2021. doi:10.26174/THESIS.LBORO.14564448.V1

34. Pollard M, Hunsicker E, Platt M. A Tunable Three-Dimensional Printed Microfluidic Resistive Pulse Sensor for the Characterization of Algae and Microplastics. *ACS Sensors*. 2020;5(8):2578-2586. doi:10.1021/ACSSENSORS.0C00987/ASSET/IMAGES/LARGE/SE0C00987_0007.JPEG

35. Zabihihesari A, Khalili A, Farshchi-Heydari MJ, Eilaghi A, Rezai P. Simple microfluidic device for simultaneous extraction and detection of microplastics in water using DC electrical signal. *New J Chem*. 2023;47(19):9050-9060. doi:10.1039/D2NJ06268B

36. Hidalgo-Ruz V, Gutow L, Thompson RC, Thiel M. Microplastics in the marine environment: A review of the methods used for identification and quantification. *Environ Sci Technol*. 2012;46(6):3060-3075. doi:10.1021/ES2031505/ASSET/IMAGES/LARGE/ES-2011-031505_0005.JPEG

37. Wang ZM, Wagner J, Ghosal S, Bedi G, Wall S. SEM/EDS and optical microscopy analyses of microplastics in ocean trawl and fish guts. *Sci Total Environ*. 2017;603-604:616-626. doi:10.1016/J.SCITOTENV.2017.06.047

38. Girão AV. SEM/EDS and Optical Microscopy Analysis of Microplastics. *Handb Microplastics Environ*. Published online January 1, 2022:57-78. doi:10.1007/978-3-030-39041-9_7/FIGURES/7

39. Girão AV, Caputo G, Ferro MC. Application of Scanning Electron Microscopy–Energy Dispersive X-Ray Spectroscopy (SEM-EDS). *Compr Anal Chem*. 2017;75:153-168. doi:10.1016/BS.COAC.2016.10.002

40. Fernández-González V, Andrade-Garda JM, López-Mahía P, Muniategui-Lorenzo S. Impact of weathering on the chemical identification of microplastics from usual packaging polymers in the marine environment. *Anal Chim Acta*. 2021;1142:179-188. doi:10.1016/J.ACA.2020.11.002

41. Shruti VC, Pérez-Guevara F, Roy PD, Kutralam-Muniasamy G. Analyzing microplastics with Nile Red: Emerging trends, challenges, and prospects. *J Hazard Mater*. 2022;423:127171. doi:10.1016/J.JHAZMAT.2021.127171

42. Prata JC, Reis V, Matos JTV, da Costa JP, Duarte AC, Rocha-Santos T. A new approach for routine quantification of microplastics using Nile Red and automated software (MP-VAT). *Sci Total Environ*. 2019;690:1277-1283. doi:10.1016/J.SCITOTENV.2019.07.060

43. Bellasi A, Binda G, Pozzi A, Boldrocchi G, Bettinetti R. The extraction of microplastics from sediments: An overview of existing methods and the proposal of a new and green alternative. *Chemosphere*. 2021;278. doi:10.1016/J.CHEMOSPHERE.2021.130357

44. Ng KL, Obbard JP. Prevalence of microplastics in Singapore's coastal marine environment. *Mar Pollut Bull*. 2006;52(7):761-767. doi:10.1016/J.MARPOLBUL.2005.11.017

45. Coppock RL, Cole M, Lindeque PK, Queirós AM, Galloway TS. A small-scale, portable method for extracting microplastics from marine sediments. *Environ Pollut*. 2017;230:829-837. doi:10.1016/J.ENVPOL.2017.07.017

46. Eriksen M, Mason S, Wilson S, et al. Microplastic pollution in the surface waters of the Laurentian Great Lakes. *Mar Pollut Bull*. 2013;77(1-2):177-182. doi:10.1016/J.MARPOLBUL.2013.10.007

47. Mohamed Nor NH, Obbard JP. Microplastics in Singapore's coastal mangrove ecosystems.

Mar Pollut Bull. 2014;79(1-2):278-283. doi:10.1016/J.MARPOLBUL.2013.11.025

48. Liu Y, Lüttjohann S, Vianello A, Lorenz C, Liu F, Vollertsen J. Detecting small microplastics down to 1.3 µm using large area ATR-FTIR. *Mar Pollut Bull*. 2024;198:115795. doi:10.1016/J.MARPOLBUL.2023.115795

49. Llorca M, Álvarez-Muñoz D, Ábalos M, et al. Microplastics in Mediterranean coastal area: toxicity and impact for the environment and human health. *Trends Environ Anal Chem*. 2020;27:e00090. doi:10.1016/J.TEAC.2020.E00090

50. Sgier L, Freimann R, Zupanic A, Kroll A. Flow cytometry combined with viSNE for the analysis of microbial biofilms and detection of microplastics. *Nat Commun 2016 71*. 2016;7(1):1-10. doi:10.1038/ncomms11587

51. Tse YT, Lo HS, Chan SMN, Sze ETP. Flow Cytometry as a Rapid Alternative to Quantify Small Microplastics in Environmental Water Samples. *Water 2022, Vol 14, Page 1436*. 2022;14(9):1436. doi:10.3390/W14091436

52. Wang XS, Song H, Liu YL, et al. Quantitively Analyzing the Variation of Micrometer-Sized Microplastic during Water Treatment with the Flow Cytometry- Fluorescent Beads Method. *ACS ES T Eng*. 2021;1(12):1668-1677. doi:10.1021/ACSESTENGG.1C00253/ASSET/IMAGES/LARGE/EE1C00253_0004.JPEG

53. Bianco A, Carena L, Peitsaro N, Sordello F, Vione D, Passananti M. Rapid detection of nanoplastics and small microplastics by Nile-Red staining and flow cytometry. 2023;21:647-653. doi:10.1007/s10311-022-01545-3

54. Li C, Campos LC, Busquets R. A novel high-throughput analytical method to quantify microplastics in water by flow cytometry. *Green Anal Chem*. 2023;5:100057. doi:10.1016/J.GREEAC.2023.100057

55. Ly NH, Kim MK, Lee H, et al. Advanced microplastic monitoring using Raman spectroscopy with a combination of nanostructure-based substrates. *J Nanostructure Chem 2022 125*. 2022;12(5):865-888. doi:10.1007/S40097-022-00506-0

56. Ece E, Hacıosmanoğlu N, Inci F. Microfluidics as a Ray of Hope for Microplastic Pollution.

Biosens 2023, Vol 13, Page 332. 2023;13(3):332. doi:10.3390/BIOS13030332

57. Spiekermann P, Rehm BHA, Kalscheuer R, Baumeister D, Steinbüchel A. A sensitive, viable-colony staining method using Nile red for direct screening of bacteria that accumulate polyhydroxyalkanoic acids and other lipid storage compounds. *Arch Microbiol*. 1999;171(2):73-80. doi:10.1007/S002030050681/METRICS

58. Fowler SD, Greenspan P. Application of Nile red, a fluorescent hydrophobic probe, for the detection of neutral lipid deposits in tissue sections: comparison with oil red O. *http://dx.doi.org/101177/3384020099*. 1985;33(8):833-836. doi:10.1177/33.8.4020099

59. Meyers N, Catarino AI, Declercq AM, et al. Microplastic detection and identification by Nile red staining: Towards a semi-automated, cost- and time-effective technique. *Sci Total Environ*. 2022;823:153441. doi:10.1016/J.SCITOTENV.2022.153441

60. Nalbone L, Panebianco A, Giarratana F, Russell M. Nile Red staining for detecting microplastics in biota: Preliminary evidence. *Mar Pollut Bull*. 2021;172:112888. doi:10.1016/J.MARPOLBUL.2021.112888

61. Sturm MT, Horn H, Schuhen K. The potential of fluorescent dyes—comparative study of Nile red and three derivatives for the detection of microplastics. *Anal Bioanal Chem*. 2021;413(4):1059-1071. doi:10.1007/S00216-020-03066-W/TABLES/4

62. Bayley H, Martin CR. Resistive-pulse sensing - from microbes to molecules. *Chem Rev*. 2000;100(7):2575-2594. doi:10.1021/CR980099G/ASSET/IMAGES/LARGE/CR980099GF00023.JPEG

63. Pollard M, Hunsicker E, Platt M. A Tunable 3D Printed Microfluidic Resistive Pulse Sensor for the Characterisation of Algae and Microplastics.

64. Peng R, Li D. Detection and sizing of nanoparticles and DNA on PDMS nanofluidic chips based on differential resistive pulse sensing. *Nanoscale*. 2017;9(18):5964-5974. doi:10.1039/C7NR00488E

65. Kim JS, Kwon SY, Lee JY, et al. High-throughput multi-gate microfluidic resistive pulse sensing for biological nanoparticle detection. *Lab Chip*. 2023;23(7):1945-1953. doi:10.1039/D2LC01064J

66. Han Z, Liu J, Liu Z, et al. Resistive pulse sensing device with embedded nanochannel (nanochannel-RPS) for label-free biomolecule and bionanoparticle analysis. *Nanotechnology*. 2021;32(29):295507. doi:10.1088/1361-6528/ABF510

67. Xu R, Ouyang L, Shaik R, Chen H, Zhang G, Zhe J. Rapid Detection of Microparticles Using a Microfluidic Resistive Pulse Sensor Based on Bipolar Pulse-Width Multiplexing. *Biosens 2023, Vol 13, Page 721*. 2023;13(7):721. doi:10.3390/BIOS13070721

68. Thompson JR, Crooks RM. Electrokinetic separation techniques for studying nano- and microplastics. *Chem Sci*. 2022;13(43):12616-12624. doi:10.1039/D2SC04019K

69. Alyasi H, Wahib S, Gomez TA, Rasool K, Mahmoud KA. The power of MXene-based materials for emerging contaminant removal from water - A review. *Desalination*. 2024;586:117913. doi:10.1016/J.DESAL.2024.117913

70. Urso M, Ussia M, Novotný F, Pumera M. Trapping and detecting nanoplastics by MXene-derived oxide microrobots. *Nat Commun 2022 131*. 2022;13(1):1-14. doi:10.1038/s41467-022-31161-2

71. Mehmood T, Mustafa B, Mackenzie K, et al. Recent developments in microplastic contaminated water treatment: Progress and prospects of carbon-based two-dimensional materials for membranes separation. *Chemosphere*. 2023;316:137704. doi:10.1016/J.CHEMOSPHERE.2022.137704

72. Ouda M, Pandey RP, Banat F, Hasan SW. Advancing water treatment sustainability: Investigating electrified Ti3C2Tx composite membranes for minimizing microplastic fouling. *Chemosphere*. 2023;343:140224. doi:10.1016/J.CHEMOSPHERE.2023.140224

73. Cao Y, Sathish CI, Guan X, et al. Advances in magnetic materials for microplastic separation and degradation. *J Hazard Mater*. 2024;461:132537. doi:10.1016/J.JHAZMAT.2023.132537

74. Yang L, Cao X, Cui J, et al. Holey Ti3C2 nanosheets based membranes for efficient separation and removal of microplastics from water. *J Colloid Interface Sci*. 2022;617:673-682. doi:10.1016/J.JCIS.2022.03.055

75. Zhao K, Wei Y, Dong J, et al. Separation and characterization of microplastic and

nanoplastic particles in marine environment. *Environ Pollut*. 2022;297. doi:10.1016/j.envpol.2021.118773

76. Muthulakshmi L, Mohan S, Tatarchuk T. Microplastics in water: types, detection, and removal strategies. *Environ Sci Pollut Res 2023 3036*. 2023;30(36):84933-84948. doi:10.1007/S11356-023-28460-6

77. Martin Z. Bazant BDS. Double Layer in Ionic Liquids: Overscreening versus Crowding. *Phys Rev Lett*. 2011;106(4):1812-1819. doi:10.1103/PHYSREVLETT.106.046102/FIGURES/4/MEDIUM

78. Wilms TFA, Verschueren ARM, Darhuber AA. Direct electrohydrodynamic simulation of electrophoretic particle mobility. *Eindhoven Univ Technol Res*. Published online 2012. doi:https://pure.tue.nl/ws/portalfiles/portal/46932704/759038-1.pdf

79. Zhang S, Bilal M, Adeel M, Barceló D, Iqbal HMN. MXene-based designer nanomaterials and their exploitation to mitigate hazardous pollutants from environmental matrices. *Chemosphere*. 2021;283:131293. doi:10.1016/J.CHEMOSPHERE.2021.131293

80. Cao H, Fang M, Jia W, Liu X, Xu Q. Remarkable improvement of corrosion resistance of silane composite coating with Ti3C2Tx MXene on copper. *Compos Part B Eng*. 2022;228:109427. doi:10.1016/J.COMPOSITESB.2021.109427

81. Zhang J, Yan S, Yuan D, et al. Fundamentals and applications of inertial microfluidics: a review. *Lab Chip*. 2015;16(1):10-34. doi:10.1039/C5LC01159K

82. Shafiei M, Kazemzadeh Y, Martyushev DA, Dai Z, Riazi M. Effect of chemicals on the phase and viscosity behavior of water in oil emulsions. *Sci Rep*. 2023;13(1):4100. doi:10.1038/S41598-023-31379-0